Pattern Formation and Dynamics of Localized Spots of a Reaction-diffusion System on the Surface of a Torus

Penghao Wang

Abstract

In this thesis, based on the higher-order matched asymptotic expansion with the analytic expression of the Green's function of the Laplace–Beltrami operator on the toroidal surface, we study the quasi-stationary states consisting of localized spots in a reaction-diffusion system on the surface of a torus with major radius R and minor radius r. Under the assumption that these localized spots persist stably, we analytically obtain the evolution equation of slow dynamics for the centers of localized spot patterns on the toroidal surface. Owing to the analytic representation of the evolution equation, we investigate the existence of equilibria with a single spot, two spots, N-ring configuration where N localized spots are equally spaced along a latitudinal line with a mathematical rigor and two N-rings configuration on the surface of torus. We show that localized spots at the innermost/outermost locations of the torus are equilibria for any aspect ratio $\alpha = \frac{R}{r}$. In addition, we obtain there exists a range of the aspect ratio in which localized spots stay at a special location of the torus and for the case of a single spot, this special location is stable. The theoretical results and the linear stability of these spot equilibria are confirmed by solving Brusselator reaction-diffusion model by numerical means. We also list some numerical simulations about spot division of Brusselator reaction-diffusion model on the torus and compare the existence and spot dynamics of spot equilibria on the toroidal surface with the unit sphere. This thesis is an extension of the study of [26] and we add some new results.

Acknowledgments

I wish to thank my supervisor Prof. Takashi Sakajo for his support and guidance during my study.

I would like to thank Prof. Axel Voigt for offering me a great opportunity to stay at Technische Universität Dresden and to study the C++ AMDiS (Adaptive MultiDimensional Simulations) library there. I would also like to thank Dr. Sebastian Reuther for his kind technical assistance in numerial simulations by AMDiS.

I would like to express my gratitude to my parents. Without their understanding, support, and encouragement, I would not have completed this thesis.

Contents

List of Figures

Chapter 1

Introduction

Self-organizing beautiful patterns of localized spot-like structures appear ubiquitously in many phenomena including animal skin, chemical reaction, cellular differentiation and many others. In order to clarify the mechanism of spot patterns theoretically, it is helpful to construct phenomenological models describing the dynamics of those localized spot structures. A well-known model for localized spot structures is obtained from reaction-diffusion (RD) systems, in which spatially homogeneous steady states self-organize into localized spot structures due to Turing instability [30]. The localized spot patterns of reaction-diffusion systems is widely observed and applied in chemistry [6, 19, 22, 28, 34], biology [11, 18, 21, 27], physics [1, 2]. More examples of localized patterns in reaction-diffusion systems are also found in [35].

In order to construct localized patterns and analyze dynamics of localized patterns of RD systems, the method of matched asymptotic expansions is often used in the studies of RD systems. By using this method, the localized spot patterns and spot dynamics of the Gierer–Meinhardt RD model [12, 13] and the Gray–Scott RD model [7, 16] are analyzed in 1D domain. For the case of 2D domain: a bounded domain of plane, this method is used to construct localized spot patterns of the Gierer–Meinhardt RD model [15], the Gray–Scott RD model [5], the Schnakenburg RD model [17], and to analyze their dynamics and stability analytically. In addition, by using the method of matched asymptotic expansions to analyze spot patterns of Schnakenburg RD model on the 2D domain, Kolokolnikov et al. [17] obtained that the direction of the self-replication should be perpendicular to the direction of the motion. Unlike the studies in 1D and 2D domain, only a few studies analyzed the dynamics of localized spot on the surface. Using the method of matched asymptotic expansions, Rozada et al. [24] constructed the quasi-equilibrium solutions of spot pattern on the sphere and obtain spot self-replication instability, competition instability and oscillatory instability. Using the higher-order matching, Trinh and Ward [29] obtained evolution equation of slow dynamics for spot patterns on the sphere. Some detailed results for the existence and bifurcation structure of N-spot patterns are also obtained in [29]. In the meantime, another remarkable geometric feature of compact surfaces is the existence of handle structures. Hence, it is interesting to investigate how the handles affect the dynamics and the stability of localized spot patterns. One of the simplest compact surfaces is a toroidal surface with major radius R and minor radius r. Different from the surface of a sphere, it has not only nonconstant curvature but also a handle that is measured by the aspect ratio $\alpha = R/r$. Tzou and Tzou [32] have proposed an analytic-numerical method for computing the Green's function for Helmholtz operators on curved surfaces, which is applied to derive an ODE describing a slow dynamics of N localized spots for Schnakenberg reaction-diffusion model. With this model, they numerically investigate the stability of one and two localized spots. Sakajo and Wang [26] utilized the

explicit analytic formula of the Green's function of the Laplace–Beltrami operator on the toroidal surface and obtained the existence and slow dynamics of localized quasi-equilibrium multispot patterns on the toroidal surface, and analyzed equilibria of 1-spot, 2-spot, N-ring spot pattern and their stabilities.

In this thesis, we consider a reaction-diffusion system of the following form on a surface $\mathcal{M}$.

$$u_t = \epsilon^2 \triangle_{\mathcal{M}} u + \epsilon^2 A + F^u(u,v), \qquad \tau v_t = \triangle_{\mathcal{M}} v + B + \frac{1}{\epsilon^2} F^v(u,v), \tag{1.1}$$

where $\triangle_{\mathcal{M}}$ is the Laplace–Beltrami operator on $\mathcal{M}$, and the reaction terms $F^u(u,v)$ and $F^v(u,v)$ are specified by

$$F^u(u,v) = a_1 u + u^2 \sum_{i,j=0}^{n} a_{i,j} u^i v^j, \qquad F^v(u,v) = b_1 u + u^2 \sum_{i,j=0}^{n} b_{i,j} u^i v^j. \tag{1.2}$$

Here, we assume that $a_1 < 0$, $\tau > 0$, $n \in \mathbb{N}_0$, $A, B, b_1, a_{i,j}, b_{i,j} \in \mathbb{R}$ are independent of ϵ and $0 < \epsilon \ll 1$. We define the parameter $E = B - \frac{b_1}{a_1} A > 0$ for later use. One example of (1.1) is Brusselator reaction-diffusion (BRD) model which is used as a mathematical model of reaction mechanism [23, 31]. It is specified by

$$u_t = \epsilon^2 \triangle_{\mathcal{M}} u + \epsilon^2 A - u + f u^2 v, \qquad \tau v_t = \triangle_{\mathcal{M}} v + \frac{1}{\epsilon^2}(u - u^2 v), \tag{1.3}$$

in which $F^u(u,v) = -u + f u^2 v$, $F^v(u,v) = u - u^2 v$, $A > 0$ and $B = 0$ in (1.1) with an additional parameter $0 < f < 1$ satisfying $\tau = \frac{1}{f^2}$. Note that the model is considered on a bounded domain of plane [4, 33] as well as on the unit sphere [24, 29]. Another example of reaction-diffusion system model (1.1) is Schnakenberg model [32], in which $\tau > 0$, $A = 0$, $B > 0$, $F^u(u,v) = -u + u^2 v$ and $F^v(u,v) = -u^2 v$.

This thesis is an extension of the study of [26]. In Chapter 2, based on the higher-order matched asymptotic expansion, we derive the quasi-equilibrium solutions of localized spot pattern and an ODE describing the slow dynamics of localized spot centers of the reaction-diffusion system (1.1) on a toroidal surface. In Chapter 3, using the ODE, we show that localized spots at the innermost or outermost locations of the torus are equilibria for any aspect ratio $\alpha = \frac{R}{r}$. Furthermore, we investigate the existence of equilibria having one spot, two spots, N-ring and two N-rings configuration. The linear stability of these equilibria are discussed. Section 3.1 and Section 3.5 are new results, and Sections 3.2 to 3.4 have been published in [26]. The explicit analytic formula of the Green's function of the Laplace–Beltrami operator on the toroidal surface [25] is used in the derivation. This is different from the derivation by [32], in which the Helmholtz Green's function is constricted numerically. Owing to the analytic formula, we can conduct rigorous mathematical analysis of the spot dynamics. We also carry out numerical simulations of the BRD model (1.3), which are compared with our theoretical results. In Chapter 4, we list some numerical simulations about spot division of BRD model (1.3) on the torus. In Chapter 5, based on the study [24, 14, 29] of the BRD model (1.3) on the unit sphere, we derive the quasi-equilibrium solutions of localized spot pattern, evolution equation of slow dynamics of RD model (1.1) and compare the existence and spot dynamics of equilibria on the toroidal surface with on the unit sphere. This chapter is new content. The last chapter is a summary. In Appendix A, we show the asymptotic expansions of the Green's function which are used in deriving the quasi-equilibrium solutions of localized spot. In Appendix B, an algorithm computing equilibria and their stability numerically is shown. In Appendix C, we briefly introduce the surface finite element method

and give an example of discrete approximation of the BRD model by using this method. In this thesis, the theoretical results of spot dynamics are confirmed by solving the numerical evolution of the BRD model (1.3) by Adaptive MultiDimensional Simulations [36, 37].

Chapter 2

Quasi-stationary Spot Solution on the Surface of a Torus

Let $\mathbb{T}_{R,r}$ denote the toroidal surface with major radius R and minor radius r that is embedded in the Euclidean space $\mathbb{E}^3$.

$$\mathbb{T}_{R,r} = \{\boldsymbol{x} \in \mathbb{E}^3 \,|\, \boldsymbol{x} = ((R - r\cos\theta)\cos\varphi, (R - r\cos\theta)\sin\varphi, r\sin\theta)\}, \tag{2.1}$$

where $(\theta, \varphi) \in (\mathbb{R}/2\pi\mathbb{Z}) \times (\mathbb{R}/2\pi\mathbb{Z})$ is the toroidal coordinates. Let us consider the reaction-diffusion model (1.1) on the torus $\mathcal{M} = \mathbb{T}_{R,r}$, where the Laplace–Beltrami operator is specified by

$$\triangle_{\mathbb{T}_{R,r}} = \frac{1}{r^2(R - r\cos\theta)}\frac{\partial}{\partial\theta}\left((R - r\cos\theta)\frac{\partial}{\partial\theta}\right) + \frac{1}{(R - r\cos\theta)^2}\frac{\partial^2}{\partial\varphi^2}.$$

2.1 Construction of localized spots

Following the asymptotic analysis in [24], we construct a quasi-stationary solution of RD model (1.1) on the toroidal surface in the limit of $\epsilon \to 0$. Suppose that the quasi-stationary spot solution solution at a scaled time $\sigma = \epsilon^2 t$ consists of N localized spots located at $(\theta_j(\sigma), \varphi_j(\sigma))$, $j = 1, \ldots, N$. Since $\frac{\partial \boldsymbol{x}}{\partial\theta} = (r\sin\theta\cos\varphi, r\sin\theta\sin\varphi, r\cos\theta)$ and $\frac{\partial \boldsymbol{x}}{\partial\varphi} = (-(R - r\cos\theta)\sin\varphi, (R - r\cos\theta)\cos\varphi, 0)$, we obtain $\frac{\partial \boldsymbol{x}}{\partial\theta} \cdot \frac{\partial \boldsymbol{x}}{\partial\varphi} = 0$, $\left|\frac{\partial \boldsymbol{x}}{\partial\varphi}\right| = r$ and $\left|\frac{\partial \boldsymbol{x}}{\partial\varphi}\right| = (R - r\cos\theta)$. Then, we introduce a local coordinate $\boldsymbol{y} = (y_1, y_2)$ of $\mathcal{O}(\epsilon)$ around the jth spot as follows.

$$y_1(\theta, \sigma) = r\epsilon^{-1}(\theta - \theta_j(\sigma)), \qquad y_2(\varphi, \sigma) = (R - r\cos\theta_j(\sigma))\epsilon^{-1}(\varphi - \varphi_j(\sigma)). \tag{2.2}$$

It follows from

$$\begin{aligned}
&\frac{1}{r^2(R - r\cos\theta)}\frac{\partial}{\partial\theta}\left((R - r\cos\theta)\frac{\partial}{\partial\theta}\right) = \frac{1}{\epsilon}\frac{\sin\theta}{R - r\cos\theta}\frac{\partial}{\partial y_1} + \frac{1}{\epsilon^2}\frac{\partial^2}{\partial y_1^2},\\
&\frac{1}{(R - r\cos\theta)^2}\frac{\partial^2}{\partial\varphi^2} = \frac{(R - r\cos\theta_j)^2}{\epsilon^2(R - r\cos\theta)^2}\frac{\partial^2}{\partial y_2^2} = \frac{1}{\epsilon^2}\left(1 - \frac{2\sin\theta}{R - r\cos\theta}\epsilon y_1 + \mathcal{O}\left(\epsilon^2\right)\right)\frac{\partial^2}{\partial y_2^2},\\
&\frac{\sin\theta}{R - r\cos\theta} = \frac{\sin\theta_j}{R - r\cos\theta_j} + \mathcal{O}(\epsilon)
\end{aligned}$$

that we obtain

$$\begin{aligned}\triangle_{\mathbb{T}_{R,r}} &= \frac{1}{\epsilon^2}\left(\frac{\partial^2}{\partial y_1^2}+\frac{\partial^2}{\partial y_2^2}+\frac{\epsilon\sin\theta_j}{R-r\cos\theta_j}\frac{\partial}{\partial y_1}-\frac{2\epsilon y_1\sin\theta_j}{R-r\cos\theta_j}\frac{\partial^2}{\partial y_2^2}+\mathcal{O}(\epsilon^2)\right)\\ &= \frac{1}{\epsilon^2}\left(\triangle_{\boldsymbol{y}}+\epsilon\mathcal{N}_j+\mathcal{O}\left(\epsilon^2\right)\right),\end{aligned} \tag{2.3}$$

where $\triangle_{\boldsymbol{y}}=\frac{\partial^2}{\partial y_1^2}+\frac{\partial^2}{\partial y_2^2}$ and

$$\mathcal{N}_j=\frac{\sin\theta_j}{R-r\cos\theta_j}\left(\frac{\partial}{\partial y_1}-2y_1\frac{\partial^2}{\partial y_2^2}\right).$$

With the local coordinates $\boldsymbol{y}=(y_1,y_2)$ and the scaled time σ in the inner region of the jth spot, the solutions u and v of RD model (1.1) can be expressed by $u(y_1,y_2,\sigma)$ and $v(y_1,y_2,\sigma)$. Owing to $|\varphi-\varphi_j|\le\mathcal{O}(\epsilon)$ in the jth inner spot, we obtain

$$\begin{aligned}\frac{\partial u}{\partial t} &= \frac{\partial u}{\partial y_1}\frac{\partial y_1}{\partial\sigma}\frac{\partial\sigma}{\partial t}+\frac{\partial u}{\partial y_2}\frac{\partial y_2}{\partial\sigma}\frac{\partial\sigma}{\partial t}+\frac{\partial u}{\partial\sigma}\frac{\partial\sigma}{\partial t}\\ &= -r\epsilon\frac{\mathrm{d}\theta_j}{\mathrm{d}\sigma}\frac{\partial u}{\partial y_1}-(R-r\cos\theta_j)\epsilon\frac{\mathrm{d}\varphi_j}{\mathrm{d}\sigma}\frac{\partial u}{\partial y_2}+\epsilon(\varphi-\varphi_j)r\sin\theta_j\frac{\mathrm{d}\theta_j}{\mathrm{d}\sigma}\frac{\partial u}{\partial y_2}+\epsilon^2\frac{\partial u}{\partial\sigma}\\ &= \epsilon\mathcal{L}_j u+\mathcal{O}(\epsilon^2)\end{aligned} \tag{2.4}$$

and similarly

$$\frac{\partial v}{\partial t}=\epsilon\mathcal{L}_j v+\mathcal{O}(\epsilon^2),$$

where

$$\mathcal{L}_j=-\left(r\frac{\mathrm{d}\theta_j}{\mathrm{d}\sigma},(R-r\cos\theta_j)\frac{\mathrm{d}\varphi_j}{\mathrm{d}\sigma}\right)\cdot\nabla_{\boldsymbol{y}},\qquad \nabla_{\boldsymbol{y}}=\left(\frac{\partial}{\partial y_1},\frac{\partial}{\partial y_2}\right). \tag{2.5}$$

The solutions of (1.1) near the jth spot are expanded with respect to ϵ as follows.

$$u(y_1,y_2,\sigma)=\sum_{n=0}^{\infty}\epsilon^n u_{jn},\qquad v(y_1,y_2,\sigma)=\sum_{n=0}^{\infty}\epsilon^n v_{jn}. \tag{2.6}$$

We here define $\boldsymbol{w}_{jn}=(u_{jn},v_{jn})^T$. In the inner region near the jth spot, substituting (2.3), (2.4) and (2.6) into (1.1), we obtain the equation for the quasi-steady solution at the leading order of ϵ on $\boldsymbol{y}\in\mathbb{R}^2$.

$$\triangle_{\boldsymbol{y}}u_{j0}+F^u(u_{j0},v_{j0})=0,\qquad \triangle_{\boldsymbol{y}}v_{j0}+F^v(u_{j0},v_{j0})=0. \tag{2.7}$$

At the next order, by introducing $\mathcal{P}=\triangle_{\boldsymbol{y}}+\mathcal{M}_j$, where $\mathcal{M}_j=\begin{pmatrix}\frac{\partial F^u}{\partial u}(u_{j0},v_{j0}) & \frac{\partial F^u}{\partial v}(u_{j0},v_{j0})\\ \frac{\partial F^v}{\partial u}(u_{j0},v_{j0}) & \frac{\partial F^v}{\partial v}(u_{j0},v_{j0})\end{pmatrix}$, the following equation for $\boldsymbol{w}_{j1}$ is derived.

$$\mathcal{P}\boldsymbol{w}_{j1}=\triangle_{\boldsymbol{y}}\boldsymbol{w}_{j1}+\mathcal{M}_j\boldsymbol{w}_{j1}=-\mathcal{N}_j\boldsymbol{w}_{j0}+\begin{pmatrix}\mathcal{L}_j u_{j0}\\ 0\end{pmatrix}. \tag{2.8}$$

In order to construct radially symmetric localized solutions $u_{j0}(\rho)$ and $v_{j0}(\rho)$ of the equation (2.7) where $\rho=|\boldsymbol{y}|$, let us consider the following boundary value problem:

$$\begin{aligned}&\triangle_\rho u_{j0}+F^u(u_{j0},v_{j0})=0,\qquad \triangle_\rho v_{j0}+F^v(u_{j0},v_{j0})=0,\qquad 0<\rho<\infty,\\ &u_{j0}'(0)=v_{j0}'(0)=0,\qquad u_{j0}\to 0,\quad v_{j0}\sim S_j\log\rho+\chi(S_j)+o(1)\quad\text{as}\quad\rho\to\infty,\end{aligned} \tag{2.9}$$

where $\chi(S_j)$ is a constant independent of ρ, $\triangle_\rho = \partial_{\rho\rho} + \frac{1}{\rho}\partial_\rho$, and u_{j0} is exponentially small as $\rho \to \infty$. This is called the *core problem*, in which parameter S_j is referred to as the *strength* of the jth spot. On the other hand, we consider the solutions of RD model (1.1) in the region outside of the spot with the scale of $\mathcal{O}(\epsilon)$. The Taylor expansion of $\boldsymbol{x}(\theta,\varphi)$ in the neighborhood of $\boldsymbol{x}_j = ((R - r\cos\theta_j)\cos\varphi_j, (R - r\cos\theta_j)\sin\varphi_j, r\sin\theta_j)$ is given by $|\boldsymbol{x}-\boldsymbol{x}_j|^2 = \epsilon^2(\boldsymbol{y}^T M_j^T M_j \boldsymbol{y}) + \mathcal{O}(\epsilon^3)$, where $\boldsymbol{x}(\theta,\varphi) = ((R - r\cos\theta)\cos\varphi, (R - r\cos\theta)\sin\varphi, r\sin\theta)$ and M_j is defined by

$$M_j = \begin{pmatrix} \cos\varphi_j \sin\theta_j & -\sin\varphi_j \\ \sin\varphi_j \sin\theta_j & \cos\varphi_j \\ \cos\theta_j & 0 \end{pmatrix}. \tag{2.10}$$

It follows from $M_j^T M_j = I$ and $\boldsymbol{y}^T\boldsymbol{y} = \rho^2$ that we obtain $|\boldsymbol{x} - \boldsymbol{x}_j| = \epsilon\rho + \mathcal{O}(\epsilon^2)$. Owing to the quasi-stationarity of the solution, u should satisfy $u_t = 0$ and $\triangle_{\mathbb{T}_{R,r}} u = 0$ in the region separated from $\mathcal{O}(\epsilon)$ neighborhoods of the localized spots at $\{\boldsymbol{x}_1, \ldots, \boldsymbol{x}_N\}$. In the outer region of the spots, since the nonlinear term is negligible, we obtain $u \sim -\frac{\epsilon^2 A}{a_1}$ for $a_1 \neq 0$. Combining the inner and outer approximations of u, we have the following asymptotic expression of u in the outer region:

$$u \sim -\epsilon^2 \frac{A}{a_1} + \sum_{j=1}^{N} u_{j0}.$$

Regarding the equation (1.1) for v in the outer region, we have $B + \frac{1}{\epsilon^2}F^v \sim B + \frac{b_1}{\epsilon^2}u \sim E$ in the outer region of spots, since the nonlinear terms are negligibly small. Since $|\boldsymbol{x} - \boldsymbol{x}_j| \sim \epsilon\rho$, $u_j \sim u_{j0}$ and $v_j \sim v_{j0}$ in the inner region of the jth spot, the contribution in $F^v(u,v)$ from the jth localized spots to the outer region is approximated by the delta function $b\delta(\boldsymbol{x} - \boldsymbol{x}_j)$ whose weight b is obtained by integrating the nonlinear term in the disk of radius $\epsilon\rho$ around the jth spot.

$$\begin{aligned} b &= \epsilon^2 \int_0^{2\pi} \mathrm{d}\theta \int_0^{\infty} F^v(u_{j0}, v_{j0})\rho \mathrm{d}\rho = -2\pi\epsilon^2 \int_0^{\infty} (\rho\partial_{\rho\rho} v_{j0} + \partial_\rho v_{j0})\mathrm{d}\rho \\ &= -2\pi\epsilon^2 \left[\rho\partial_\rho v_{j0}\right]_0^{\infty} = -2\pi\epsilon^2 S_j. \end{aligned}$$

Hence, by combining the inner and outer approximations for $B + \frac{1}{\epsilon^2}F^v(u,v)$, we obtain

$$B + \frac{1}{\epsilon^2}F^v(u,v) \sim E - 2\pi \sum_{j=1}^{N} S_j \delta(\boldsymbol{x} - \boldsymbol{x}_j). \tag{2.11}$$

Using (2.11) and the far-field behavior of the inner solution (2.9), we finally obtain the following outer problem for v subject to the matching condition:

$$\triangle_{\mathbb{T}_{R,r}} v + E = 2\pi \sum_{j=1}^{N} S_j \delta(\boldsymbol{x} - \boldsymbol{x}_j), \qquad |\boldsymbol{x} - \boldsymbol{x}_j| > \mathcal{O}(\epsilon), \quad j = 1, \ldots, N, \tag{2.12}$$

$$v \sim v_{j0} + \epsilon v_{j1} \sim S_j \log\rho + \chi(S_j) + \epsilon v_{j1} + o(1), \quad |\boldsymbol{x} - \boldsymbol{x}_j| \to \mathcal{O}(\epsilon), \quad j = 1, \ldots, N. \tag{2.13}$$

To solve (2.12), we make use of the Green's function $G(\boldsymbol{x};\boldsymbol{x}_0)$ associated with the toroidal surface, satisfying

$$\triangle_{\mathbb{T}_{R,r}} G(\boldsymbol{x};\boldsymbol{x}_0) = -\delta(\boldsymbol{x} - \boldsymbol{x}_0) + \frac{1}{4\pi^2 Rr}, \qquad G(\boldsymbol{x};\boldsymbol{x}_0) = G(\boldsymbol{x}_0;\boldsymbol{x}). \tag{2.14}$$

According to [25], the Green's function on the toroidal surface is explicitly represented by

$$G(\boldsymbol{x};\boldsymbol{x}_0) = -\frac{1}{2\pi}\log\left|P\left(\frac{\zeta}{\zeta_0}\right)\right| - F(\theta) - F(\theta_0) - \frac{1}{4\pi^2\mathcal{A}}K(\theta)K(\theta_0) + \frac{1}{4\pi}K(\theta) - \frac{1}{4\pi}K(\theta_0), \tag{2.15}$$

where

$$K(\theta) = -\int_0^\theta \frac{\mathrm{d}\eta}{\alpha-\cos\eta}, \quad F(\theta) = -\frac{1}{4\pi^2\alpha}\int_0^\theta \frac{\alpha\eta-\sin\eta}{\alpha-\cos\eta}\mathrm{d}\eta, \quad \zeta(\theta,\varphi) = e^{i\varphi}\exp\left(K(\theta)\right) \in \mathbb{C} \tag{2.16}$$

and $\mathcal{A} = (\alpha^2-1)^{-1/2}$ with $\alpha = R/r$. Note that the variables $\boldsymbol{x}$, (θ,φ) and ζ are related to each other through the relations (2.1) and (2.16). In (2.15), the function $P(\zeta)$ denotes the Schottky–Klein prime function associated with the annular domain $D_\zeta = \{\zeta \in \mathbb{C} | e^{-2\pi\mathcal{A}} < |\zeta| < 1\}$.

$$P(\zeta) = (1-\zeta)\prod_{n\geq 1}\left(1-e^{-2n\pi\mathcal{A}}\zeta\right)\left(1-e^{-2n\pi\mathcal{A}}\zeta^{-1}\right). \tag{2.17}$$

If S_j satisfies $\sum_{j=1}^N S_j = 2\pi rRE$, the solution of (2.12) is expressed by

$$v = -2\pi\sum_{j=1}^N S_j G(\boldsymbol{x};\boldsymbol{x}_j) + \overline{v} \tag{2.18}$$

with a constant $\overline{v}$ to be determined. In order to compute $\overline{v}$, we match the behavior of the outer solution (2.18) as $|\boldsymbol{x}-\boldsymbol{x}_j| \to \mathcal{O}(\epsilon)$ and the far-field behavior of the inner solution (2.13) of the jth spot as $\rho \to \infty$. Let us rewrite $G_j(\boldsymbol{x}) = G(\boldsymbol{x};\boldsymbol{x}_j)$ for $j = 1, 2, \ldots, N$, which is divided into three parts:

$$2\pi G_j(\boldsymbol{x}) = -\log\left|1-\frac{\zeta(\theta,\varphi)}{\zeta(\theta_j,\varphi_j)}\right| - \log W_j(\theta,\varphi) - Q_j(\theta), \tag{2.19}$$

where

$$W_j(\theta,\varphi) = \left|\prod_{n\geq 1}\left(1-e^{-2n\pi\mathcal{A}}\frac{\zeta(\theta,\varphi)}{\zeta(\theta_j,\varphi_j)}\right)\left(1-e^{-2n\pi\mathcal{A}}\left(\frac{\zeta(\theta,\varphi)}{\zeta(\theta_j,\varphi_j)}\right)^{-1}\right)\right|, \tag{2.20}$$

$$Q_j(\theta) = 2\pi\left(F(\theta)+F(\theta_j)+\frac{1}{4\pi^2\mathcal{A}}K(\theta)K(\theta_j) - \frac{1}{4\pi}K(\theta) + \frac{1}{4\pi}K(\theta_j)\right). \tag{2.21}$$

As $\boldsymbol{x} \to \boldsymbol{x}_j$, it follows from (A.2) in Appendix A that we obtain

$$\log\left|1-\frac{\zeta(\theta,\varphi)}{\zeta(\theta_j,\varphi_j)}\right| = \log\rho + \log\epsilon - \log\left(R-r\cos\theta_j\right) - \frac{\epsilon(1+\sin\theta_j)y_1}{2(R-r\cos\theta_j)} + \frac{\epsilon\sin\theta_j y_1 y_2^2}{2\rho^2(R-r\cos\theta_j)} + \mathcal{O}(\epsilon^2).$$

Owing to (2.22) and (A.7) in Appendix A, we also have

$$\begin{aligned}\log W_j(\theta,\varphi) =& \log W_j(\theta_j,\varphi_j) + \left.\frac{\partial(\log W_j(\theta,\varphi_j))}{\partial\theta}\right|_{\theta=\theta_j}(\theta-\theta_j)\\ &+ \left.\frac{\partial(\log W_j(\theta_j,\varphi))}{\partial\varphi}\right|_{\varphi=\varphi_j}(\varphi-\varphi_j)+\mathcal{O}(\epsilon^2)\\ =& k+\mathcal{O}(\epsilon^2),\\ Q_j(\theta) =& Q_j(\theta_j)+\left.\frac{\partial Q_j}{\partial\theta}\right|_{\theta=\theta_j}(\theta-\theta_j)+\mathcal{O}(\epsilon^2) = q_j + Q_j'(\theta_j)\frac{\epsilon y_1}{r}+\mathcal{O}(\epsilon^2),\end{aligned}$$

where $k=\log W_j(\theta_j,\varphi_j)=2\log\left(\prod_{n\geq 1}\left(1-e^{-2n\pi\mathcal{A}}\right)\right)$, $q_j=Q_j(\theta_j)$ and

$$Q_j'(\theta) = -\frac{1}{2\pi\alpha}\frac{\alpha\theta-\sin\theta}{\alpha-\cos\theta}-\frac{1}{2\pi\mathcal{A}}K(\theta_j)\frac{1}{\alpha-\cos\theta}+\frac{1}{2}\frac{1}{\alpha-\cos\theta}. \tag{2.22}$$

Hence, as $\boldsymbol{x}\to\boldsymbol{x}_j$, we have

$$\begin{aligned}2\pi G_j(\boldsymbol{x}_j) =& -\log\rho-\log\epsilon+\log(R-r\cos\theta_j)+\frac{\epsilon(1+\sin\theta_j)y_1}{2(R-r\cos\theta_j)}-\frac{\epsilon\sin\theta_j y_1 y_2^2}{2\rho^2(R-r\cos\theta_j)}\\ &-k-q_j-Q_j'(\theta_j)\frac{\epsilon y_1}{r}+\mathcal{O}(\epsilon^2).\end{aligned}$$

On the other hand, by Taylor expansion, as $\boldsymbol{x}\to\boldsymbol{x}_i$ for $i\neq j$, we have

$$\begin{aligned}2\pi G_j(\boldsymbol{x}) \sim& 2\pi G_j(\boldsymbol{x}_i)+2\pi\left.\frac{\partial G_j(\theta,\varphi)}{\partial\theta}\right|_{(\theta,\varphi)=(\theta_i,\varphi_i)}(\theta-\theta_i)+2\pi\left.\frac{\partial G_j(\theta,\varphi)}{\partial\varphi}\right|_{(\theta,\varphi)=(\theta_i,\varphi_i)}(\varphi-\varphi_i)\\ =& -\left(\widetilde{G}_{ji}+\nabla_{(\theta,\varphi)}\widetilde{G}_j\Big|_{(\theta,\varphi)=(\theta_i,\varphi_i)}\cdot\left(\frac{\epsilon y_1}{r},\frac{\epsilon y_2}{R-r\cos\theta_i}\right)\right),\end{aligned}$$

where $\widetilde{G}_j=-2\pi G_j$, $\widetilde{G}_{ji}=\widetilde{G}_j(\boldsymbol{x}_i)$, and $\nabla_{(\theta,\varphi)}=(\frac{\partial}{\partial\theta},\frac{\partial}{\partial\varphi})$. Then, as $|\boldsymbol{x}-\boldsymbol{x}_j|\to\mathcal{O}(\epsilon)$, by matching the outer solution (2.18) of v and the far-field behavior of the inner solution (2.13) of the jth spot, we have

$$-2\pi\sum_{i=1}^{N}S_iG_i(\boldsymbol{x})+\overline{v}\sim S_j\log\rho+\chi(S_j)+\epsilon v_{j1},\qquad |\boldsymbol{x}-\boldsymbol{x}_j|\to\mathcal{O}(\epsilon),$$

which implies

$$\begin{aligned}&S_j\left(\log\rho+\log\epsilon-\log(R-r\cos\theta_j)-\frac{\epsilon(1+\sin\theta_j)y_1}{2(R-r\cos\theta_j)}+\frac{\epsilon\sin\theta_j y_1y_2^2}{2\rho^2(R-r\cos\theta_j)}\right)+S_jk+S_jq_j\\ &+\frac{\epsilon S_j}{r}Q_j'(\theta_j)y_1+\sum_{\substack{i=1\\ i\neq j}}^{N}S_i\left(\widetilde{G}_{ij}+\nabla_{(\theta,\varphi)}\widetilde{G}_i\Big|_{(\theta,\varphi)=(\theta_j,\varphi_j)}\cdot\left(\frac{\epsilon y_1}{r},\frac{\epsilon y_2}{R-\cos\theta_j}\right)\right)+\overline{v}\\ &\sim S_j\log\rho+\chi(S_j)+\epsilon v_{j1}.\end{aligned} \tag{2.23}$$

Matching the leading order of (2.23), we obtain

$$\chi(S_j)=S_j(\log\epsilon-\log(R-r\cos\theta_j)+k+q_j)+\overline{v}+\sum_{i\neq j}^{N}S_i\widetilde{G}_{ij},\quad j=1,\ldots,N. \tag{2.24}$$

Let us recall that the expression (2.18) is valid under the assumption that

$$\sum_{j=1}^{N} S_j = 2\pi r R E. \tag{2.25}$$

Hence, the matrix form of (2.24) and (2.25) is given by

$$\boldsymbol{\chi}(\boldsymbol{S}) - (\mathcal{G} + (\log\epsilon)I - \mathbf{P} + \mathcal{K} + \mathcal{Q})\boldsymbol{S} = \overline{v}\boldsymbol{e}, \qquad \boldsymbol{e}^T\boldsymbol{S} = 2\pi r R E, \tag{2.26}$$

where

$$\begin{aligned}
&\boldsymbol{S} = \begin{pmatrix} S_1 \\ \vdots \\ S_N \end{pmatrix}, \quad \boldsymbol{e} = \begin{pmatrix} 1 \\ \vdots \\ 1 \end{pmatrix}, \quad \boldsymbol{\chi}(\boldsymbol{S}) = \begin{pmatrix} \chi(S_1) \\ \vdots \\ \chi(S_N) \end{pmatrix}, \quad \mathcal{G} = \begin{pmatrix} 0 & \widetilde{G}_{12} & \cdots & \widetilde{G}_{1N} \\ \widetilde{G}_{21} & \ddots & & \vdots \\ \vdots & & & \\ \widetilde{G}_{N1} & \cdots & & 0 \end{pmatrix}, \\
&\mathbf{P} = \begin{pmatrix} p_1 & & & 0 \\ & p_2 & & \\ & & \ddots & \\ 0 & & & p_N \end{pmatrix}, \quad \mathcal{K} = \begin{pmatrix} k & & & 0 \\ & k & & \\ & & \ddots & \\ 0 & & & k \end{pmatrix}, \quad \mathcal{Q} = \begin{pmatrix} q_1 & & & 0 \\ & q_2 & & \\ & & \ddots & \\ 0 & & & q_N \end{pmatrix}.
\end{aligned} \tag{2.27}$$

Here, $p_j = \log(R - r\cos\theta_j)$ and $q_j = Q_j(\theta_j)$ for $j = 1, 2, \ldots, N$. Since $\boldsymbol{e}^T\boldsymbol{S} = \sum_{j=1}^{N} S_j = 2\pi r R E$ and $\boldsymbol{e}^T\boldsymbol{e} = N$, by taking the inner product between $\boldsymbol{e}^T$ and the first equation of (2.26), we have the following formula deriving the constant $\overline{v}$ from $\boldsymbol{S}$ and $\boldsymbol{\chi}(\boldsymbol{S})$.

$$\begin{aligned}
\overline{v} =& \frac{1}{N}(\boldsymbol{e}^T\boldsymbol{\chi}(\boldsymbol{S}) - (\boldsymbol{e}^T\mathcal{G} + (\log\epsilon)\boldsymbol{e}^T I - \boldsymbol{e}^T\mathbf{P} + \boldsymbol{e}^T\mathcal{K} + \boldsymbol{e}^T\mathcal{Q})\boldsymbol{S}) \\
=& -\frac{2\pi r R E \log\epsilon}{N} + \frac{1}{N}(\boldsymbol{e}^T\boldsymbol{\chi}(\boldsymbol{S}) - (\boldsymbol{e}^T\mathcal{G} - \boldsymbol{e}^T\mathbf{P} + \boldsymbol{e}^T\mathcal{K} + \boldsymbol{e}^T\mathcal{Q})\boldsymbol{S}).
\end{aligned} \tag{2.28}$$

Substituting (2.28) into (2.26), we have

$$\boldsymbol{S} + \frac{1}{\log\epsilon}(I - \boldsymbol{e}_0)(\mathcal{G} - \mathbf{P} + \mathcal{K} + \mathcal{Q})\boldsymbol{S} = \frac{1}{\log\epsilon}(I - \boldsymbol{e}_0)\boldsymbol{\chi}(\boldsymbol{S}) + \frac{2\pi r R E}{N}\boldsymbol{e}, \tag{2.29}$$

where $\boldsymbol{e}_0 = \frac{1}{N}\boldsymbol{e}\boldsymbol{e}^T$ is the matrix whose components are all $\frac{1}{N}$. The equation (2.29) gives rise to a nonlinear equation $\boldsymbol{g}(\boldsymbol{S}) = \mathbf{0}$ for $\boldsymbol{S}$. Suppose that there exist solutions S_j, $u_{j0}(\rho)$, $v_{j0}(\rho)$, $j = 1, \ldots, N$, of (2.29) and (2.9) for given N spot centers (θ_j, φ_j). In addition, if the solutions $u_{j0}(\rho)$ and $v_{j0}(\rho)$ are spot-shaped for $j = 1, 2 \ldots, N$, then the localized spot solutions u_{qe} and v_{qe} of RD model (1.1) are represented by

$$u_{\mathrm{qe}} \sim -\epsilon^2\frac{A}{a_1} + \sum_{j=1}^{N} u_{j0}(\epsilon^{-1}|\boldsymbol{x} - \boldsymbol{x}_j|), \tag{2.30}$$

$$v_{\mathrm{qe}} \sim \begin{cases} v_{j0}(\epsilon^{-1}|\boldsymbol{x} - \boldsymbol{x}_j|), & |\boldsymbol{x} - \boldsymbol{x}_j| \le \mathcal{O}(\epsilon), \\ -2\pi\sum\limits_{j=1}^{N} S_j G(\boldsymbol{x}; \boldsymbol{x}_j) + \overline{v}, & |\boldsymbol{x} - \boldsymbol{x}_j| > \mathcal{O}(\epsilon). \end{cases} \tag{2.31}$$

2.2 Stability of localized spots

We assume that the quasi-equilibrium solution of (2.30) and (2.31) is stable up to eigenvalues of $\mathcal{O}(1)$ when we derive the evolution equation for spot cores in the next section. Hence, we discuss the stability of the quasi-stationary spot solutions $u_{\rm qe}$ and $v_{\rm qe}$ based on the analysis in [24]. Substituting $u = u_{\rm qe} + e^{\lambda t}\psi$, $v = v_{\rm qe} + e^{\lambda t}\phi$ into RD model (1.1) and linearizing the equation, we obtain the following eigenvalue problem:

$$\begin{aligned} &\epsilon^2 \triangle_{\mathbb{T}_{R,r}}\psi + \frac{\partial F^u}{\partial u}(u_{\rm qe}, v_{\rm qe})\psi + \frac{\partial F^u}{\partial v}(u_{\rm qe}, v_{\rm qe})\phi = \lambda\psi, \\ &\triangle_{\mathbb{T}_{R,r}}\phi + \frac{1}{\epsilon^2}\left(\frac{\partial F^v}{\partial u}(u_{\rm qe}, v_{\rm qe})\psi + \frac{\partial F^v}{\partial v}(u_{\rm qe}, v_{\rm qe})\phi\right) = \tau\lambda\phi. \end{aligned} \tag{2.32}$$

Since we are concerned with the stability of a localized spot in the inner region of the jth spot, we expand

$$u_{\rm qe}(y_1, y_2, \sigma) = \sum_{n=0}^{\infty} \epsilon^n u_{jn}, \qquad v_{\rm qe}(y_1, y_2, \sigma) = \sum_{n=0}^{\infty} \epsilon^n v_{jn}. \tag{2.33}$$

Note that we have $u_{\rm qe} \sim u_{j0}$ and $v_{\rm qe} \sim v_{j0}$ in the inner region of the jth spot with the strength S_j as the leading order. Assume now that u_{j0} and v_{j0} are radially symmetric functions, say $u_{j0}(\rho)$ and $v_{j0}(\rho)$ which are solutions of the core problem (2.9). Using the local coordinates (2.2) and (2.3) in the inner region of the jth spot, the eigenvalue problem (2.32) is reduced to

$$\begin{aligned} &\triangle_{\boldsymbol{y}}\psi + \frac{\partial F^u}{\partial u}(u_{j0}, v_{j0})\psi + \frac{\partial F^u}{\partial v}(u_{j0}, v_{j0})\phi + \mathcal{O}(\epsilon) = \lambda\psi, \\ &\triangle_{\boldsymbol{y}}\phi + \frac{\partial F^v}{\partial u}(u_{j0}, v_{j0})\psi + \frac{\partial F^v}{\partial v}(u_{j0}, v_{j0})\phi + \mathcal{O}(\epsilon) = \epsilon^2\tau\lambda\phi. \end{aligned} \tag{2.34}$$

Furthermore, we assume $\tau\lambda \ll \mathcal{O}(\epsilon^{-2})$ and neglect the $\mathcal{O}(\epsilon)$ term. Then, we obtain the eigenvalue problem at the leading order.

$$\begin{aligned} &\triangle_{\boldsymbol{y}}\psi + \frac{\partial F^u}{\partial u}(u_{j0}, v_{j0})\psi + \frac{\partial F^u}{\partial v}(u_{j0}, v_{j0})\phi = \lambda\psi, \\ &\triangle_{\boldsymbol{y}}\phi + \frac{\partial F^v}{\partial u}(u_{j0}, v_{j0})\psi + \frac{\partial F^v}{\partial v}(u_{j0}, v_{j0})\phi = 0. \end{aligned} \tag{2.35}$$

By the separation of variables with $\psi = \widehat{\psi}(\rho)e^{i\omega m}$ and $\phi = \widehat{\phi}(\rho)e^{i\omega m}$ around the inner region of the jth spot in the coordinates $\boldsymbol{y} = (y_1, y_2) = (\rho\cos\omega, \rho\sin\omega)$ and $m = 0, 1, 2\ldots$, the equations (2.35) are reduced to those for the shape of the jth spot.

$$\begin{aligned} &\triangle_\rho\widehat{\psi} - \frac{m^2}{\rho^2}\widehat{\psi} + (a_1 - \lambda)\widehat{\psi} + \frac{\partial(u^2 f^u)}{\partial u}(u_{j0}, v_{j0})\widehat{\psi} + \frac{\partial F^u}{\partial v}(u_{j0}, v_{j0})\widehat{\phi} = 0, \\ &\triangle_\rho\widehat{\phi} - \frac{m^2}{\rho^2}\widehat{\phi} + \frac{\partial F^v}{\partial u}(u_{j0}, v_{j0})\widehat{\psi} + \frac{\partial F^v}{\partial v}(u_{j0}, v_{j0})\widehat{\phi} = 0, \end{aligned} \tag{2.36}$$

where $f^u(u, v) = \sum_{i,j=0}^{n} a_{i,j}u^i v^j$. Owing to the existence of $(a_1 - \lambda)\widehat{\psi}$ in the equation (2.36) for $\widehat{\psi}$, we impose that $\widehat{\psi} \to 0$ as $\rho \to \infty$ if $\mathrm{Re}\lambda > a_1$. The far-field condition for $\widehat{\psi}$ is given by $\widehat{\psi}'(0) = \widehat{\phi}'(0) = 0$ and $\widehat{\psi} \to 0$ as $\rho \to \infty$. In what follows, we consider the modes $m \geq 2$, since $(\widehat{\psi}, \widehat{\phi}) = (\partial_\rho u_{j0}, \partial_\rho v_{j0})$ is the solution of (2.36) corresponding to the $\lambda = 0$ for $m = 1$, which is obtained by differentiating core problem (2.9). Hence, owing to the existence of $-\frac{m^2}{\rho^2}\widehat{\phi}$ in the equation (2.36) for $\widehat{\phi}$, the boundary condition for $\widehat{\phi}$ is given by $\widehat{\phi} \to 0$ as $\rho \to \infty$ for $m \geq 2$. By solving the eigenvalue problem (2.36) numerically, we can observe the stability of the jth spot.

2.3 Derivation of evolution equation for spot cores

Based on the asymptotic analysis in [29], the evolution equation of N spot centers is derived from the second-order inner core problem (2.8) with the operator $\mathcal{L}_j$ containing the temporal derivative in terms of σ. The boundary condition of $v_{j1}(y_1, y_2, \sigma)$ as $\rho \to \infty$ is obtained by matching the next order $\mathcal{O}(\epsilon)$ in (2.23).

$$\begin{aligned} v_{j1} =& S_j \left(\frac{1}{r} Q_j'(\theta_j) y_1 - \frac{(1+\sin\theta_j) y_1}{2(R - r\cos\theta_j)} + \frac{\sin\theta_j y_1 y_2^2}{2\rho^2 (R - r\cos\theta_j)} \right) \\ &+ \sum_{\substack{i=1 \\ i\neq j}}^{N} S_i \nabla_{(\theta,\varphi)} \widetilde{G}_i(\theta_j, \varphi_j) \cdot \left(\frac{y_1}{r}, \frac{y_2}{R - r\cos\theta_j} \right) \\ =& Y_j + \frac{S_j \sin\theta_j y_1 y_2^2}{2\rho^2 (R - r\cos\theta_j)}, \quad j = 1, 2, \ldots, N, \end{aligned} \tag{2.37}$$

where

$$Y_j = S_j \left(\frac{1}{r} Q_j'(\theta_j) y_1 - \frac{(1+\sin\theta_j) y_1}{2(R - r\cos\theta_j)} \right) + \sum_{\substack{i=1 \\ i\neq j}}^{N} S_i \nabla_{(\theta,\varphi)} \widetilde{G}_i(\theta_j, \varphi_j) \cdot \left(\frac{y_1}{r}, \frac{y_2}{R - r\cos\theta_j} \right).$$

Regarding the boundary condition of $u_{j1}(y_1, y_2, \sigma)$, owing to $u \sim -\epsilon^2 A/a_1$ as $\rho \to \infty$, the $\mathcal{O}(\epsilon)$ term of u in (2.6) becomes $u_{j1} = 0$ as $\rho \to \infty$ for $\boldsymbol{w}_{j1} = (u_{j1}, v_{j1})^T$. This gives rise to the following boundary value problem:

$$\begin{aligned} &\mathcal{P}\boldsymbol{w}_{j1} = \triangle_{\boldsymbol{y}} \boldsymbol{w}_{j1} + \mathcal{M}_j \boldsymbol{w}_{j1} = -\mathcal{N}_j \boldsymbol{w}_{j0} + \begin{pmatrix} \mathcal{L}_j u_{j0} \\ 0 \end{pmatrix}, \quad \boldsymbol{y} = (y_1, y_2) \in \mathbb{R}^2, \\ &\boldsymbol{w}_{j1} \sim \begin{pmatrix} 0 \\ \frac{S_j}{2\rho^2} \frac{\sin\theta_j}{R - r\cos\theta_j} y_1 y_2^2 + Y_j \end{pmatrix} \quad \text{as} \quad \rho = |\boldsymbol{y}| \to \infty. \end{aligned} \tag{2.38}$$

We solve this equation by considering the decomposition of $\boldsymbol{w}_{j1}$,

$$\boldsymbol{w}_{j1} = \begin{pmatrix} u_{j1} \\ v_{j1} \end{pmatrix} = \boldsymbol{w}_{j1}^e + \boldsymbol{w}_{j1}^d, \quad \boldsymbol{w}_{j1}^e = \begin{pmatrix} u_{j1}^e \\ v_{j1}^e \end{pmatrix}, \quad \boldsymbol{w}_{j1}^d = \begin{pmatrix} u_{j1}^d \\ v_{j1}^d \end{pmatrix}, \tag{2.39}$$

where $\boldsymbol{w}_{j1}^e$ and $\boldsymbol{w}_{j1}^d$ satisfy the following inhomogeneous boundary value problems:

$$\mathcal{P}\boldsymbol{w}_{j1}^e = -\mathcal{N}_j \boldsymbol{w}_{j0}, \quad \mathcal{P}\boldsymbol{w}_{j1}^d = \begin{pmatrix} \mathcal{L}_j u_{j0} \\ 0 \end{pmatrix}, \quad \boldsymbol{y} \in \mathbb{R}^2, \tag{2.40}$$

$$\boldsymbol{w}_{j1}^e \sim \begin{pmatrix} 0 \\ \frac{S_j}{2\rho^2} \frac{\sin\theta_j}{R - r\cos\theta_j} y_1 y_2^2 \end{pmatrix}, \quad \boldsymbol{w}_{j1}^d \sim \begin{pmatrix} 0 \\ \boldsymbol{\alpha}_j \cdot \boldsymbol{y} \end{pmatrix}, \quad \rho = |y| \to \infty. \tag{2.41}$$

Here, the function $\boldsymbol{\alpha}_j = (\alpha_{j,1}, \alpha_{j,2})^T$ is introduced so that $\boldsymbol{\alpha}_j \cdot \boldsymbol{y} = Y_j$ for $j = 1, 2, \ldots, N$. Each $\boldsymbol{\alpha}_j$ is a function from $(\theta_1, \theta_2, \ldots, \theta_N, \varphi_1, \varphi_2, \cdots \varphi_N) \in \mathbb{R}^{2N}$ to $\mathbb{R}^2$, and it is explicitly given by

$$\boldsymbol{\alpha}_j = \begin{pmatrix} \alpha_{j,1} \\ \alpha_{j,2} \end{pmatrix} = \sum_{\substack{i=1 \\ i\neq j}}^{N} S_i \left(\begin{array}{c} \frac{1}{r} \frac{\partial \widetilde{G}_i}{\partial \theta} \\ \frac{1}{R - r\cos\theta_j} \frac{\partial \widetilde{G}_i}{\partial \varphi} \end{array} \right) \Bigg|_{(\theta,\varphi)=(\theta_j,\varphi_j)} + S_j \begin{pmatrix} \frac{1}{r} Q_j'(\theta_j) - \frac{(1+\sin\theta_j)}{2(R - r\cos\theta_j)} \\ 0 \end{pmatrix}. \tag{2.42}$$

As shown in [32], $w^e_{j1} = \frac{\sin\theta_j}{R-r\cos\theta_j}(-\frac{y_2^2}{2}\frac{\partial w_{j0}}{\partial y_1} + y_1 y_2 \frac{\partial w_{j0}}{\partial y_2})$ is the solution of the first equation, which contains no temporal derivative term. Hence, it has nothing to do with the spot dynamics. Hence, we construct the evolution equation for the jth spot by solving the second equation of (2.40) for $\boldsymbol{w}^d_{j1}$. By differentiating (2.7), we obtain $\mathcal{P}\frac{\partial \boldsymbol{w}_{j0}}{\partial y_i} = 0$ for $i = 1, 2$, which means the dimension of the null-space of the adjoint operator $\mathcal{P}^* = (\triangle_{\boldsymbol{y}} + \mathcal{M}_j^T)$ is at least two. Let us consider the homogeneous adjoint problem $\mathcal{P}^*\boldsymbol{\Psi} = 0$, which is solved by the separation of variables in terms of the local coordinates $\boldsymbol{y} = (\rho\cos\omega, \rho\sin\omega)^T$,

$$\boldsymbol{\Psi}(\rho,\omega) = \boldsymbol{P}(\rho)T(\omega), \quad \boldsymbol{P}(\rho) = \begin{pmatrix} P_1(\rho) \\ P_2(\rho) \end{pmatrix}, \tag{2.43}$$

where $T(\omega) = \cos\omega$ or $\sin\omega$. Substituting (2.43) into the equation, we obtain the equation for $\boldsymbol{P}(\rho)$

$$\triangle_\rho \boldsymbol{P} - \frac{1}{\rho^2}\boldsymbol{P} + \mathcal{M}_j^T\boldsymbol{P} = 0, \quad \boldsymbol{P}(0) = \boldsymbol{0}, \quad \boldsymbol{P} \sim \left(-\frac{b_1}{a_1\rho}, \frac{1}{\rho}\right)^T, \quad \rho \to \infty. \tag{2.44}$$

The boundary condition of $\boldsymbol{P}$ as $\rho \to \infty$ is obtained as follows. Owing to (2.8) with $u_{j0} \to 0$ and $u_{j0}v_{j0} \to 0$ as $\rho \to \infty$, $\mathcal{M}_j^T$ should satisfy

$$\mathcal{M}_j^T \to \begin{pmatrix} a_1 & b_1 \\ 0 & 0 \end{pmatrix}, \qquad \rho \to \infty. \tag{2.45}$$

This yields $\triangle_\rho P_2 - \rho^{-2}P_2 = 0$ as $\rho \to \infty$ and we thus have $P_2 = \mathcal{O}(\rho^{-1})$ as $\rho \to \infty$. Normalizing $\boldsymbol{P}$ so that $P_2 \sim \frac{1}{\rho}$ as $\rho \to \infty$, we have $P_1 \sim -\frac{b_1}{a_1\rho}$ as $\rho \to \infty$. Hence, we obtain another boundary condition $\boldsymbol{P} \sim (-\frac{b_1}{a_1\rho}, \frac{1}{\rho})^T$ as $\rho \to \infty$.

Let $B_\kappa = \{\boldsymbol{y} \,|\, |\boldsymbol{y}| \le \kappa\}$. By using Green's second identity to $\boldsymbol{w}^d_{j1}$ and $\boldsymbol{\Psi}$, we obtain

$$\begin{aligned} \Lambda &= \lim_{\kappa\to\infty} \int_{B_\kappa} \left[\boldsymbol{\Psi}^T\mathcal{P}\boldsymbol{w}^d_{j1} - (\boldsymbol{w}^d_{j1})^T\mathcal{P}^*\boldsymbol{\Psi}\right] \mathrm{d}\boldsymbol{y} \qquad (2.46) \\ &= \lim_{\kappa\to\infty} \int_{B_\kappa} \left[\boldsymbol{\Psi}^T(\triangle_{\boldsymbol{y}} + \mathcal{M}_j)\boldsymbol{w}^d_{j1} - (\boldsymbol{w}^d_{j1})^T(\triangle_{\boldsymbol{y}} + \mathcal{M}_j^T)\boldsymbol{\Psi}\right] \mathrm{d}\boldsymbol{y} \\ &= \lim_{\kappa\to\infty} \int_0^{2\pi} \left(\boldsymbol{\Psi}^T\partial_\rho\boldsymbol{w}^d_{j1} - (\boldsymbol{w}^d_{j1})^T\partial_\rho\boldsymbol{\Psi}\right)\Big|_{\rho=\kappa} \rho \mathrm{d}\omega. \qquad (2.47) \end{aligned}$$

Using the far-field asymptotic behavior as $\rho \to \infty$,

$$\boldsymbol{w}^d_{j1} \sim \begin{pmatrix} 0 \\ \boldsymbol{\alpha}_j \cdot \boldsymbol{y} \end{pmatrix} = \begin{pmatrix} 0 \\ \alpha_{j,1}\rho\cos\omega + \alpha_{j,2}\rho\sin\omega \end{pmatrix}, \qquad \Psi \sim \begin{pmatrix} -\frac{b_1}{a_1\rho} \\ \frac{1}{\rho} \end{pmatrix} T(\omega), \tag{2.48}$$

we calculate (2.47) as

$$\Lambda = \int_0^{2\pi} (2\alpha_{j,1}\cos\omega + 2\alpha_{j,2}\sin\omega)T(\omega)\mathrm{d}\omega = \begin{cases} 2\pi\alpha_{j,1} & \text{if } T(\omega) = \cos\omega, \\ 2\pi\alpha_{j,2} & \text{if } T(\omega) = \sin\omega. \end{cases} \tag{2.49}$$

On the other hand, since $\mathcal{P}^*\boldsymbol{\Psi} = 0$, substituting (2.40) into the left-hand side of (2.46) and

using $\frac{\partial u_{j0}}{\partial y_1} = \frac{\partial u_{j0}}{\partial \rho}\cos\omega$, $\frac{\partial u_{j0}}{\partial y_2} = \frac{\partial u_{j0}}{\partial \rho}\sin\omega$, we obtain

$$\begin{aligned}\Lambda &= \lim_{\kappa\to\infty}\int_{B_\kappa}\left[\boldsymbol{\Psi}^T\mathcal{P}\boldsymbol{w}^d_{j1}\right]\mathrm{d}\boldsymbol{y} = \int_0^\infty\int_0^{2\pi}\rho P_1(\rho)T(\omega)\mathcal{L}_j u_{j0}\mathrm{d}\rho\mathrm{d}\omega \\ &= -\int_0^\infty\int_0^{2\pi}\rho P_1(\rho)T(\omega)\left(r\frac{\mathrm{d}\theta_j}{\mathrm{d}\sigma}\frac{\partial u_{j0}}{\partial\rho}\cos\omega + (R-r\cos\theta_j)\frac{\mathrm{d}\varphi_j}{\mathrm{d}\sigma}\frac{\partial u_{j0}}{\partial\rho}\sin\omega\right)\mathrm{d}\rho\mathrm{d}\omega \qquad (2.50)\\ &= \begin{cases} -r\pi\mathcal{C}_j\frac{\mathrm{d}\theta_j}{\mathrm{d}\sigma}, & \text{if } T(\omega)=\cos\omega,\\ -(R-r\cos\theta_j)\pi\mathcal{C}_j\frac{\mathrm{d}\varphi_j}{\mathrm{d}\sigma}, & \text{if } T(\omega)=\sin\omega.\end{cases}\end{aligned}$$

Here, the constant $\mathcal{C}_j$ is defined by

$$\mathcal{C}_j = \int_0^\infty \rho\frac{\partial u_{j0}}{\partial\rho}P_1(\rho)\mathrm{d}\rho. \qquad (2.51)$$

We note that since the solution u_{j0} of (2.9) depends on the strength S_j and the parameters F^u, F^v, so does $\mathcal{C}_j$. Equating (2.49) and (2.50) for $T(\omega)=\cos\omega$ and $T(\omega)=\sin\omega$, we obtain the equation of the jth spot,

$$\frac{\mathrm{d}\theta_j}{\mathrm{d}\sigma} = -\frac{2\alpha_{j,1}}{r\mathcal{C}_j}, \qquad \frac{\mathrm{d}\varphi_j}{\mathrm{d}\sigma} = -\frac{2\alpha_{j,2}}{(R-r\cos\theta_j)\mathcal{C}_j}. \qquad (2.52)$$

The evolution equation is valid as long as the localized spots of RD model (1.1) with the strengths $\boldsymbol{S}$ persist stably for a long time, and the constant $\mathcal{C}_j$ has a fixed sign independently of S_j. These conditions are validated numerically for BRD model (1.3) in the next section.

2.4 Validation of the theory for Brusselator reaction-diffusion system

We construct quasi-stationary solutions u_{qe} and v_{qe} for BRD model (1.3) by numerical means to validate the existence of stable localized spots. That is to say, we determine the source strength $\boldsymbol{S}\in\mathbb{R}^N$, $\boldsymbol{\chi}\in\mathbb{R}^N$ and $\overline{v}\in\mathbb{R}$ so that they satisfy (2.9), (2.28) and (2.29) and check its stability. Let us first consider the following boundary value problem on $0\le\rho\le\rho_0$ for $\rho_0\gg 1$ for a given scalar S.

$$\begin{aligned}&\triangle_\rho\widehat{u} - \widehat{u} + f\widehat{u}^2\widehat{v} = 0, \qquad \triangle_\rho\widehat{v} + \widehat{u} - \widehat{u}^2\widehat{v} = 0, \qquad 0<\rho\le\rho_0,\\ &\widehat{u}'(0) = \widehat{v}'(0) = 0, \qquad \widehat{u}(\rho_0) = 0, \quad \text{and} \quad \widehat{v}'(\rho_0) = \frac{S}{\rho_0}.\end{aligned} \qquad (2.53)$$

Taking $\rho_0 = 20$, we solve this equation with the COLNEW method [3] in the bvpSolve R library [20]. We then set $\overline{\chi}(S) = \widehat{v}(\rho_0) - S\log\rho_0$. This defines a map $\overline{\chi}: S\in\mathbb{R}\mapsto\overline{\chi}(S)\in\mathbb{R}$. Then, for the jth component S_j of $\boldsymbol{S}$, we obtain the approximation $\chi(S_j)\approx\overline{\chi}(S_j)$. Consequently, $\widehat{u}$ and $\widehat{v}$ are the approximate solutions u_{j0} and v_{j0} of (2.9) with S_j. In addition, it is important to observe that the shape of the solution depends on the parameters f and S. Figure 2.1(a) shows that the radial solution $\widehat{u}(\rho)$ is localized When $S=2$, but it tends to be volcano-shaped as S increases for $f=0.7$. As a matter of fact, it is numerically confirmed that the radial solution remains localized for $S\le 3.44$. Since the solution is assumed to be localized in the present asymptotic analysis, we need to restrict our attention to small S. The algorithm solving $\boldsymbol{g}(\boldsymbol{S})=\boldsymbol{0}$ is described in Appendix B. The plot of $\overline{\chi}(S)$ for various

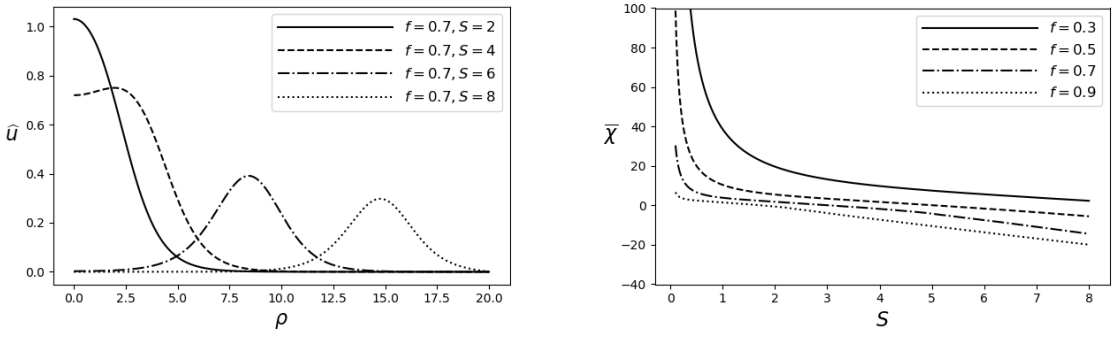

(a) (b)

Figure 2.1: (a) Numerical solution $\widehat{u}(\rho)$ of the approximate core problem (2.53) for BRD model (1.3) with $f = 0.7$ and various S. (b) The constant $\overline{\chi}(S)$ in (2.9) that is obtained by solving $\boldsymbol{g}(\boldsymbol{S}) = \boldsymbol{0}$ numerically for $f = 0.3, 0.5, 0.7, 0.9$ and $S \in [0.1, 8.0]$.

f is shown in Figure 2.1(b). Note that Figure 2.1(a) and (b) are the same as those in [24], although the chosen parameters are different.

Next, we confirm the stability of the localized spot solutions of the BRD model (1.3) described in Section 2.2. With $F^u(u,v) = -u + fu^2v$ and $F^v(u,v) = u - u^2v$, the linearized problem (2.36) is reduced to

$$\triangle_\rho\widehat{\psi} - \frac{m^2}{\rho^2}\widehat{\psi} - (1+\lambda)\widehat{\psi} + 2fu_{j0}v_{j0}\widehat{\psi} + fu_{j0}^2\widehat{\phi} = 0, \quad \triangle_\rho\widehat{\phi} - \frac{m^2}{\rho^2}\widehat{\phi} + \widehat{\psi} - 2u_{j0}v_{j0}\widehat{\psi} - u_{j0}^2\widehat{\phi} = 0. \tag{2.54}$$

The boundary condition is given by $\widehat{\psi}'(0) = \widehat{\phi}'(0) = 0$, $\widehat{\psi} \to 0$ and $\widehat{\phi} \to 0$ as $\rho \to \infty$. For the approximate solutions u_{j0} and v_{j0} of the core problem (2.9) and given m, we solve (2.54) by using the finite central differences on $0 < \rho < \rho_0 = 20$, which gives rise to a generalized matrix eigenvalue problem. We pay attention to the eigenvalue of (2.54) having the largest real part, say the principal eigenvalue λ_{max}. Figure 2.2 shows the real part of λ_{max} for fixed $f = 0.7$ and $m = 2, 3, 4$, which is the same plot as that in [24]. It indicates that λ_{max} is negative for small S and gets larger as S increases monotonically, and it finally becomes positive for large S. Hence, there exists a unique threshold, denoted by $\Sigma_m(f)$, where the principal eigenvalue becomes zero. If $S > \Sigma_m(f)$, since the principal eigenvalue is real, the spot becomes unstable, while it is stable for $S < \Sigma_m(f)$. Since $\Sigma_2(f) < \Sigma_3(f) < \Sigma_4(f)$ for $f = 0.7$, the spot is unstable for any modes of perturbations with $m \geq 2$ if $S > \Sigma_2(f)$. It is important to notice that the stability of the localized spot depends not on the locations but on the strength $\boldsymbol{S}$, the parameter f, and the mode m.

Finally, the value of $\mathcal{C}_j$ is computed. We solve the following boundary value problem on $0 \leq \rho \leq \rho_0$ with $\rho_0 \gg 1$ to approximate (P_1, P_2) satisfying (2.44).

$$\begin{aligned}
&\triangle_\rho\widehat{P_1} - \frac{1}{\rho^2}\widehat{P_1} + (2f\widehat{u}\widehat{v} - 1)\widehat{P_1} + (1 - 2\widehat{u}\widehat{v})\widehat{P_2} = 0, \quad \triangle_\rho\widehat{P_2} - \frac{1}{\rho^2}\widehat{P_2} + f\widehat{u}^2\widehat{P_1} - \widehat{u}^2\widehat{P_2} = 0, \\
&\widehat{P_1}(0) = \widehat{P_2}(0) = 0, \quad \widehat{P_1}(\rho_0) = \frac{1}{\rho_0}, \quad \widehat{P_2}(\rho_0) = \frac{1}{\rho_0}.
\end{aligned} \tag{2.55}$$

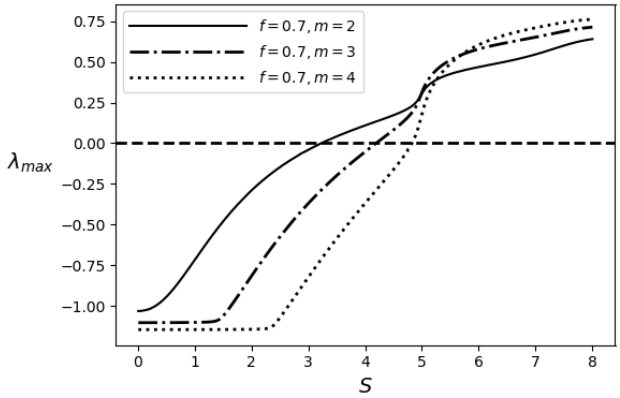

Figure 2.2: Plots of the principal eigenvalue λ_{max} of (2.54) when $f = 0.7$ and $S_j \in [0.01, 8]$ for $m = 2, 3, 4$.

With $\widehat{P_1}$ and $\widehat{u}'$ obtained in this way, we can define a map $\mathcal{C}\colon S \in \mathbb{R} \mapsto \mathcal{C}(S) \in \mathbb{R}$ by

$$\mathcal{C} = \int_0^{\rho_0} \rho \widehat{u}'(\rho)\widehat{P_1}(\rho)\mathrm{d}\rho. \tag{2.56}$$

We thus have $\mathcal{C}_j \approx \mathcal{C}(S_j)$ for given S_j. Figure 2.3 shows the plot of $\mathcal{C}(S)$ of the BRD model (1.3) with $f = 0.7$, which is the same plot as that in [29]. Let us note that $\mathcal{C}_j$ is independent of the location of the jth spot by construction, and it is always negative for $0 < S < \Sigma_2(0.7)$. Consequently, we conclude that the stable localized spots with $0 < S < \Sigma_2(0.7)$ with a negative $\mathcal{C}$ exist, where the equation (2.52) of the spot cores remains valid.

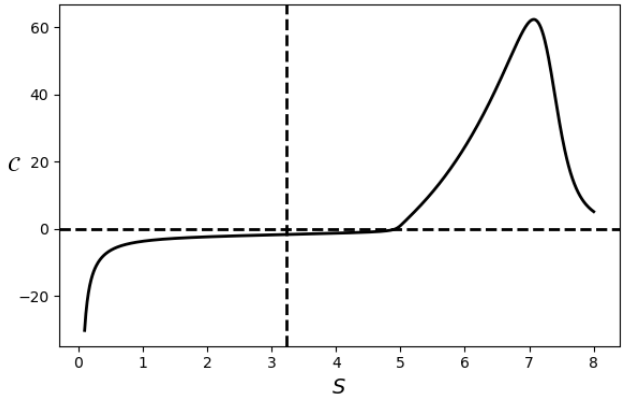

Figure 2.3: Plot of $\mathcal{C}(S)$ of the BRD model (1.3) for $f = 0.7$ and $S \in [0.1, 8]$. The vertical dotted line represents $S = \Sigma_2(f)$, which determines the stability of the quasi-steady spot solution. For $S > \Sigma_2(f)$, it is unstable. For $0 < S < \Sigma_2(f)$, we observe $\mathcal{C} < 0$.

Chapter 3

Dynamics of Quasi-stationary Localized Spots

In this chapter, under the assumption that localized N spots persist stably and $\mathcal{C}_j < 0$ for $j = 1, \ldots, N$, we study the equilibrium states of evolution equation (2.52), meaning that N spots of RD model (1.1) are in a quasi-equilibrium state moving very slowly with $\mathcal{O}(\epsilon^{-2})$ time scale. Since $\mathcal{C}_j < 0$ and $R - r\cos\theta_j > 0$, the N spots configuration centered at (θ_j, φ_j) is an equilibrium state if and only if $\alpha_{j,1} = \alpha_{j,2} = 0$, $j = 1, \ldots, N$. It is important to note that $\alpha_{j,1}$ and $\alpha_{j,2}$ are independent of the choice of the reaction terms F^u and F^v if we ignore the constraint (2.29). On the other hand, we need to specify the reaction terms to discuss the linear stability, since the matrix generally depends on $\frac{\partial S_j}{\partial \theta_i}$ and $\frac{\partial S_j}{\partial \varphi_i}$, $i, j = 1, 2, \ldots, N$, except the one-spot case. The theoretical results are compared with the nonlinear evolutions of the BRD model (1.3) that are obtained numerically.

3.1 $\theta_j = 0$ or π

When spots are located at the innermost or the outermost locations of the torus, i.e $\theta_j = 0$ or π for $j = 1, 2, \ldots, N$, by the symmetry of the torus, independent of φ_j, the spots should satisfy $\frac{\mathrm{d}\theta_j}{\mathrm{d}\sigma} = 0$ for $j = 1, 2, \ldots, N$. This result can be confirmed by computing (2.42) as follows.

Theorem 3.1.1. Suppose that $\theta_j = 0$ or π for $j = 1, 2, \ldots, N$ and there exists $S_j, j = 1, \ldots, N$ satisfying (2.29). Then, wherever the location of φ_j is, we have $\alpha_{j,1} = 0$ for $j = 1, 2, \ldots, N$. Hence, $\frac{\mathrm{d}\theta_j}{\mathrm{d}\sigma} = 0$ for $j = 1, 2, \ldots, N$.

Proof. It follows from (2.52) and (2.42) that

$$\alpha_{j,1} = \sum_{\substack{i=1 \\ i\neq j}}^{N} \frac{S_i}{r} \frac{\partial \widetilde{G}_i}{\partial \theta}\bigg|_{(\theta,\varphi)=(\theta_j,\varphi_j)} + S_j \left(\frac{1}{r} Q_j'(\theta_j) - \frac{(1+\sin\theta_j)}{2(R - r\cos\theta_j)} \right), \tag{3.1}$$

where $\frac{\partial \widetilde{G}_i}{\partial \theta}\Big|_{(\theta,\varphi)=(\theta_j,\varphi_j)} = h_{i,j,n} + t_{i,j} + Q_i'(\theta_j)$. Here Q_i', $h_{i,j,n}$ and $t_{i,j}$ are defined by (2.22), (A.3) and (A.5). It follows from (2.22) that $\frac{1}{r} Q_j'(\theta_j) - \frac{(1+\sin\theta_j)}{2(R - r\cos\theta_j)} = 0$ when $\theta_j = 0$ or π, since $K(0) = 0$ and $K(\pi) = -\pi\mathcal{A}$. When $\theta_i = \theta_j = 0$ or $\theta_i = \theta_j = \pi$, from (A.3) and (A.5), we have $h_{i,j,n} = h_{j,i,n} = 0$, $t_{i,j} = t_{j,i} = -\frac{1}{2(\alpha - \cos\theta_j)}$ and $Q_i'(\theta_j) = Q_j'(\theta_i) = Q_j'(\theta_j) = \frac{1}{2(\alpha - \cos\theta_j)}$. Hence,

when $\theta_i = \theta_j = 0$ or $\theta_i = \theta_j = \pi$, we obtain $\frac{\partial \widetilde{G}_i}{\partial \theta}(\theta_j, \varphi_j) = 0$. Next, we show that when $\theta_i = 0$ and $\theta_j = \pi$, we obtain $\frac{\partial \widetilde{G}_i}{\partial \theta}(\theta_j, \varphi_j) = \frac{\partial \widetilde{G}_j}{\partial \theta}(\theta_i, \varphi_i) = 0$. Setting

$$E_{i,j} = \exp\left(-\int_{\theta_i}^{\theta_j} \frac{\mathrm{d}\eta}{\alpha - \cos\eta}\right) \quad \text{and} \quad s = \exp(-2\pi\mathcal{A}),$$

we have $E_{i,j} = E_{j,i}^{-1} = \exp(-\pi\mathcal{A}) = s^{\frac{1}{2}}$ when $\theta_i = 0$ and $\theta_j = \pi$. Since $s < 1$, we obtain $\lim_{k\to\infty} s^k = 0$. Then, it follows from (2.22), (A.3) and (A.5) that

$$\begin{aligned}
(\alpha - \cos\theta_j)\sum_{n\geq 1} h_{i,j,n} =& \left(\frac{s^{\frac{3}{2}}\cos(\varphi_j - \varphi_i) - s^3}{1 - 2s^{\frac{3}{2}}\cos(\varphi_j - \varphi_i) + s^3} - \frac{s^{\frac{1}{2}}\cos(\varphi_j - \varphi_i) - s^1}{1 - 2s^{\frac{1}{2}}\cos(\varphi_j - \varphi_i) + s^1}\right) \\
&+ \left(\frac{s^{\frac{5}{2}}\cos(\varphi_j - \varphi_i) - s^5}{1 - 2s^{\frac{5}{2}}\cos(\varphi_j - \varphi_i) + s^5} - \frac{s^{\frac{3}{2}}\cos(\varphi_j - \varphi_i) - s^3}{1 - 2s^{\frac{3}{2}}\cos(\varphi_j - \varphi_i) + s^3}\right) + \cdots \\
=& -\frac{s^{\frac{1}{2}}\cos(\varphi_j - \varphi_i) - s^1}{1 - 2s^{\frac{1}{2}}\cos(\varphi_j - \varphi_i) + s^1}, \\
(\alpha - \cos\theta_j)t_{i,j} =& \frac{s^{\frac{1}{2}}\cos(\varphi_j - \varphi_i) - s^1}{1 - 2s^{\frac{1}{2}}\cos(\varphi_j - \varphi_i) + s^1}, \\
(\alpha - \cos\theta_j)Q_i'(\theta_j) =& -\frac{1}{2\pi\alpha}(\alpha\theta_j - \sin\theta_j) - \frac{1}{2\pi\mathcal{A}}K(\theta_i) + \frac{1}{2} = 0,
\end{aligned}$$

and

$$\begin{aligned}
(\alpha - \cos\theta_i)\sum_{n\geq 1} h_{j,i,n} =& \left(\frac{s^{\frac{1}{2}}\cos(\varphi_j - \varphi_i) - s^1}{1 - 2s^{\frac{1}{2}}\cos(\varphi_j - \varphi_i) + s^1} - \frac{s^{\frac{3}{2}}\cos(\varphi_j - \varphi_i) - s^3}{1 - 2s^{\frac{3}{2}}\cos(\varphi_j - \varphi_i) + s^3}\right) \\
&+ \left(\frac{s^{\frac{3}{2}}\cos(\varphi_j - \varphi_i) - s^3}{1 - 2s^{\frac{3}{2}}\cos(\varphi_j - \varphi_i) + s^3} - \frac{s^{\frac{5}{2}}\cos(\varphi_j - \varphi_i) - s^5}{1 - 2s^{\frac{5}{2}}\cos(\varphi_j - \varphi_i) + 5^3}\right) + \cdots \\
=& \frac{s^{\frac{1}{2}}\cos(\varphi_j - \varphi_i) - s^1}{1 - 2s^{\frac{1}{2}}\cos(\varphi_j - \varphi_i) + s^1}, \\
(\alpha - \cos\theta_i)t_{j,i} =& \frac{s^{-\frac{1}{2}}\cos(\varphi_j - \varphi_i) - s^{-1}}{1 - 2s^{-\frac{1}{2}}\cos(\varphi_j - \varphi_i) + s^{-1}} = -1 - \frac{s^{\frac{1}{2}}\cos(\varphi_j - \varphi_i) - s^1}{1 - 2s^{\frac{1}{2}}\cos(\varphi_j - \varphi_i) + s^1}, \\
(\alpha - \cos\theta_i)Q_j'(\theta_i) =& -\frac{1}{2\pi\alpha}(\alpha\theta_i - \sin\theta_i) - \frac{1}{2\pi\mathcal{A}}K(\theta_j) + \frac{1}{2} = 1.
\end{aligned}$$

Then, we obtain $\frac{\partial \widetilde{G}_i}{\partial \theta}(\theta_j, \varphi_j) = \frac{\partial \widetilde{G}_j}{\partial \theta}(\theta_i, \varphi_i) = 0$ and

$$\alpha_{j,1} = \sum_{\substack{i=1 \\ i\neq j}}^{N} \frac{S_i}{r}\frac{\partial \widetilde{G}_i}{\partial \theta}\bigg|_{(\theta,\varphi)=(\theta_j,\varphi_j)} + S_j\left(\frac{1}{r}Q_j'(\theta_j) - \frac{(1+\sin\theta_j)}{2(R - r\cos\theta_j)}\right) = 0. \tag{3.2}$$

Similarly, we obtain $\alpha_{i,1} = 0$. Hence, we obtain $\frac{\mathrm{d}\theta_j}{\mathrm{d}\sigma} = \alpha_{j,1} = 0$ when $\theta_j = 0$ or π, $j = 1, \ldots, N$. □

3.2 A single spot

Suppose that the spot is located at (θ_1, φ_1) with the strength S_1 on the toroidal surface. For one spot, $S_1 = 2\pi rRE$ is the solution of (2.29) and independent of (θ_1, φ_1). We then find the equilibrium state, in which the spot is in a quasi-equilibrium state moving very slowly with $\mathcal{O}(\epsilon^{-2})$ time scale. This is the solution of

$$\alpha_{1,1}(\theta_1) = \frac{S_1}{r(\alpha - \cos\theta_1)} \left(-\frac{\alpha\theta_1 - \sin\theta_1}{2\pi\alpha} - \frac{K(\theta_1)}{2\pi\mathcal{A}} - \frac{\sin\theta_1}{2} \right), \qquad \alpha_{1,2}(\theta_1) = 0,$$

where $K(\theta_1) = -2\mathcal{A} \arctan\left(\sqrt{\frac{\alpha+1}{\alpha-1}} \tan\frac{\theta_1}{2}\right)$. Since $\alpha_{1,2}$ always vanishes, it is sufficient to solve the equation $\alpha_{1,1}(\theta_1) = 0$ for θ_1.

Theorem 3.2.1. There exists a unique $\alpha_s > 1$ such that the following holds. For $1 < \alpha < \alpha_s$, there exists a unique $\vartheta_s(\alpha) \in (0, \pi)$ such that the single spots at $\theta_1 = 0, \vartheta_s(\alpha), \pi, 2\pi - \vartheta_s(\alpha)$ are equilibria. Then the spots at $\theta_1 = 0$ and π are unstable, while those at $\theta_1 = \vartheta_s(\alpha)$ and $2\pi - \vartheta_s(\alpha)$ are stable. On the other hand, for $\alpha_s \le \alpha$, there exist the stable spot at $\theta_1 = 0$ and the unstable spot at $\theta_1 = \pi$.

Proof. When the spot is located at the innermost and the outermost points of the torus, i.e. $\theta_1 = 0$ and $\theta_1 = \pi$, as shown in Theorem 3.1.1, $\alpha_{1,1}(0) = \alpha_{1,1}(\pi) = 0$. We now find the other equilibrium. Let us rewrite

$$\alpha_{1,1}(\theta_1) = \frac{S_1\beta_1(\theta_1)}{r(\alpha - \cos\theta_1)}, \qquad \beta_1(\theta_1) = -\frac{\alpha\theta_1 - \sin\theta_1}{2\pi\alpha} - \frac{K(\theta_1)}{2\pi\mathcal{A}} - \frac{\sin\theta_1}{2}.$$

The zeros of $\beta_1(\theta_1) = 0$ are equivalent to those of $\alpha_{1,1}(\theta_1) = 0$ owing to $\alpha - \cos\theta_1 > 0$. It follows from

$$\beta_1'(\theta_1) = -\frac{\alpha - \cos\theta_1}{2\pi\alpha} + \frac{1}{2\pi\mathcal{A}} \frac{1}{\alpha - \cos\theta_1} - \frac{\cos\theta_1}{2} \tag{3.3}$$

that there exist $\theta_b \in [0, 2\pi)$ satisfying $\beta_1'(\theta_b) = 0$ if and only if $\theta = \theta_b$ satisfies

$$\alpha - \mathcal{A}(\alpha - \cos\theta)^2 - \pi\alpha\mathcal{A}\cos\theta(\alpha - \cos\theta) = 0. \tag{3.4}$$

With $x = \cos\theta$, it gives rise to the quadratic equation $\alpha - \mathcal{A}(\alpha - x)^2 - \pi\alpha\mathcal{A}x(\alpha - x) = 0$. It has the solutions $x_1 = \sqrt{\gamma + \delta^2} + \delta$ and $x_2 = -\sqrt{\gamma + \delta^2} + \delta$, where

$$\gamma = \frac{\alpha^2 - \alpha\sqrt{\alpha^2 - 1}}{\pi\alpha - 1} > 0, \qquad \delta = \frac{\pi\alpha^2 - 2\alpha}{2(\pi\alpha - 1)} > 0.$$

Note that $x_2 < x_1$. Hence, owing to the one-to-one correspondence between $x \in [-1, 1]$ and $\theta \in [0, \pi]$ and the symmetry $x = \cos\theta = \cos(2\pi - \theta)$, (3.4) has two solutions at most in $\theta \in (0, \pi)$ and two solutions at most in $\theta \in (\pi, 2\pi)$ corresponding to x_1 and x_2. It is easy to see $x_2 = -\sqrt{\gamma + \delta^2} + \delta < 0 < 1$. Since $x_2 = -\sqrt{\gamma + \delta^2} + \delta > -1$, it is reduced to $1 + 2\delta > \gamma$, which is equivalent to $-\alpha\sqrt{\alpha^2 - 1} < (\alpha + 1)((\pi - 1)\alpha - 1)$. This inequality always holds true owing to $(\alpha + 1)((\pi - 1)\alpha - 1) > 0$ for $\alpha > 1$. Hence, we obtain $-1 < x_2 < 1$. We then consider the range of α where $x_1 < 1$. Let us first confirm that $\delta < 1$ for $1 < \alpha < \sqrt{1 + \frac{1}{\pi^2}} + \frac{1+\pi}{\pi} \approx 2.3677$. In this range, $x_1 < 1$ is reduced to $\gamma < 1 - 2\delta$, which is equivalent to

$$(\alpha - 1)((\pi^2 + 2\pi)\alpha^3 - (2 + \pi)^2\alpha^2 + (3 + 2\pi)\alpha - 1) < 0.$$

Since the cubic equation $(\pi^2+2\pi)\alpha^3-(2+\pi)^2\alpha^2+(3+2\pi)\alpha-1=0$ has only one real solution, say $\alpha=\alpha_s\approx 1.2010$, we obtain $x_1<1$ for $\alpha\in(1,\alpha_s)$. Hence, owing to $-1<x_2<1\le x_1$ for $\alpha\ge\alpha_s$, the equation $\beta_1'(\theta_b)=0$ has the solutions $\theta_b=\cos^{-1}x_2\in(0,\pi)$ and $2\pi-\cos^{-1}x_2\in(\pi,2\pi)$. Accordingly, since $\beta_1(0)=\beta_1(\pi)=0$, there is no solution of $\beta_1(\theta)=0$ except $\theta=0,\pi$. In addition, it follows from $\beta_1'(0)\le 0$ and $\beta_1'(\pi)>0$ for $\alpha\ge\alpha_s$ that the spot at $\theta_1=0$ is stable and that at $\theta_1=\pi$ is unstable. On the other hand, since $-1<x_2<x_1<1$ for $\alpha\in(1,\alpha_s)$, (3.4) has two solutions in $(0,\pi)$ and the other two solutions in $(\pi,2\pi)$, which indicates that there exists $\vartheta_s(\alpha)\in(0,\pi)$ such that one spot solutions at $\theta_1=0$, $\vartheta_s(\alpha)$, π, and $2\pi-\vartheta_s(\alpha)$ are the solutions of $\beta_1(\theta_1)=0$ by the continuity of β_1. Owing to $\beta_1'(\pi)>0$, we also obtain $\beta_1'(0)>0$, $\beta_1'(\vartheta_s(\alpha))<0$ and $\beta_1'(2\pi-\vartheta_s(\alpha))<0$. Hence, the single spots at $\theta_1=0$ and π are unstable, while those at $\vartheta_s(\alpha)$, $2\pi-\vartheta_s(\alpha)$ are stable. □

To confirm the linear stability of the one-spot case, we solve BRD model (1.3) numerically from the initial condition (2.30) and (2.31) having one spot on the torus of $(R,r)=(1.1,1.0)$ and $(R,r)=(1.3,1.0)$. The numerical parameters are given by $f=0.7$, $\epsilon=0.05$, $S_1=3$, $A=\frac{S_1}{2\pi Rr}$. After computing the solution up to $t=100$ when the localized spot is formed, we add a 2% random perturbation to the solution. For $\alpha=1.1<\alpha_s$, the present theory expects that the spot at $\vartheta_s(1.1)\approx 0.64295$ is stable, whereas that at $\theta=0$ and π are unstable. Figure 3.1 shows that the spot centered at $\theta_1=0$ is moving toward the stable one spot at $\theta_1=\vartheta_s(1.1)$ after the perturbation. When $\alpha=1.3>\alpha_s$, the spot at $\theta_1=0$ is stable and that at $\theta_1=\pi$ is unstable. Figure 3.2 confirms that the spot centered at $\theta_1=\pi$ is moving toward $\theta_1=0$ after a long-time evolution.

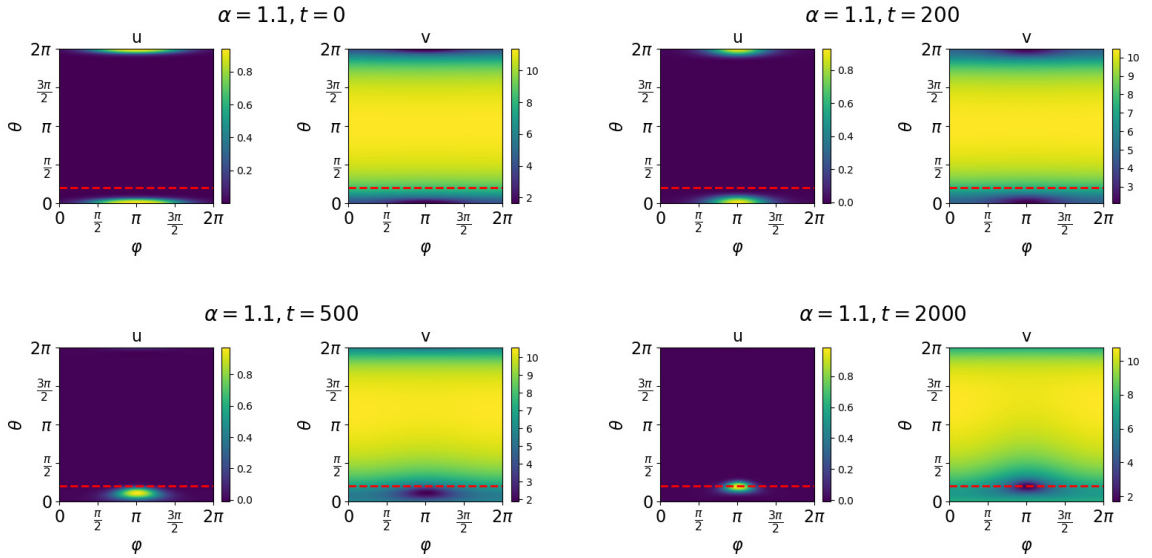

Figure 3.1: Evolution of the BRD model (1.3) from a one-spot initial condition (2.30) and (2.31) centered at $\theta_1=0$ and $\varphi_1=\pi$ on the torus of $R=1.1$ and $r=1.0$, i.e., $\alpha=1.1$. The numerical parameters are $f=0.7$, $\epsilon=0.05$, $S_1=3$, $A=\frac{S_1}{2\pi Rr}$. The red horizontal dotted line represents the reference lines of $\vartheta_s(1.1)\approx 0.64295$. Since the spot is unstable, it starts moving toward $\vartheta_s(1.1)$.

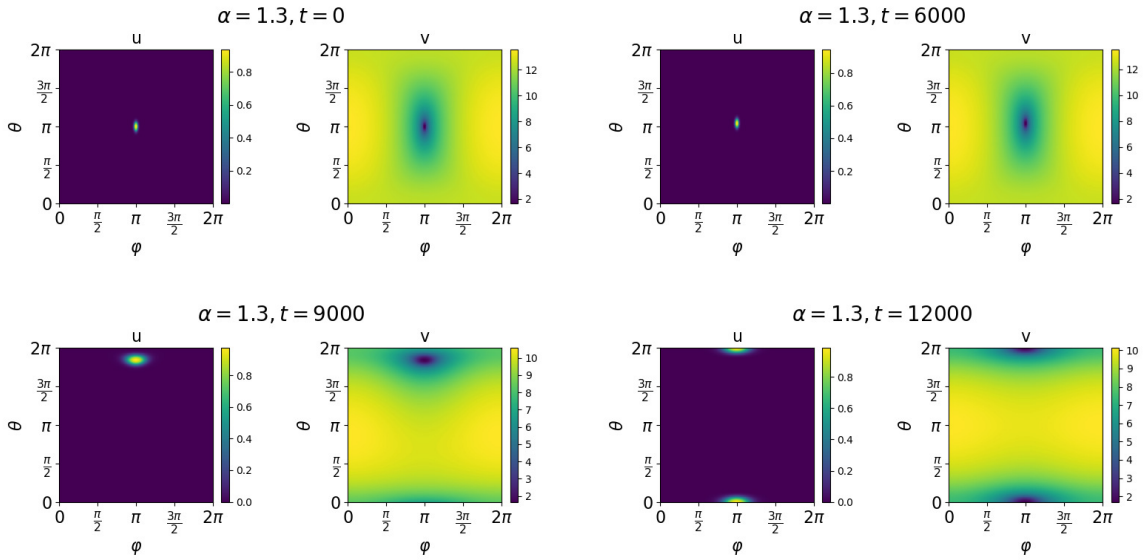

Figure 3.2: Evolution of the BRD model (1.3) from a one-spot initial condition (2.30) and (2.31) centered at $\theta_1 = \pi$ and $\varphi_1 = \pi$ on the torus of $R = 1.3$ and $r = 1.0$, i.e., $\alpha = 1.3$. The numerical parameters are the same as Figure 3.1. The unstable spot starts moving toward the stable spot at $\theta = 0$ as expected.

3.3 Two spots

Suppose that two spots are centered at (θ_1, φ_1) and (θ_2, φ_2) on the toroidal surface. Then the source strengths S_1 and $S_2 > 0$ satisfy $S_1 + S_2 = 2\pi RrE$ owing to (2.25). Then, we have the following theorem.

Theorem 3.3.1. Suppose that $0 \le \varphi_2 \le \varphi_1 < 2\pi$. Two spots pattern is an equilibrium only if $\varphi_1 - \varphi_2 = \pi$ or 0. Moreover, $\varphi_1 - \varphi_2 = 0$ is unstable.

Proof. It follows from (2.42) with (A.4) and (A.6) that $\alpha_{1,2}$ is given by

$$\begin{aligned}\alpha_{1,2} &= \frac{S_2}{R - r\cos\theta_1}\frac{\partial \widetilde{G}_2}{\partial \varphi}\bigg|_{(\theta,\varphi)=(\theta_1,\varphi_1)} \\ &= \frac{S_2}{R - r\cos\theta_1}\frac{E_{2,1}\sin(\varphi_1 - \varphi_2)}{(1 - E_{2,1}\cos(\varphi_1 - \varphi_2))^2 + E_{2,1}^2\sin^2(\varphi_1 - \varphi_2)} + \frac{S_2}{R - r\cos\theta_1}\sum_{n=1}^{\infty} w_{2,1,n},\end{aligned} \tag{3.5}$$

where

$$w_{2,1,n} = \frac{\sin(\varphi_1 - \varphi_2)s^n\left(\left(E_{2,1} + E_{2,1}^{-1}\right)(1 + s^{2n}) - 4s^{2n}\cos(\varphi_1 - \varphi_2)\right)}{(1 + s^{2n} - s^n\cos(\varphi_1 - \varphi_2)(E_{2,1} + E_{2,1}^{-1}))^2 + (s^n(E_{2,1} - E_{2,1}^{-1})\sin(\varphi_1 - \varphi_2))^2}$$

with $s = \exp(-2\pi\mathcal{A}) < 1$. Since $(E_{2,1}+E_{2,1}^{-1})(1+s^{2n})-4s^{2n}\cos(\varphi_1 - \varphi_2) \ge 2(1+s^{2n})-4s^{2n} > 0$, we obtain $\alpha_{1,2} = 0$ if and only if $\varphi_1 - \varphi_2 = k\pi$, $k \in \mathbb{Z}$. Similarly, we have $\alpha_{2,2} = 0$ if and only if $\varphi_1 - \varphi_2 = k\pi$, $k \in \mathbb{Z}$. Under the supposition that $0 \le \varphi_2 \le \varphi_1 < 2\pi$, we have $\varphi_1 - \varphi_2 = 0$ or π. The linear stability of $\varphi_1 = \varphi_2 = \pi$ is unstable. Indeed, with a small perturbation to

the spot centers at $(\theta_1, \theta_2, \varphi_1 = \Delta\varphi, \varphi_2 = -\Delta\varphi)$ where $\Delta\varphi > 0$, by (3.5), we have $\alpha_{1,2} > 0$ and $\alpha_{2,2} < 0$. Hence, the two spots thus tend to $\varphi_1 - \varphi_2 = \pi$, which means $\varphi_1 - \varphi_2 = 0$ is unstable. □

3.4 The N-ring configuration

Let us consider a ring configuration of N spots at $\theta_j = \vartheta_N$ and $\varphi_j = (2j-1)\pi/N$ on the toroidal surface for $j = 1, \ldots, N$, which is called the N-ring at ϑ_N. Then the strengths of the N spots become identical according to (2.29) and are set as $S_j = S_c = \frac{2\pi rRE}{N}$, which means that the existence of the N-ring is independent of the choice of the reaction terms F^u and F^v. It follows from (2.42) with (A.4) and (A.6) that we have

$$\alpha_{j,2} = \frac{S_c}{R - r\cos\theta_j} \sum_{\substack{i=1 \\ i\neq j}}^{N} \left(\frac{\partial \log \left| 1 - \frac{\zeta(\theta_j,\varphi)}{\zeta(\theta_i,\varphi_i)} \right|}{\partial \varphi} \bigg|_{\varphi=\varphi_j} + \frac{\partial \log W_i(\theta_j,\varphi)}{\partial \varphi} \bigg|_{\varphi=\varphi_j} \right) = 0. \tag{3.6}$$

From (2.42), we have

$$\begin{aligned} \alpha_{j,1} =& \frac{S_c}{r} \sum_{\substack{i=1 \\ i\neq j}}^{N} \left(\frac{\partial \log \left| 1 - \frac{\zeta(\theta,\varphi_j)}{\zeta(\theta_i,\varphi_i)} \right|}{\partial \theta} \bigg|_{\theta=\theta_j} + \frac{\partial \log W_i(\theta,\varphi_j)}{\partial \theta} \bigg|_{\theta=\theta_j} + Q_i'(\theta_j) \right) \\ &+ \frac{S_c}{r} \left(Q_j'(\theta_j) - \frac{1 + \sin\theta_j}{2(\alpha - \cos\theta_j)} \right). \end{aligned}$$

From (A.3) and (A.5) with $\theta_i = \theta_j$, we obtain

$$\frac{\partial \log W_i(\theta,\varphi_j)}{\partial \theta} \bigg|_{\theta=\theta_j} = 0, \qquad \frac{\partial \log \left| 1 - \frac{\zeta(\theta,\varphi_j)}{\zeta(\theta_i,\varphi_i)} \right|}{\partial \theta} \bigg|_{\theta=\theta_j} = -\frac{1}{2(\alpha - \cos\theta_j)}.$$

Substituting $\theta_j = \vartheta$, we have

$$\begin{aligned} \alpha_{j,1}(\vartheta) &= \frac{S_c}{r} \left(N \left(Q_1'(\vartheta) - \frac{1}{2(\alpha - \cos\vartheta)} \right) - \frac{\sin\vartheta}{2(\alpha - \cos\vartheta)} \right) \\ &= \frac{S_c}{r} \frac{1}{\alpha - \cos\vartheta} \left(-\frac{N}{2\pi\alpha}(\alpha\vartheta - \sin\vartheta) - \frac{N}{2\pi\mathcal{A}} K(\vartheta) - \frac{1}{2}\sin\vartheta \right). \end{aligned}$$

As shown in Theorem 3.1.1, we have $\alpha_{j,1} = 0$ for $j = 1, 2, \ldots, N$, when $\vartheta = 0$ or π. Hence, the N-ring at the innermost/outermost locations of the torus becomes an equilibrium state of N spots for any $\alpha > 1$. For $\vartheta \neq 0, \pi$, it is sufficient to consider the existence of equilibrium N-ring at $\vartheta \in (0, \pi)$ by symmetry. We thus have the following theorem.

Theorem 3.4.1. The N-rings at $\vartheta_N = 0$ and π are equilibria for any $\alpha > 1$. For $N \geq 2$, there are $\alpha_m(N)$ and $\alpha_M(N)$ with $1 < \alpha_m(N) < \alpha_M(N)$ for which the following is satisfied. For $\alpha \in (\alpha_m(N), \alpha_M(N))$, there exists a unique $\vartheta_N(\alpha) \in (0, \pi)$ such that the N-ring at $\vartheta_N(\alpha)$ becomes an equilibrium. Moreover, $\lim_{\alpha \searrow \alpha_m(N)} \vartheta_N(\alpha) = \pi$ and $\lim_{\alpha \nearrow \alpha_M(N)} \vartheta_N(\alpha) = 0$.

Proof. Let us define $\beta_N(\theta) = -\frac{N}{2\pi\alpha}(\alpha\theta - \sin\theta) - \frac{N}{2\pi\mathcal{A}}K(\theta) - \frac{1}{2}\sin\theta$. Owing to $\frac{1}{\alpha-\cos\theta} \neq 0$ for $\alpha > 1$, $\alpha_{j,1}(\theta) = 0$ is equivalent to $\beta_N(\theta) = 0$. Owing to

$$\beta_N'(\theta) = \frac{1}{\alpha - \cos\theta}\left(-\frac{N}{2\pi\alpha}(\alpha - \cos\theta)^2 + \frac{N}{2\pi\mathcal{A}} - \frac{1}{2}\cos\theta(\alpha - \cos\theta)\right),$$

we introduce $m_N(x,\alpha) = -\frac{N}{2\pi\alpha}(\alpha - x)^2 + \frac{N}{2\pi\mathcal{A}} - \frac{1}{2}x(\alpha - x)$ by the change of variable, $x = \cos\theta$. Then $m_N(x,\alpha) = 0$ becomes a quadratic equation with respect to x, whose discriminant $\mathcal{D}(N,\alpha)$ is given by

$$\mathcal{D}(N,\alpha) = \left(\frac{N}{\pi} - \frac{1}{2}\alpha\right)^2 - \frac{N}{\pi}\left(1 - \frac{N}{\pi\alpha}\right)\left(\frac{1}{\mathcal{A}} - \alpha\right) \tag{3.7}$$

$$= \frac{1}{4}\alpha^2 - \left(1 - \frac{N}{\pi\alpha}\right)\frac{N}{\pi\mathcal{A}}. \tag{3.8}$$

When $\alpha > \frac{N}{\pi}$, it follows from (3.7) that $\mathcal{D}(N,\alpha) > 0$ owing to $\frac{1}{\mathcal{A}} < \alpha$. On the other hand, for $\alpha \leq \frac{N}{\pi}$, (3.8) yields $\mathcal{D}(N,\alpha) > 0$. Hence, $m_N(x) = 0$ has two real roots, and so does $\beta_N'(\theta) = 0$ for $\theta \in [0,\pi]$ owing to $\alpha - \cos\theta \in [\alpha - 1, \alpha + 1]$. Hence, it follows from $\beta_N(0) = \beta_N(\pi) = 0$ that $\beta_N(\theta) = 0$ has one unique solution $\vartheta_N(\alpha) \in (0,\pi)$ if and only if $\beta_N'(0)\beta_N'(\pi) > 0$. This condition is confirmed by checking $m_N(-1,\alpha)m_N(1,\alpha) > 0$ owing to $\alpha - \cos\theta > 0$. Since

$$m_N(1,\alpha) = -\frac{N}{2\pi\alpha}(\alpha-1)^2 + \frac{N}{2\pi\mathcal{A}} - \frac{1}{2}(\alpha-1), \quad m_N(-1,\alpha) = -\frac{N}{2\pi\alpha}(\alpha+1)^2 + \frac{N}{2\pi\mathcal{A}} + \frac{1}{2}(\alpha+1),$$

we have

$$\frac{\mathrm{d}}{\mathrm{d}\alpha}m_N(1,\alpha) = -\frac{N}{2\pi} + \frac{N}{2\pi\alpha^2} + \frac{N\alpha}{2\pi\sqrt{\alpha^2-1}} - \frac{1}{2},$$
$$\frac{\mathrm{d}}{\mathrm{d}\alpha}m_N(-1,\alpha) = -\frac{N}{2\pi} + \frac{N}{2\pi\alpha^2} + \frac{N\alpha}{2\pi\sqrt{\alpha^2-1}} + \frac{1}{2}$$

and

$$\frac{\mathrm{d}^2}{\mathrm{d}\alpha^2}m_N(1,\alpha) = \frac{\mathrm{d}^2}{\mathrm{d}\alpha^2}m_N(-1,\alpha) = \frac{N}{2\pi}\left(-\frac{2}{\alpha^3} - (\alpha^2-1)^{-\frac{3}{2}}\right) < 0.$$

On the other hand, it follows from

$$\lim_{\alpha\searrow 1} m_N(1,\alpha) = 0, \quad \lim_{\alpha\to\infty} m_N(1,\alpha) = -\infty,$$
$$\lim_{\alpha\searrow 1} \frac{\mathrm{d}}{\mathrm{d}\alpha}m_N(1,\alpha) = \infty, \quad \lim_{\alpha\to\infty} \frac{\mathrm{d}}{\mathrm{d}\alpha}m_N(1,\alpha) = -\frac{1}{2}$$

that there exists a unique $\alpha_M(N) > 1$ such that $m_N(1,\alpha) > 0$ for $1 < \alpha < \alpha_M(N)$, while $m_N(1,\alpha) < 0$ for $\alpha > \alpha_M(N)$. Similarly, since

$$\lim_{\alpha\searrow 1} m_N(-1,\alpha) = -\frac{2N}{\pi} + 1 < 0, \quad \lim_{\alpha\to\infty} m_N(-1,\alpha) = \infty,$$
$$\lim_{\alpha\searrow 1} \frac{\mathrm{d}}{\mathrm{d}\alpha}m_N(-1,\alpha) = \infty, \quad \lim_{\alpha\to\infty} \frac{\mathrm{d}}{\mathrm{d}\alpha}m_N(-1,\alpha) = \frac{1}{2},$$

there exists a unique $\alpha_m(N) > 1$ such that $m_N(-1,\alpha) < 0$ for $1 < \alpha < \alpha_m(N)$, and $m_N(-1,\alpha) > 0$ for $\alpha > \alpha_m(N)$.

With $\alpha_0 = \frac{2N}{\pi} > 1$ for $N \geq 2$, we have

$$\begin{aligned} m_N(1,\alpha_0) &= -\frac{N}{2\pi\alpha_0}(\alpha_0-1)^2 + \frac{N\sqrt{\alpha_0^2-1}}{2\pi} - \frac{1}{2}(\alpha_0-1) \\ &= \frac{\pi\alpha_0}{2}\left(-\frac{1}{2\pi\alpha_0}(\alpha_0-1)^2 + \frac{1}{2\pi}\sqrt{\alpha_0^2-1}\right) - \frac{1}{2}(\alpha_0-1) \\ &= -\frac{1}{4}(\alpha_0-1)^2 + \frac{\alpha_0}{4}\sqrt{\alpha_0^2-1} - \frac{1}{2}(\alpha_0-1) = \frac{1}{4}\left(-(\alpha_0^2-1) + \alpha_0\sqrt{\alpha_0^2-1}\right) > 0. \end{aligned}$$

Recalling that $m_N(1,\alpha) > 0$ for $1 < \alpha < \alpha_M(N)$, we have $\alpha_0 = \frac{2N}{\pi} < \alpha_M(N)$. On the other hand, let us notice $m_N(-1,\alpha_M(N)) = m_N(-1,\alpha_M(N)) - m_N(1,\alpha_M(N)) = \alpha_M(N) - \frac{2N}{\pi} > 0$. We thus have $\alpha_m(N) < \alpha_M(N)$, since $m_N(-1,\alpha)$ is monotone increasing. Moreover, by $m_N(-1,\alpha) = 0$ at $\alpha = \alpha_m(N)$ and $m_N(1,\alpha) = 0$ at $\alpha = \alpha_M(N)$, it is easy to see that $\lim_{\alpha\searrow\alpha_m(N)} \vartheta_N(\alpha) = \pi$ and $\lim_{\alpha\nearrow\alpha_M(N)} \vartheta_N(\alpha) = 0$ owing to the one-to-one correspondence of $x = \cos\theta$ for $\theta \in [0,\pi]$. □

We observe the linear stability of the N-ring configuration of the BRD model (1.3) for $N = 2,\ldots,6$ on the torus of $(R,r) = (\frac{\alpha}{2},\frac{1}{2})$ with $\alpha = [1.01, 10]$ by numerical means. The parameters are $f = 0.7$, $\epsilon = 0.05$, $S_c = 1.5$, and $A = \frac{NS_c}{2\pi Rr}$. We compute the eigenvalues of the linearized matrix of $\frac{\mathrm{d}\theta_j}{\mathrm{d}\sigma}$ and $\frac{\mathrm{d}\varphi_j}{\mathrm{d}\sigma}$ (2.52) for $j = 1,2,\ldots,N$ at the equilibria, thereby observing the principal eigenvalue, say λ_{max}. We note that 0 is always an eigenvalue of this equilibrium originated from the invariance of the infinitesimal translation of the torus in the φ direction. Figure 3.3(a) shows the real part of the principal eigenvalue, indicating that there exists $\alpha_s(N)$ such that the N-ring at $\vartheta = 0$ is neutrally stable for $\alpha > \alpha_s(N)$, and it is unstable otherwise. Figure 3.3(b) shows that the N-ring at $\vartheta = \pi$ is always unstable. The real part of the principal eigenvalue $\lambda_{max}(\alpha)$ for the N-ring at $\vartheta_N(\alpha) \in (0,\pi)$ with $N = 2,\ldots,6$ in the range of $\alpha \in (\alpha_m(N), \alpha_M(N))$ is shown in Figure 3.3(c). This indicates that it is unstable. Let us compare the result with that of the one-spot case in the previous section, which is equivalent to the 1-ring. According to theorem 3.2.1, we find that the stable 1-ring at $\vartheta_1(\alpha) = \vartheta_s(\alpha)$ exists for $1 < \alpha_M(1) = \alpha_s(1) = \alpha_s$, although $\alpha_m(1)$ is not defined. On the other hand, Figure 3.3 indicates that $\alpha_m(N) < \alpha_M(N) < \alpha_s(N)$ for $N \geq 2$. Moreover, the stability of the 1-ring at $\vartheta_1(\alpha)$ is stable, whereas the N-ring at $\vartheta_N(\alpha)$ for $N \geq 2$ is unstable.

We solve BRD model (1.3) numerically for the localized 5-ring initial condition (2.30) and (2.31) on the torus of $(R,r) = (1.7, 0.5)$, $(R,r) = (2.1, 0.5)$, and $(R,r) = (2.2, 0.5)$ with $f = 0.7$, $\epsilon = 0.05$, $S_c = 1.5$ and $A = \frac{NS_c}{2\pi Rr}$. After solving the equations until the localized spots are formed, we add a 2% random perturbation to the solution. For the 5-ring, the parameters are $\alpha_m(5) \approx 2.990$, $\alpha_M(5) \approx 3.495$, $\alpha_s(5) \approx 4.296$. Let us remember that the 5-ring at $\vartheta = \pi$ is always unstable and that at $\vartheta = 0$ is stable for $\alpha = 4.4 > \alpha_s(5)$. As a matter of fact, Figure 3.4 shows that the spots centered at $\vartheta = \pi$ are moving toward those at $\vartheta = 0$ after a long-time evolution. On the other hand, since the 5-ring at $\vartheta = 0$ becomes unstable for $\alpha = 4.2 < \alpha_s(5)$, the spots centered at $\vartheta = 0$ initially are moving toward another quasi-equilibrium solution consisting of nonsymmetric spot centers after the perturbation as shown in Figure 3.5. When $\alpha = 3.4 \in (\alpha_m(5), \alpha_M(5))$ where an unstable 5-ring at $\vartheta_5(\alpha)$ exists, we confirm in fig. 3.6 that the unstable 5-ring at $\vartheta_5(\alpha)$ moves toward another quasi-equilibrium state.

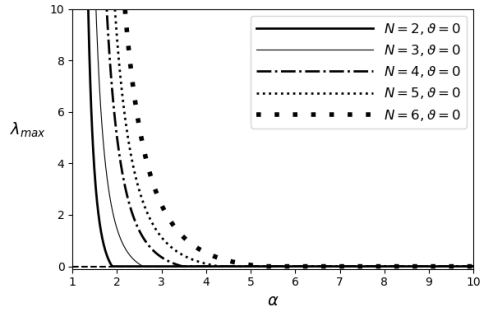

(a)

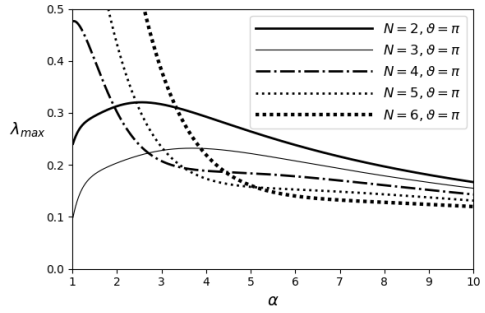

(b)

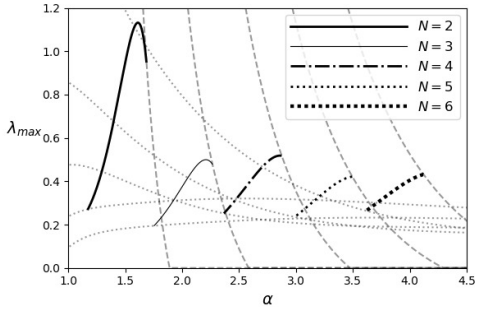

(c)

Figure 3.3: The real part of the principal eigenvalue $\lambda_{max}(\alpha)$ for the N-ring for $N = 2, \ldots, 6$ on the torus of $(R, r) = (\frac{\alpha}{2}, \frac{1}{2})$, $\alpha \in [1.01, 10]$. The numerical parameters are $f = 0.7$, $\epsilon = 0.05$, $S_c = 1.5$, and $A = \frac{NS_c}{2\pi Rr}$. (a) $\lambda_{max}(\alpha)$ for the N-ring at $\vartheta = 0$. (b) $\lambda_{max}(\alpha)$ for the N-ring at $\vartheta = \pi$. (c) Each curve is the plot of $\lambda_{max}(\alpha)$ for the N-ring at $\vartheta_N(\alpha) \in (0, \pi)$ in the range of $\alpha \in (\alpha_m(N), \alpha_M(N))$. The plots of $\lambda_{max}(\alpha)$ in Figure 3.3(a) and (b) are shown for reference.

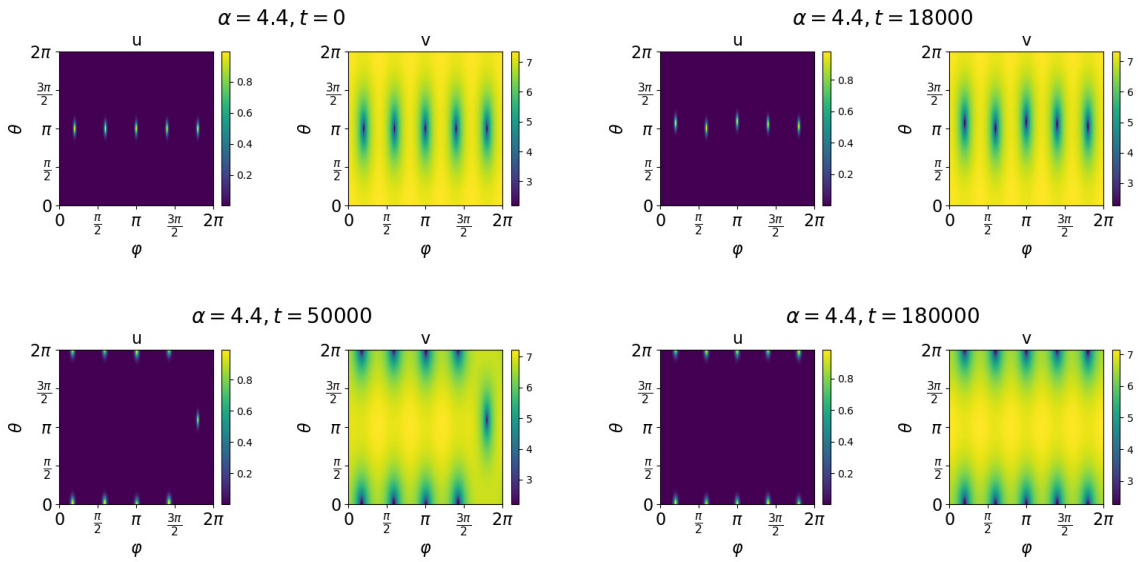

Figure 3.4: Evolution of the BRD model (1.3) from the 5-ring initial condition (2.30) and (2.31) centered at $\theta_j = \pi$ and $\varphi_j = \frac{(2j-1)\pi}{5}, j = 1, 2, \ldots, 5$ on the torus of $R = 2.2$ and $r = 0.5$. The numerical parameters are $f = 0.7$, $\epsilon = 0.05$, $S_c = 1.5$, $A = \frac{5S_c}{2\pi Rr}$. The spots approach a quasi-stationary state having spots at $\theta_j = 0$, $j = 1, 2, \ldots, 5$.

3.5 The two N-rings configuration

We consider the quasi-equilibrium state of two kinds of two N-rings, where N localized spots are equally spaced along latitudinal line $\theta_j = \vartheta_1$ with strength S_1 for $j = 1, 3, \ldots, 2N-1$ and the other N localized spots are equally spaced along latitudinal line $\theta_j = \vartheta_2$ with strength S_2 for $j = 2, 4, \ldots, 2N$. Two special configuration are considered. The first case is called *untwisted* two N-rings satisfying $\varphi_{2j-1} = \varphi_{2j} = (2j-2)\pi/N$ for $j = 1, 2, \ldots, N$. The second case is called *twisted* two N-rings $\varphi_{2j-1} = (2j-2)\pi/N$ and $\varphi_{2j} = (2j-1)\pi/N$ for $j = 1, 2, \ldots, N$.

3.5.1 Two N-rings at $(\vartheta_1, \vartheta_2) = (0, \pi)$

Let us consider untwisted and twisted two N-rings at $(\vartheta_1, \vartheta_2) = (0, \pi)$ on the toroidal surface. As shown in Theorem 3.1.1, in both cases, we have $\alpha_{j,1} = 0$, $j = 1, 2, \ldots, 2N$. It follows from (2.42) with (A.4) and (A.6) that, by the symmetry of two N-rings, in both cases, we obtain

$$\begin{aligned}\alpha_{2j-1,2} =& \frac{S_1}{R - r\cos\theta_{2j-1}} \sum_{\substack{i=1 \\ i\neq j}}^{N} \left(\frac{\partial \log \left| 1 - \frac{\zeta(\theta_{2j-1},\varphi)}{\zeta(\theta_{2i-1},\varphi_{2i-1})} \right|}{\partial \varphi} \bigg|_{\varphi=\varphi_{2j-1}} + \frac{\partial \log W_{2i-1}(\theta_{2j-1},\varphi)}{\partial \varphi} \bigg|_{\varphi=\varphi_{2j-1}} \right) \\ &+ \frac{S_2}{R - r\cos\theta_{2j}} \sum_{i=1}^{N} \left(\frac{\partial \log \left| 1 - \frac{\zeta(\theta_{2j-1},\varphi)}{\zeta(\theta_{2i},\varphi_{2i})} \right|}{\partial \varphi} \bigg|_{\varphi=\varphi_{2j-1}} + \frac{\partial \log W_{2i}(\theta_{2j-1},\varphi)}{\partial \varphi} \bigg|_{\varphi=\varphi_{2j-1}} \right) = 0.\end{aligned}$$

Similarly, we can obtain $\alpha_{2j,2} = 0$ for $j = 1, 2, \ldots, N$. Hence, if there exist S_j, $j = 1, 2, \ldots, 2N$ satisfying (2.29), the untwisted and twisted two N-rings at $(\vartheta_1, \vartheta_2) = (0, \pi)$ are equilibria.

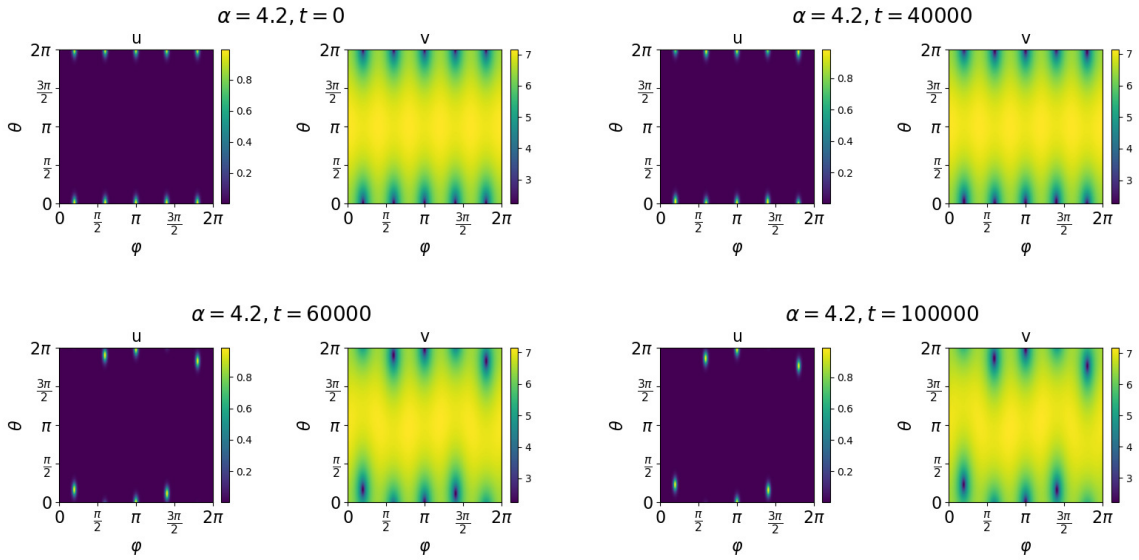

Figure 3.5: Evolution of the BRD model (1.3) from the 5-ring initial condition (2.30) and (2.31) centered at $\theta_j = 0$ and $\varphi_j = \frac{(2j-1)\pi}{5}$, $j = 1, 2, \ldots, 5$ on the torus of $R = 2.1$ and $r = 0.5$. The numerical parameters are the same as Figure 3.4. The 5-ring at $\vartheta = 0$ starts moving toward another equilibrium point, since it is unstable.

When the two N-rings are not on the symmetric latitude, S_1 and S_2 no longer have the same value in general, which makes the situation more complicated. As an example, we compute the strengths of two 1-ring, i.e. $(\theta_1, \varphi_1) = (0, 0)$ and $(\theta_2, \varphi_2) = (\pi, \pi)$ for the BRD model (1.3) on the torus of $(R, r) = (\frac{\alpha}{2}, \frac{1}{2})$ for $\alpha \in [1.01, 2]$ numerically with the parameters $f = 0.7$ $\epsilon = 0.05$ and $A = \frac{3}{2\pi Rr}$, i.e., $S_1 + S_2 = 3$. Figure 3.7(a) shows that the strength $S_1(\alpha)$ is not unique for $\alpha > \alpha_4 \approx 1.021$. For each value of $S_1(\alpha)$ on this curve, the largest real part of the eigenvalue λ_{max} is shown in Figure 3.7(b). The case 1 is unstable for $\alpha \in [1.1, 2]$. When $\alpha = \alpha_4 \approx 1.021$, unstable case 2 and case 3 appear. As α increase, case 2 and case 3 change their stabilities. Then, as α increase, these two cases become unstable again.

3.5.2 Two N-rings at $(\vartheta_1, \vartheta_2) = (\vartheta_N, 2\pi - \vartheta_N)$

Let us consider untwisted and twisted two N-rings at $(\vartheta_1, \vartheta_2) = (\vartheta_N, 2\pi - \vartheta_N)$ on the toroidal surface for $\vartheta_N \in (0, \pi)$. In both cases, the strengths of the N spots become identical according to (2.29). Hence, they are set as $S_j = S_c = \frac{\pi r R E}{N}$ for $j = 1, 2, \ldots, 2N$, which means that the existence of the untwisted and twisted two N-rings at $(\vartheta_1, \vartheta_2) = (\vartheta_N, 2\pi - \vartheta_N)$ are independent of the choice of the reaction terms F^u and F^v. As similar to the untwisted and twisted two N-rings $(\vartheta_1, \vartheta_2) = (0, \pi)$, we obtain $\alpha_{j,2} = 0$ for $j = 1, 2, \ldots, 2N$ in the untwisted and twisted

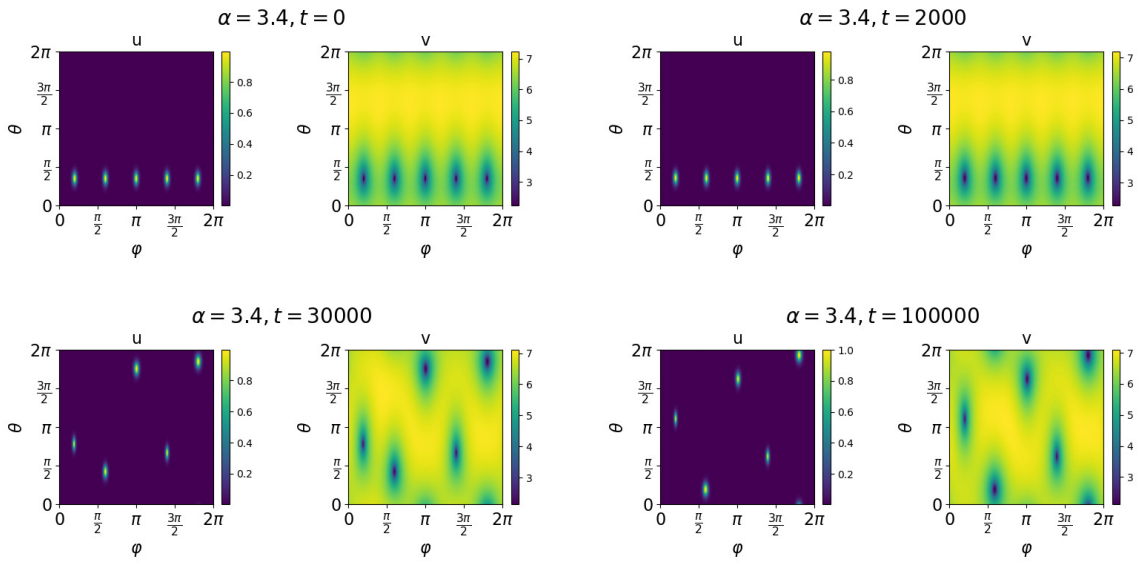

Figure 3.6: Evolution of the BRD model (1.3) from the 5-ring initial condition (2.30) and (2.31) centered at $\theta_j = 1.1$ and $\varphi_j = \frac{(2j-1)\pi}{5}$, $j = 1, 2, \ldots, 5$ on the torus of $R = 1.7$ and $r = 0.5$. The numerical parameters are the same as Figure 3.4. At $t = 2000$, the solution is close to the 5-ring at $\vartheta_5(3.4) \in (0, \pi)$. The unstable 5-ring starts moving toward another equilibrium state since it is unstable.

two N-rings $(\vartheta_1, \vartheta_2) = (\vartheta_N, 2\pi - \vartheta_N)$, by the symmetry of two N-rings. From (2.42), we have

$$\begin{aligned}\alpha_{2j-1,1} =& \frac{S_c}{r} \sum_{\substack{i=1 \\ i \neq j}}^{N} \left(\frac{\partial \log \left| 1 - \frac{\zeta(\theta, \varphi_{2j-1})}{\zeta(\theta_{2i-1}, \varphi_{2i-1})} \right|}{\partial \theta} \bigg|_{\theta=\theta_{2j-1}} + \frac{\partial \log W_{2i-1}(\theta, \varphi_{2j-1})}{\partial \theta} \bigg|_{\theta=\theta_{2j-1}} + Q'_{2i-1}(\theta_{2j-1}) \right) \\ &+ \frac{S_c}{r} \left(Q'_{2j-1}(\theta_{2j-1}) - \frac{1 + \sin \theta_{2j-1}}{2(\alpha - \cos \theta_{2j-1})} \right) \\ &+ \frac{S_c}{r} \sum_{i=1}^{N} \left(\frac{\partial \log \left| 1 - \frac{\zeta(\theta, \varphi_{2j-1})}{\zeta(\theta_{2i}, \varphi_{2i})} \right|}{\partial \theta} \bigg|_{\theta=\theta_{2j-1}} + \frac{\partial \log W_{2i}(\theta, \varphi_{2j-1})}{\partial \theta} \bigg|_{\theta=\theta_{2j-1}} + Q'_{2i}(\theta_{2j-1}) \right).\end{aligned}$$

By the symmetry of two N-rings, we have $\alpha_{1,1} = \alpha_{3,1} = \cdots = \alpha_{2N-1,1} = -\alpha_{2,1} = -\alpha_{4,1} = \cdots = -\alpha_{2N,1}$. Then, we first consider the existence of the untwisted two N-rings at $(\vartheta_1, \vartheta_2) = (\vartheta_N(\alpha), 2\pi - \vartheta_N(\alpha))$ that is in a quasi-stationary state. Let $E_\theta = \exp\left(\int_\theta^{2\pi - \theta} \frac{\mathrm{d}\eta}{\alpha - \cos \eta} \right)$. We then obtain $E_\theta \in (1, s^{-1})$ and $E_\theta^{-1} \in (s, 1)$ for $\theta \in (0, \pi)$. Owing to $E_\theta \nearrow s^{-1}$ as $\theta \searrow 0$, it

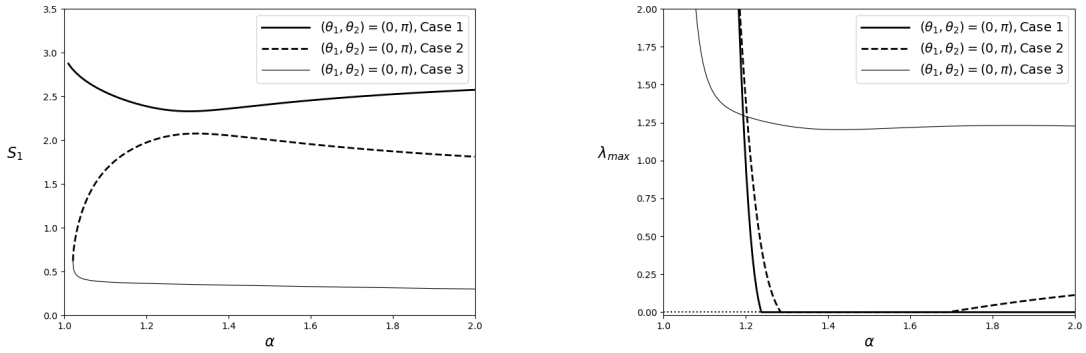

(a) (b)

Figure 3.7: (a) The strength $S_1(\alpha)$ for the spot $(\theta_1, \varphi_1) = (0, 0)$ of the twisted two 1-rings $(\vartheta_1, \vartheta_2) = (0, \pi)$ of the BRD model (1.3) on the torus of $(R, r) = (\frac{\alpha}{2}, \frac{1}{2})$ for $\alpha \in [1.01, 2]$. They are obtained by solving (2.29) numerically with the parameters $f = 0.7$ $\epsilon = 0.05$ and $A = \frac{3}{2\pi Rr}$, satisfying $S_1(\alpha) + S_2(\alpha) = 3$. When $\alpha > \alpha_4 \approx 1.021$, we have three solutions. (b) The real part of the principal eigenvalue λ_{max} corresponding to the strength in Figure 3.7(a).

follows from (A.3) and $\varphi_{2j-1} = \varphi_{2j}$ that

$$h_{2j,2j-1,1} = \lim_{\theta_{2j-1} \searrow 0} \left. \frac{\partial \log \left| \left(1 - e^{-2\pi\mathcal{A}\frac{\zeta(\theta,\varphi_{2j-1})}{\zeta(\theta_{2j},\varphi_{2j})}}\right) \left(1 - e^{-2\pi\mathcal{A}\left(\frac{\zeta(\theta,\varphi_{2j-1})}{\zeta(\theta_{2j},\varphi_{2j})}\right)^{-1}}\right) \right|}{\partial\theta} \right|_{\theta=\theta_{2j-1}}$$

$$= \lim_{\theta_{2j-1} \searrow 0} \frac{1}{\alpha - \cos\theta_{2j-1}} \frac{-s\left(E_{\theta_{2j-1}}^{-1} - E_{\theta_{2j-1}}\right)}{1 + s^2 - s\left(E_{\theta_{2j-1}} + E_{\theta_{2j-1}}^{-1}\right)} = +\infty.$$

From (A.3), we have

$$\lim_{n\to\infty} \frac{h_{i,j,n+1}}{h_{i,j,n}} = \lim_{n\to\infty} \frac{-(1+s^{2n+2})s^{n+1}\cos(\varphi_j - \varphi_i) + s^{2n+2}(E_{i,j}^{-1} + E_{i,j})}{-(1+s^{2n})s^n\cos(\varphi_j - \varphi_i) + s^{2n}(E_{i,j}^{-1} + E_{i,j})} = s < 1.$$

Hence, the other terms in $\alpha_{2j-1,1}$ remain bounded as $\theta \searrow 0$, we obtain $\alpha_{2j-1,1} \to +\infty$. Similarly, since $E_\theta \searrow 1$ as $\theta \nearrow \pi$, from (A.5), we obtain

$$\lim_{\theta_{2j-1} \nearrow \pi} \left. \frac{\partial \log \left| 1 - \frac{\zeta(\theta,\varphi_{2j-1})}{\zeta(\theta_{2j},\varphi_{2j})} \right|}{\partial\theta} \right|_{\theta=\theta_{2j-1}} = \lim_{\theta_{2j-1} \nearrow \pi} \frac{1}{\alpha - \cos\theta_{2j-1}} \frac{E_{\theta_{2j-1}}}{1 - E_{\theta_{2j-1}}} = -\infty$$

and the other terms in $\alpha_{2j-1,1}$ are bounded. Hence, $\lim_{\theta \nearrow \pi} \alpha_{2j-1,1} \to -\infty$. Since $\alpha_{j,1}$ is continuous function of ϑ_N, there exist $\vartheta_N(\alpha) \in (0, \pi)$ such that $\alpha_{2j-1,1} = \alpha_{2j,1} = 0$ for $j = 1, 2, \ldots, N$, for any $\alpha > 1$.

Next, we consider the existence of the twisted two N-rings at $(\vartheta_1, \vartheta_2) = (\vartheta_N(\alpha), 2\pi - \vartheta_N(\alpha))$ that is in a quasi-stationary state. When $\vartheta_N = 0$ or π, the twisted two N-rings at $(\vartheta_1, \vartheta_2) = (\vartheta_N(\alpha), 2\pi - \vartheta_N(\alpha))$ is a $2N$-ring with $\vartheta_{2N} = 0$ or π. The twisted two N-rings at

$(\vartheta_1, \vartheta_2) = (\vartheta_N(\alpha), 2\pi - \vartheta_N(\alpha))$ is a equilibrium if and only if $\alpha_{1,1} = 0$. Hence, it is sufficient to consider the equation

$$\begin{aligned}\alpha_{1,1}(\theta) &= \frac{S_c}{r}\frac{1}{\alpha - \cos\theta}\left((\alpha - \cos\theta)Q_1'(\theta) - \frac{1}{2}(1+\sin\theta) + \sum_{i=2}^{2N}\left(t_{i,1} + h_{i,1} + (\alpha - \cos\theta)Q_i'(\theta)\right)\right)\\ &= 0,\end{aligned}$$

where $t_i = (\alpha - \cos\theta)t_{i,1}$ and $h_i = (\alpha - \cos\theta)h_{i,1}$. Here $\theta_1 = \theta_3 = \cdots = \theta_{2N-1} = \theta$, $\theta_2 = \theta_4 = \cdots = \theta_{2N} = 2\pi - \theta$ and $t_{i,1}$, $h_{i,1}$ are defined in (A.3) and (A.5). When $\theta_i = \theta$, we have $t_i = -\frac{1}{2}$ and $h_i = 0$. Hence, from (2.22), (A.3) and (A.5), we obtain

$$\begin{aligned}\alpha_{1,1}(\theta) =& \frac{S_c}{r}\frac{1}{\alpha - \cos\theta}\left(-\frac{2N}{2\pi\alpha}(\alpha\theta - \sin\theta) - \frac{1}{2}(1+\sin\theta) + 2N - \frac{1}{2}(N-1)\right)\\ &+ \frac{S_c}{r}\frac{1}{\alpha - \cos\theta}\sum_{i=1}^{N}(t_{2i,1} + h_{2i,1})\\ =& \frac{S_c}{r}\frac{1}{\alpha - \cos\theta}\left(-\frac{N}{\pi\alpha}(\alpha\theta - \sin\theta) - \frac{1}{2}\sin\theta + \frac{3}{2}N + \sum_{i=1}^{N}(t_{2i,1} + h_{2i,1})\right).\end{aligned}$$

Let us here introduce the function $\beta_N(\theta, \alpha)$ by

$$\begin{aligned}&\beta_N(\theta,\alpha) = \frac{\mathrm{d}\alpha_{1,1}(\theta)}{\mathrm{d}\theta}\\ &= \frac{S_c}{r(\alpha - \cos\theta)^2}e_N(\theta,\alpha) + \frac{\mathrm{d}\left(\frac{S_c}{r}\frac{1}{\alpha-\cos\theta}\right)}{\mathrm{d}\theta}\left(-\frac{N}{\pi\alpha}(\alpha\theta - \sin\theta) - \frac{1}{2}\sin\theta + \frac{3}{2}N + \sum_{i=1}^{N}(t_{2j,1} + h_{2j,1})\right),\end{aligned}$$

where

$$\begin{aligned}e_N(\theta,\alpha) =& (\alpha - \cos\theta)\frac{\mathrm{d}}{\mathrm{d}\theta}\left(-\frac{N}{\pi\alpha}(\alpha\theta - \sin\theta) - \frac{1}{2}\sin\theta + \frac{3}{2}N + \sum_{i=1}^{N}(t_{2j,1} + h_{2j,1})\right)\\ =& -\frac{N}{\pi\alpha}(\alpha - \cos\theta)^2 - \frac{1}{2}\cos\theta(\alpha - \cos\theta) + (\alpha - \cos\theta)\frac{\mathrm{d}}{\mathrm{d}\theta}\left(\sum_{i=1}^{N}(t_{2j,1} + h_{2j,1})\right).\end{aligned}$$

Notice that $\alpha_{1,1}(\theta)$ vanishes at $\theta = 0, \pi$, and it is continuous. Hence, if $\beta_N(0,\alpha)\beta_N(\pi,\alpha) > 0$, there must exist $\vartheta_N(\alpha) \in (0,\pi)$ such that $\alpha_{1,1}(\vartheta_N(\alpha)) = 0$. The condition is equivalent to $e_N(0,\alpha)e_N(\pi,\alpha) > 0$ owing to $\beta_N(0,\alpha) = \frac{S_c}{r(\alpha-1)^2}e_N(0,\alpha)$ and $\beta_N(\pi,\alpha) = \frac{S_c}{r(\alpha+1)^2}e_N(\pi,\alpha)$. The plots of $e_{N,0}(\alpha) = e_N(0,\alpha)$ and $e_{N,\pi}(\alpha) = e_N(\pi,\alpha)$ are shown in Figure 3.8 indicating that there exist $\alpha_d(N)$ for $N = 1, \ldots, 5$, such that for $1 < \alpha < \alpha_d(N)$, the twisted two N-rings $(\vartheta_1, \vartheta_2) = (\vartheta_N(\alpha), 2\pi - \vartheta_N(\alpha))$ becomes an quasi-stationary state.

We confirm the existence of two 1-rings by solving the BRD model (1.3) from the initial condition (2.30) and (2.31). The numerical parameters are $\epsilon = 0.05, f = 0.7$, $A = \frac{3}{2\pi Rr}$. The center of the two spots at the initial moment is $(\theta_1, \varphi_1, \theta_2, \varphi_2) = (0, \frac{\pi}{2}, 0, \frac{3\pi}{2})$ with $S_1 = S_2 = 1.5$ on the torus of $(R, r) = (0.925, 0.5)$, i.e. $\alpha = 1.85$. After the localized two spots are formed, we add a 2% random perturbation to check the stability. Figure 3.9 shows that when $\alpha = 1.85 < \alpha_s(2) \approx 1.89$, the 2-ring at $\theta_1 = \theta_2 = 0$ is unstable and moves toward the stable quasi-stationary state the twisted two 1-rings at $(\vartheta_1, \vartheta_2) = (\vartheta_1(1.85), 2\pi - \vartheta_1(1.85))$ as expected. On the other hand, when $\alpha = 1.65 < \alpha_d(1) \approx 1.76$, the twisted two 1-rings

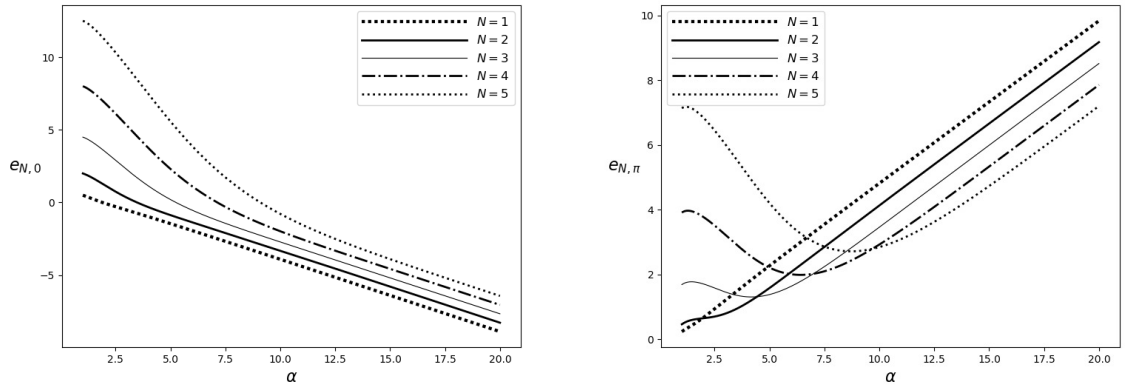

(a) (b)

Figure 3.8: Plots of $e_{N,0}(\alpha) = e_N(0,\alpha)$ and $e_{N,\pi}(\alpha) = e_N(\pi,\alpha)$ for $1.01 \le \alpha \le 20$, showing $e_{N,\pi}(\alpha) > 0$ and $e_{N,0}(\alpha)$ are monotone decreasing.

$(\vartheta_1, \vartheta_2) = (\vartheta_1(1.65), 2\pi - \theta_1(1.65))$ are unstable and moving toward a quasi-stationary state of the twisted two 1-rings at $(\vartheta_1, \vartheta_2) = (\pi, 0)$ after a long-time evolution as shown in Figure 3.10. The center of the two spots of another example at the initial moment is the untwisted two 1-rings at $(\vartheta_1, \vartheta_2) = (\theta_0, 2\pi - \theta_0)$ on the torus of $(R, r) = (0.6, 0.5)$ with $S_1 = S_2 = 1.5$ and $\theta_0 \approx 0.8934$, which is the numerical solution of $\alpha_{1,1}(\theta_0, 2\pi - \theta_0, \pi, \pi) = 0$. The numerical parameters are $f = 0.7$, $\epsilon = 0.05$, $A = \frac{3}{2\pi Rr}$, $\varphi_1 = \frac{\pi}{2}, \varphi_2 = \frac{3\pi}{2}$, $S_1 = S_2 = 1.5$. As shown in Figure 3.11, the two spots are moving towards a stable quasi-stationary state, the twisted two 1-rings at $(\vartheta_1, \vartheta_2) = (\vartheta_c(1.2), 2\pi - \theta_c(1.2))$.

We observe the linear stability of the untwisted and twisted two N-rings configuration of the BRD model (1.3) for $N = 1, \ldots, 5$ on the torus of $(R, r) = (\frac{\alpha}{2}, \frac{1}{2})$ with $\alpha = [1.01, 10]$ by numerical means. The parameters are $\epsilon = 0.05$, $f = 0.7$, $S_c = 1.5$ and $A = \frac{NS_c}{\pi Rr}$. We compute the eigenvalues of the linearized matrix of $\frac{\mathrm{d}\theta_j}{\mathrm{d}\sigma}$ and $\frac{\mathrm{d}\varphi_j}{\mathrm{d}\sigma}$ (2.52) for $j = 1, 2, \ldots, 2N$ at the equilibria, thereby observing the real part of principal eigenvalue, say λ_{max}. Figure 3.12(a) shows the real part of the principal eigenvalue of the untwisted two N-rings at $(\vartheta_1, \vartheta_2) = (\vartheta_N(\alpha), 2\pi - \vartheta_N(\alpha))$, indicating that these cases are unstable for $\alpha > 1$. Figure 3.12(b) shows the real part of the principal eigenvalue of the twisted two N-rings at $(\vartheta_1, \vartheta_2) = (\vartheta_N(\alpha), 2\pi - \vartheta_N(\alpha))$. There exist two unstable peaks for $N > 1$. By the numerical results, there exists $\alpha_e(N)$ such that the twisted two N-rings at $(\vartheta_1, \vartheta_2) = (\vartheta_N(\alpha), 2\pi - \vartheta_N(\alpha))$ only exist when $\alpha \in (1, \alpha_e(N))$. When $\alpha \to \alpha_e(N)$, a supercritical pitchfork bifurcation occurs: the twisted two N-rings $(\vartheta_1, \vartheta_2) = (\vartheta_N(\alpha), 2\pi - \vartheta_N(\alpha))$ vanish and $2N$-ring $\vartheta = 0$ change its stability. The bifurcation diagram of θ_1 with respect to stable equilibria about the second peak of the twisted two 2-rings of the BRD model (1.3) is shown in Figure 3.13 for $\alpha \in [1.5, 5]$ with parameters $\epsilon = 0.05, f = 0.7, S_c = 1.5$. The equilibria in Figure 3.13 are located at $(\varphi_1, \varphi_2, \varphi_3, \varphi_4) = (0, \frac{\pi}{2}, \pi, \frac{3\pi}{2})$. There exist four special twisted two 2-rings equilibria, $(\vartheta_1, \vartheta_2) = (\vartheta_a, \vartheta_b)$, $(\vartheta_b, \vartheta_a)$, $(-\vartheta_a, -\vartheta_b)$ and $(-\vartheta_b, -\vartheta_a)$ where $\vartheta_a(\alpha) \in (0, \pi)$, $\vartheta_b(\alpha) \in (\pi, 2\pi)$ satisfying $2\pi < \vartheta_a(\alpha) + \vartheta_b(\alpha) < 3\pi$. As α increases, there exists a supercritical pitchfork bifurcation such that the twisted two 2-rings $(\vartheta_1, \vartheta_2) = (\vartheta_2, 2\pi - \vartheta_2)$ and $(2\pi - \vartheta_2, \vartheta_2)$ change their stability. By the bifurcation, there appear those four special twisted two 2-rings equilibria appear. As α increases, another supercritical pitchfork bifurcation happens, those four special equilibria vanish and the twisted 2-rings $(\vartheta_1, \vartheta_2) = (0, \pi)$ and $(\pi, 0)$ change

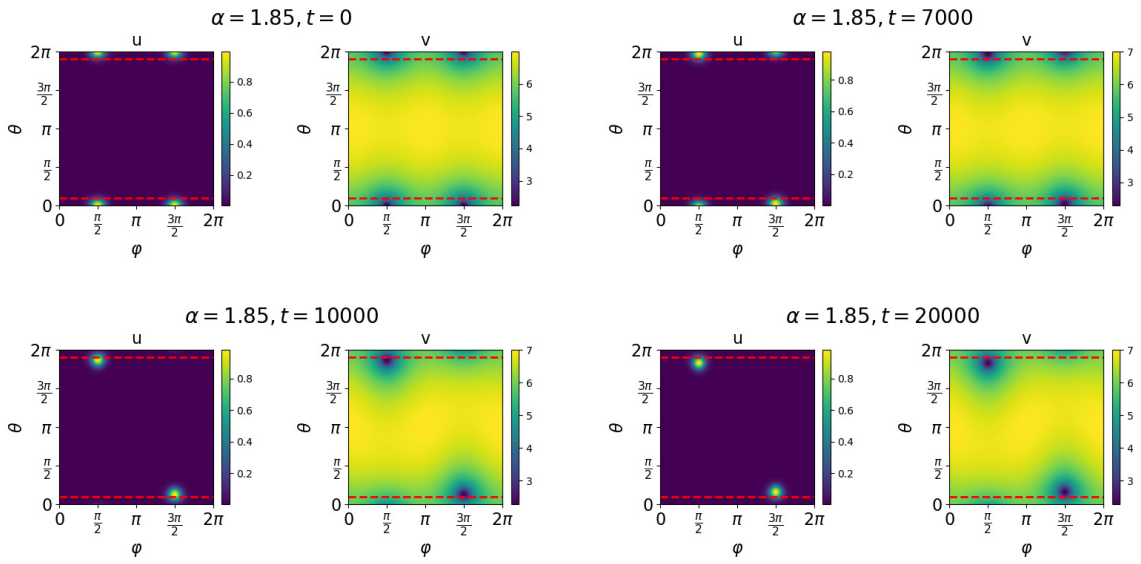

Figure 3.9: Evolution of the BRD model (1.3) from the initial condition (2.30) and (2.31) consisting of two spots centered at $\theta_1 = \theta_2 = 0$ and $\varphi_1 = \frac{\pi}{2}, \varphi_2 = \frac{3\pi}{2}$ on the torus of $R = 0.925$ and $r = 0.5$. The numerical parameters are $f = 0.7$, $\epsilon = 0.05$, $A = \frac{S_c}{\pi Rr}$ and $S_c = 1.5$. The 2-ring starts moving toward $(\theta_1, \theta_2) = (\vartheta_1(1.85), 2\pi - \vartheta_1(1.85))$. The horizontal dotted line represents the reference lines of $\vartheta_1(1.85) \approx 0.3067$ and $2\pi - \vartheta_1(1.85) \approx 5.9765$.

their stability. Then, as α increases, we observe the opposite process: another supercritical pitchfork bifurcation happens, those four special equilibria appear and the twisted 2-rings $(\vartheta_1, \vartheta_2) = (0, \pi)$ and $(\pi, 0)$ change their stability and, as α increases, another supercritical pitchfork bifurcation happens, those four special equilibria vanish and the twisted 2-rings $(\vartheta_1, \vartheta_2) = (\vartheta_2, 2\pi - \vartheta_2)$ and $(2\pi - \vartheta_2, \vartheta_2)$ change their stability. And there exists another supercritical pitchfork bifurcation such that two 2-rings vanish and 4-ring $\theta = 0$ change its stability which bifurcation is $\alpha_s(2N)$ introduced in Section 3.4. By our numerical results, we obtain the similar four special equilibria and supercritical pitchfork bifurcations in the second peak when $N = 3, 4, 5$ and first peak when $N = 1$ in Figure 3.12(b). To confirm the linear stability of second peak, we solve the BRD model (1.3) numerically from the twisted two 2-rings at $(\vartheta_1, \vartheta_2) = (\vartheta_2(2.5), 2\pi - \vartheta_2(2.5))$ on the torus of $(R, r) = (1.25, 0.5)$. The numerical parameters are given by $\epsilon = 0.05$, $f = 0.7$, $S_c = 1.5$, $A = \frac{2S_c}{\pi Rr}$. After computing the solution up to $t = 1000$ when the localized spot is formed, we add a 2% random perturbation to the solution. Figure 3.14 shows that the these two 2-rings are moving toward the twisted two 2-rings at $(\vartheta_1, \vartheta_2) = (0, \pi)$ after the perturbation as we expected.

For the first peak in Figure 3.12(b) for $N = 2, 3, 4, 5$, we observe the unstable two twisted $2N$-rings $(\vartheta_1, \vartheta_2) = (\vartheta_N(\alpha), 2\pi - \vartheta_N(\alpha))$ move to a certain special location after the perturbation. For example, We solve the BRD model (1.3) numerically for the twisted two 4-rings $(\vartheta_1, \vartheta_2) = (\vartheta_4(\alpha), 2\pi - \vartheta_4(\alpha))$ on the torus of $(R, r) = (0.75, 0.5)$ with $f = 0.7$, $\epsilon = 0.05$, $S_c = 1.5$, $A = \frac{4S_c}{\pi Rr}$ and $\vartheta_4 \approx 1.8647$. When $t = 1000$, we add a 2% random perturbation to the solution. For $\alpha = 1.5$, as show in Figure 3.12(b), these twisted two 4-rings are unstable. Figure 3.15 shows that this two 4-rings pattern is unstable after a long-time evolution, and it is moving to a special location. To show this sepcial pattern more specifically, the evolution of this simulation on the 3D torus model is shown in Figure 3.16.

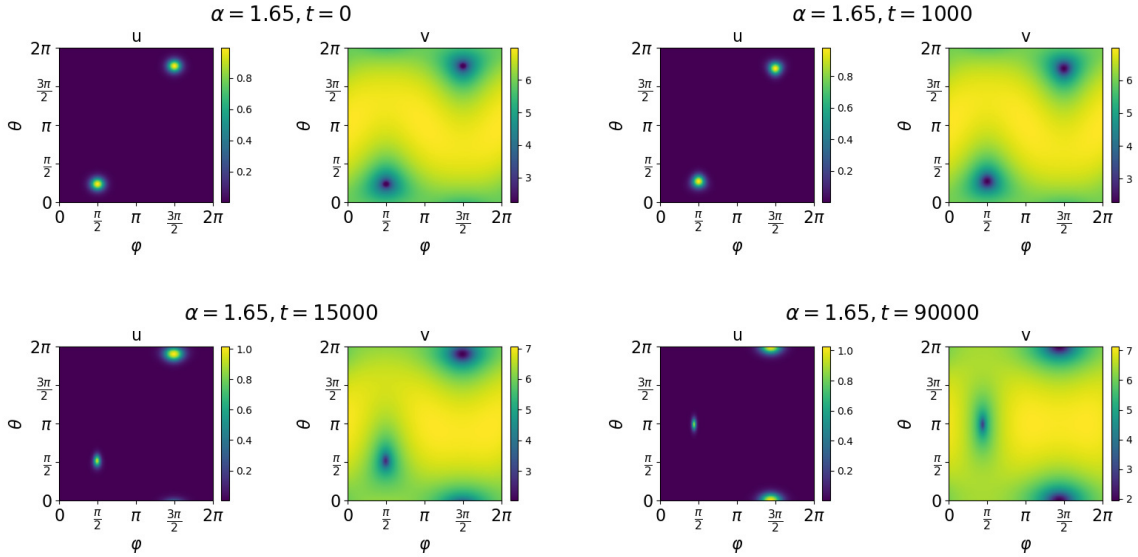

Figure 3.10: Evolution of BRD model (1.3) from the initial condition (2.30) and (2.31) consisting of two spots centered at $(\theta_1, \theta_2) = (\theta_0, 2\pi - \theta_0)$ and $\varphi_1 = \frac{\pi}{2}, \varphi_2 = \frac{3\pi}{2}$ on the torus of $R = 0.825$ and $r = 0.5$, where $\theta_0 \approx 0.7378$ is the solution of $\alpha_{1,1}(\theta_0, 2\pi - \theta_0, \pi, 0) = 0$. The numerical parameters are $f = 0.7$, $\epsilon = 0.05$, $S_c = 1.5$ and $A = \frac{S_c}{\pi R r}$. At first, two spots move toward a quasi-stationary state of two spots at $(\vartheta_c, 2\pi - \vartheta_c)$. The two spots become unstable and starts moving toward $(\theta_1, \theta_2) = (\pi, 0)$.

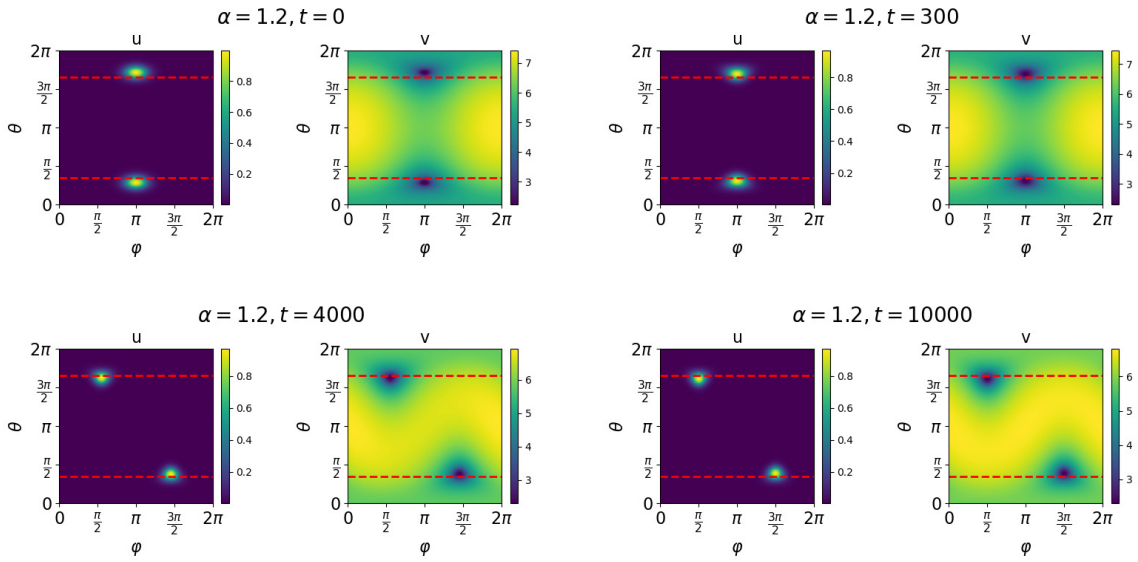

Figure 3.11: Evolution of the BRD model (1.3) from the initial condition (2.30) and (2.31) centered at $(\theta_1, \theta_2, \varphi_1, \varphi_2) = (\theta_0, 2\pi - \theta_0, \pi, \pi)$ on the torus of $R = 0.6$ and $r = 0.5$, where $\theta_0 \approx 0.8934$. The numerical parameters are $f = 0.7$, $\epsilon = 0.05$, $S_c = 1.5$ and $A = \frac{3}{2\pi R r}$. The two-spot configuration becomes unstable and is moving toward $\varphi_1 - \varphi_2 = \pi$. The horizontal dotted line represents the reference lines of $\vartheta_c(1.2) \approx 1.0970$ and $2\pi - \vartheta_c(1.2) \approx 5.1862$ which is the numerical solution of $\alpha_{1,1}(\vartheta_c, 2\pi - \vartheta_c, \pi, 0) = 0$.

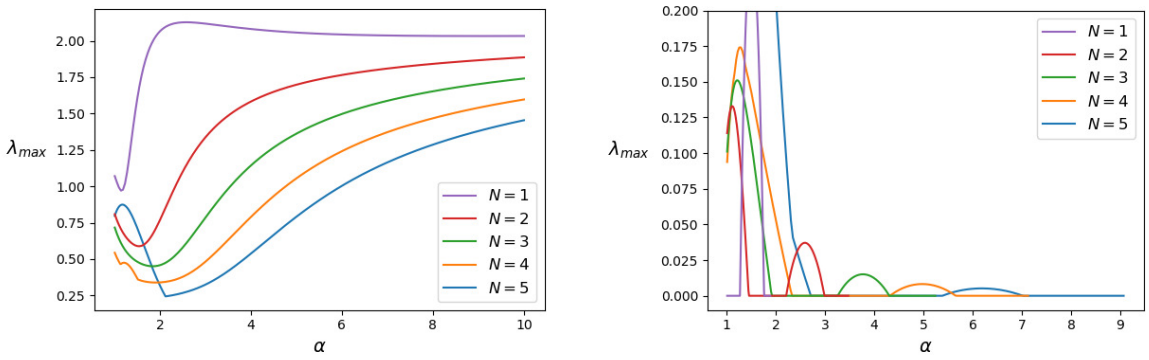

(a) (b)

Figure 3.12: The real part of the principal eigenvalue $\lambda_{max}(\alpha)$ for the untwisted and twisted two N-rings at $(\vartheta_1, \vartheta_2) = (\vartheta_N(\alpha), 2\pi - \vartheta_N(\alpha))$, $N = 1, \ldots, 5$ on the torus of $(R, r) = (\frac{\alpha}{2}, \frac{1}{2})$ with $\alpha \in [1.01, 10]$. The numerical parameters are $\epsilon = 0.05$, $f = 0.7$, $S_c = 1.5$ and $A = \frac{NS_c}{\pi Rr}$. (a) The untwisted two N-rings. (b) The twisted two N-rings.

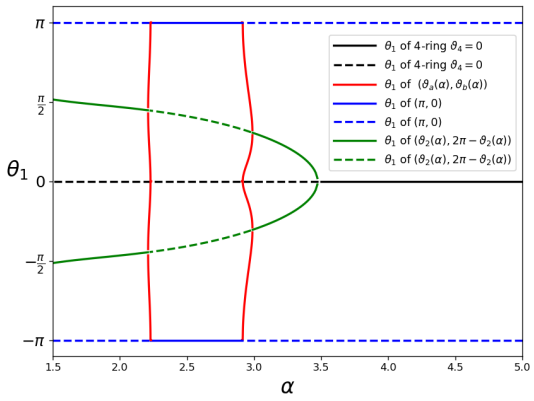

Figure 3.13: A part of bifurcation diagram with respect to θ_1 of the twisted two 2-rings with $\alpha \in [1.5, 5.0]$. The numerical parameters are $\epsilon = 0.05$, $f = 0.7$, $S_c = 1.5$ and $A = \frac{2S_c}{\pi Rr}$. The solid line represents the stable solutions and the dotted line depicts the unstable solutions. The equilibria are located at $(\varphi_1, \varphi_2, \varphi_3, \varphi_4) = (0, \frac{\pi}{2}, \pi, \frac{3\pi}{2})$. The black line represents the 4-ring $\vartheta_4 = 0$. The green line represents the twisted two 2-rings at $(\vartheta_2(\alpha), 2\pi - \vartheta_2(\alpha))$ and $(2\pi - \vartheta_2(\alpha), \vartheta_2(\alpha))$. The blue line represents the twisted two 2-rings at $(\vartheta_1, \vartheta_2) = (0, \pi)$ and $(\pi, 0)$. The red line represents special twisted two 2-rings solutions with $(\vartheta_1, \vartheta_2) = (\vartheta_a, \vartheta_b)$, $(\vartheta_b, \vartheta_a)$, $(-\vartheta_a, -\vartheta_b)$ and $(-\vartheta_b, -\vartheta_a)$ where $\vartheta_a(\alpha) \in (0, \pi), \vartheta_b(\alpha) \in (\pi, 2\pi)$ and $2\pi < \vartheta_a(\alpha) + \vartheta_b(\alpha) < 3\pi$.

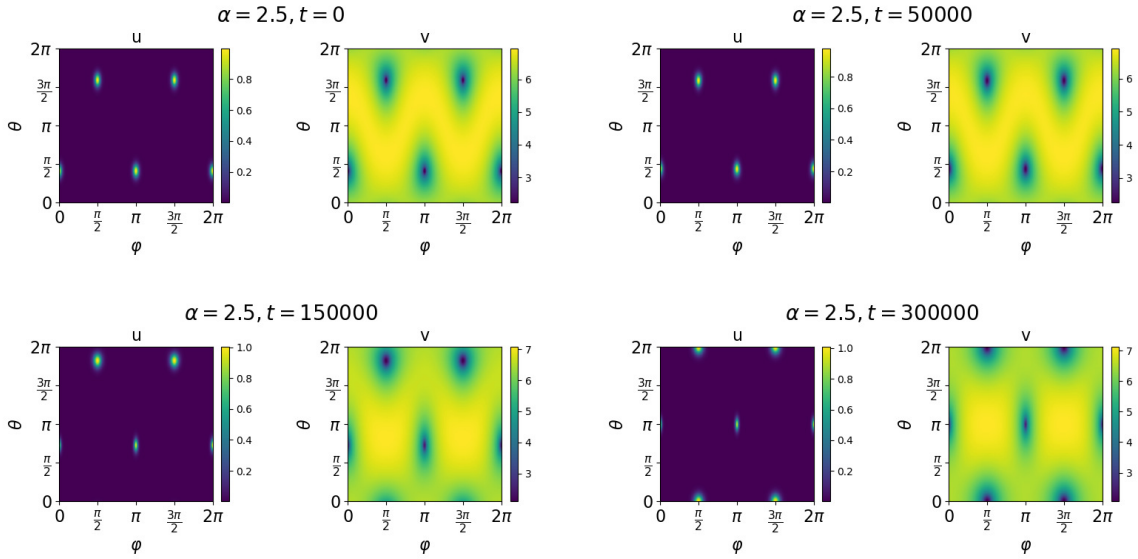

Figure 3.14: Evolution of the BRD model (1.3) from the initial condition (2.30) and (2.31) centered at $(\theta_1, \theta_2, \theta_3, \theta_4, \varphi_1, \varphi_2, \varphi_3, \varphi_4) = (\theta_0, 2\pi - \theta_0, \theta_0, 2\pi - \theta_0, 0, \frac{\pi}{2}, \pi, \frac{3\pi}{2})$ on the torus of $R = 1.25$ and $r = 0.5$, where $\theta_0 \approx 1.2854$. The numerical parameters are $\epsilon = 0.05$, $f = 0.7$, $S_c = 1.5$ and $A = \frac{3}{\pi Rr}$. When $t = 1000$, we add a 2% random perturbation to the solution. The two 2-rings configuration becomes unstable and is moving toward $(\theta_1, \theta_2, \theta_3, \theta_4) = (\pi, 2\pi, \pi, 2\pi)$.

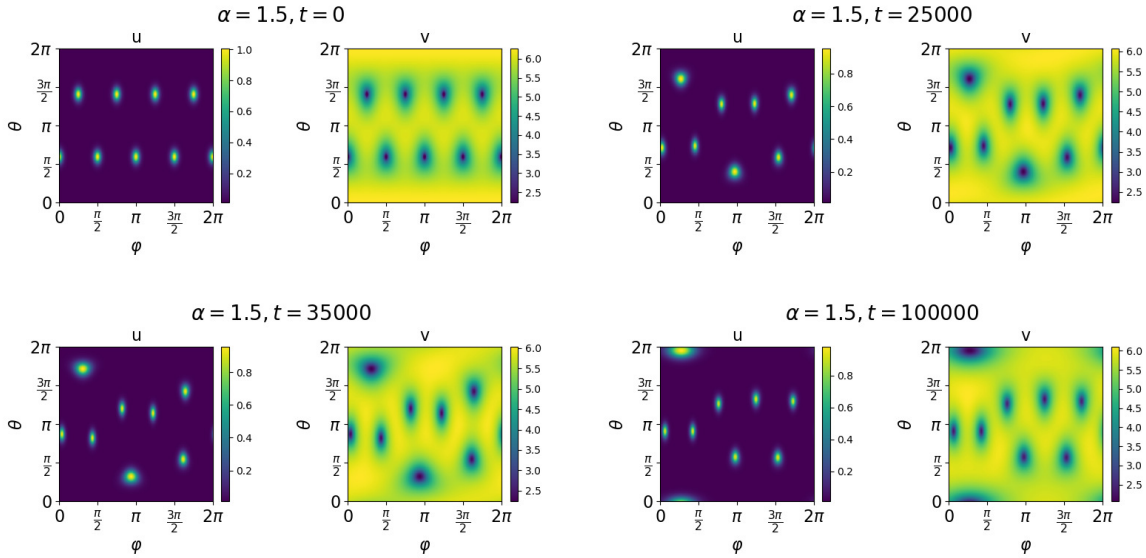

Figure 3.15: Evolution of the BRD model (1.3) from the initial condition (2.30) and (2.31) centered at the two twisted 4-rings $(\vartheta_1, \vartheta_2) = (\theta_0, 2\pi - \theta_0)$ on the torus of $R = 0.75$ and $r = 0.5$, where $\theta_0 \approx 1.8647$. The numerical parameters are $f = 0.7$, $\epsilon = 0.05$, $S_c = 1.5$ and $A = \frac{6}{\pi Rr}$. When $t = 1000$, we add a 2% random perturbation to the solution. The two 4-rings configuration becomes unstable and is moving toward a special position.

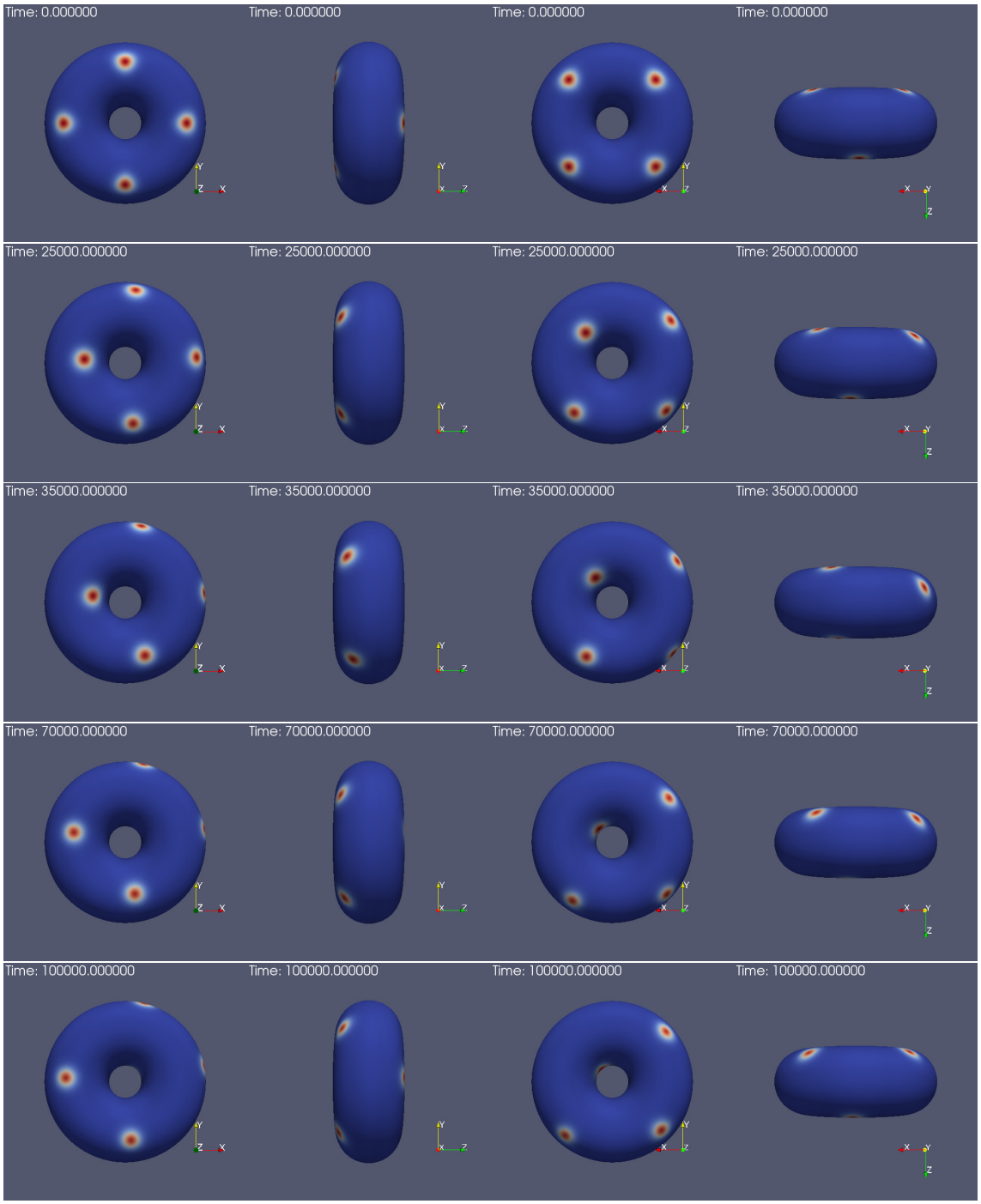

Figure 3.16: Evolution of u of the BRD model (1.3) centered at the two twisted 4-rings $(\vartheta_1, \vartheta_2) = (\theta_0, 2\pi - \theta_0)$ on the torus of $R = 0.75$ and $r = 0.5$, where $\theta_0 \approx 1.8647$. The numerical parameters and the initial condition are the same as Figure 3.15. The two 4-rings configuration becomes unstable and is moving toward a special position. The right-handed coordinates are shown in each figure.

Chapter 4

Some Numerical Simulations of Brusselator Reaction-diffusion model

In this chapter, we list some numerical simulations about spot division of BRD model (1.3) on the torus which are left open for future research. The numerical parameters of numerical simulations are given by $f = 0.7$, $\epsilon = 0.05$, $A = \frac{S_1}{2\pi Rr}$ and when $t < 100$, $S_1 = 3$. The the initial condition is given by (2.30) and (2.31).

The first experiment is shown in Figure 4.1. The initial condition is one spot at $(\theta_1, \varphi_1) = (0, \pi)$ on the torus of $(R, r) = (0.75, 0.5)$. When $t \geq 100$, we set $S_1 = 14$. Fist, this spot is divided into four spots. Then, each spot is divided into two spots and a pattern of eight spots is formed. When $t = 1000$, the pattern is close to the unstable untwisted two 4-rings at $(\vartheta_1, 2\pi - \vartheta_1)$. When $t = 5500$, the pattern is close to the unstable twisted two 4-rings at $(\vartheta_1, 2\pi - \vartheta_1)$. After a long-time evolution, the pattern is moving toward a special position which is similar to the stable pattern shown in Figure 3.15, although $A = \frac{\sum_{j=1}^{8} S_j}{2\pi Rr}$ is different between these two simulations : $\sum_{j=1}^{8} S_j = 12$ in Figure 3.15 and $\sum_{j=1}^{8} S_j = 14$ in Figure 4.1.

The second experiment is shown in Figure 4.2. The initial condition is one spot at $(\theta_1, \varphi_1) = (0, \pi)$ on the torus of $(R, r) = (2.0, 0.5)$. When $t \geq 100$, same as the first experiment, we set $S_1 = 14$. Different from the division process in the first experiment, one spot is first divided into two spots. Then, each spot is divided into three spots. From $t = 180$ to $t = 230$, it seems that two spots at $\theta = 0$ is divided into six spots, but new spots vanish. Finally, two spots at $\theta = 0$ split in the φ direction, and we obtain a pattern of eight spots. From $t = 180$ to $t = 240$, these two spots at $\theta = 0$ are moving in the φ direction. Hence, the direction of division of these two spots are parallel to the direction of the motion. In the meantime, as shown in [17], when $S_j \approx \Sigma_2(f)$, the direction of the self-replication should be perpendicular to the direction of the motion. Hence, when $S_j > \Sigma_2(f)$, the direction of self-replication could be different.

The third experiment is shown in Figure 4.3. The initial condition is one spot at $(\theta_1, \varphi_1) = (\pi, \pi)$ on the torus of $(R, r) = (2.0, 0.5)$. When $t \geq 100$, same as the above two experiment, we set $S_1 = 14$. This spot is first divided into four symmetric spots with $S_c = 3.5 > \Sigma_2(f) \approx 3.2$. Hence, these four spots pattern is unstable. Since these four spots are symmetric, each spot should be divided into two spots. It seems that each spot is divided into two spots, but two of them vanish and we finally obtain a pattern of six spots. The reason of vanishing phenomenon arises because of our torus model: the vertices of model are not symmetric. Hence, we found

that spot division may be unstable.

The fourth experiment is shown in Figure 4.4. The initial condition is one spot at $(\theta_1, \varphi_1) = (0, \pi)$ on the torus of $(R, r) = (2.0, 0.5)$. When $t \geq 100$, we set $S_1 = 20$. As similar to the division process in the second experiment, one spot is first divided into two spots, and then each spot is divided into three spots. But different from the division process in the second experiment, the two spots at $\theta = 0$ do not split in the φ direction, but are divided into six spots. Finally, each spot at $\theta = 0$ is divided into three spots again, and we obtain a pattern of fourteen spots.

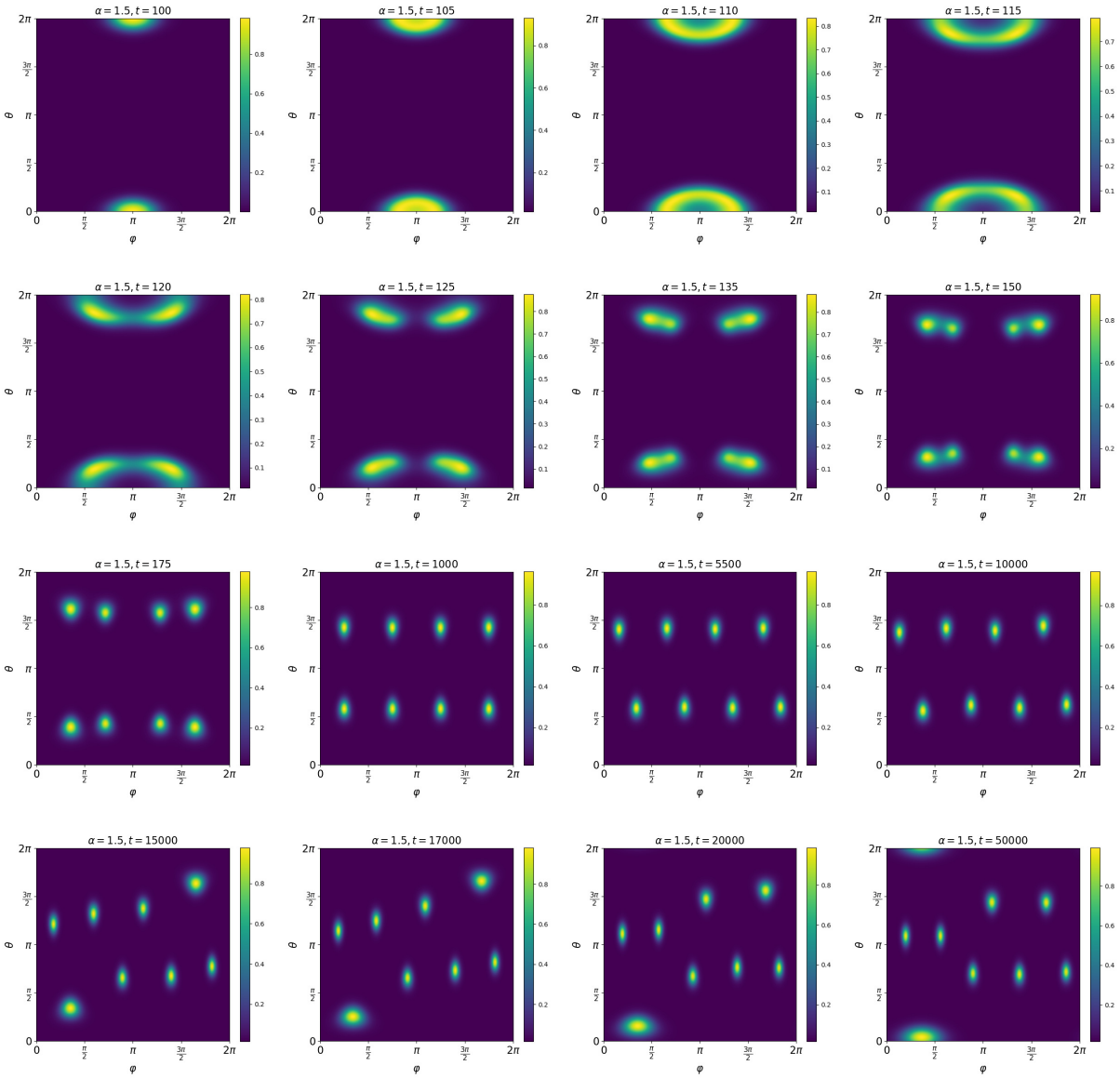

Figure 4.1: Evolution of the BRD model (1.3) from one spot centered at $(\theta_1, \varphi_1) = (0, \pi)$ on the torus of $R = 0.75$ and $r = 0.5$. The numerical parameters are $f = 0.7$, $\epsilon = 0.05$, $A = \frac{S_1}{2\pi Rr}$. When $t < 100$, $S_1 = 3$. When $t = 100$, we set $S_1 = 14$. Then, the division of spot is observed and a pattern of eight spots is formed. After a long-time evolution, the pattern is moving toward a special position which is similar to the stable pattern shown in Figure 3.15.

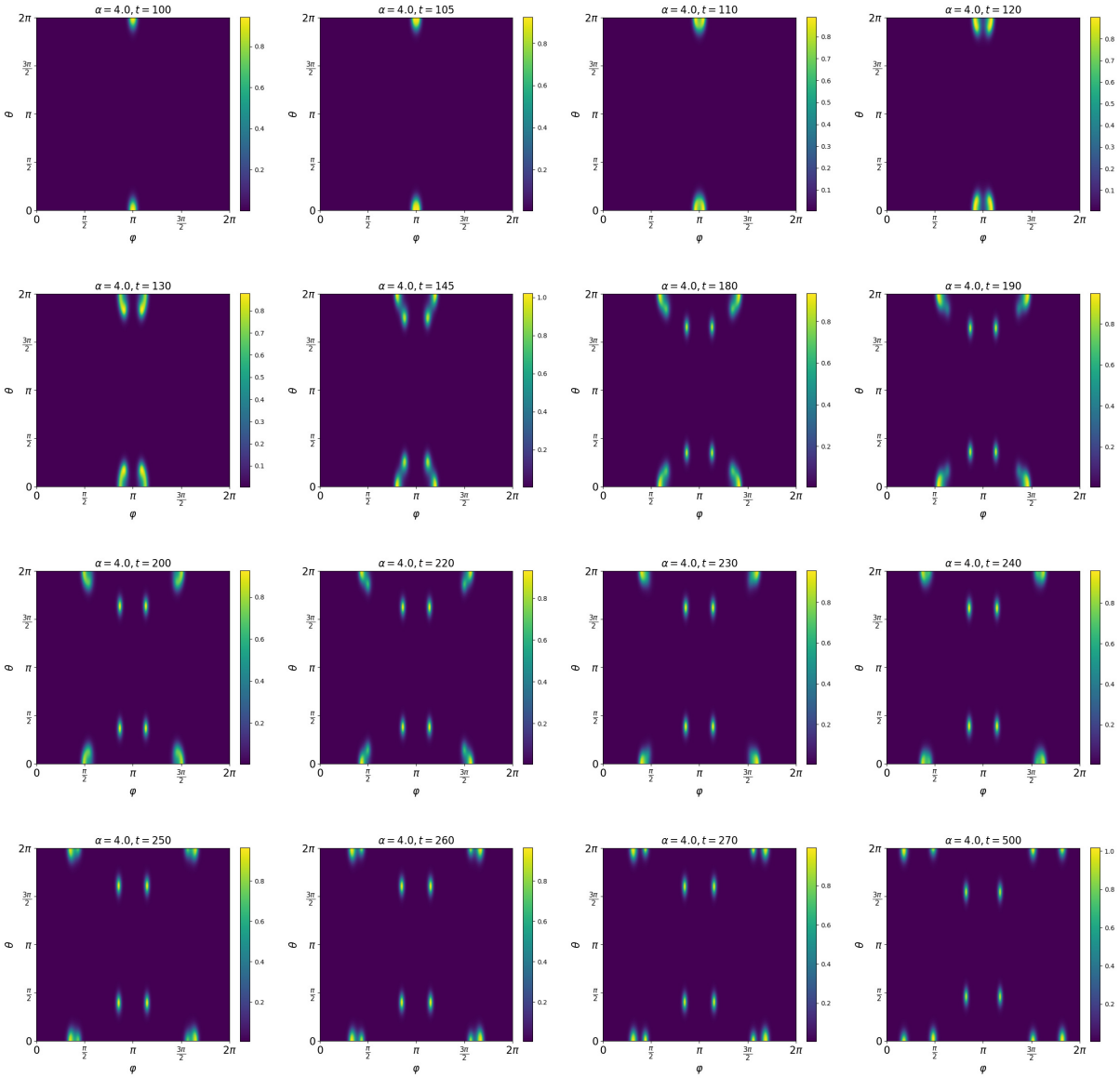

Figure 4.2: Evolution of the BRD model (1.3) from one spot centered at $(\theta_1, \varphi_1) = (0, \pi)$ on the torus of $R = 2.0$ and $r = 0.5$. The numerical parameters are $f = 0.7$, $\epsilon = 0.05$, $A = \frac{S_1}{2\pi Rr}$. When $t < 100$, $S_1 = 3$. When $t = 100$, we set $S_1 = 14$. Then, the division of spot is observed and a pattern of eight spots is formed.

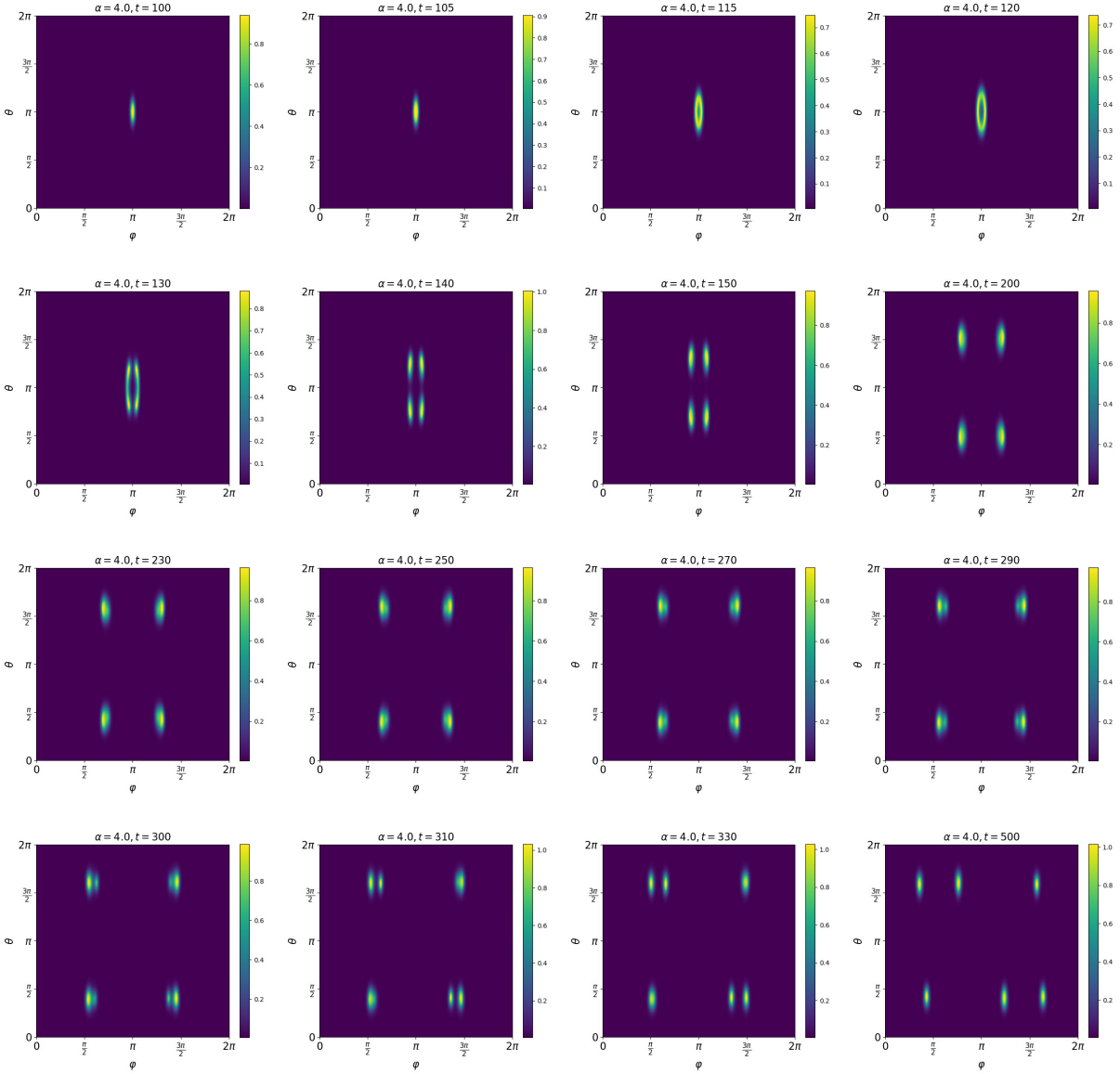

Figure 4.3: Evolution of the BRD model (1.3) from one spot centered at $(\theta_1, \varphi_1) = (\pi, \pi)$ on the torus of $R = 2.0$ and $r = 0.5$. The numerical parameters are $f = 0.7$, $\epsilon = 0.05$, $A = \frac{S_1}{2\pi Rr}$. When $t < 100$, $S_1 = 3$. When $t = 100$, we set $S_1 = 14$. Then, the division of spot is observed and a pattern of six spots is formed.

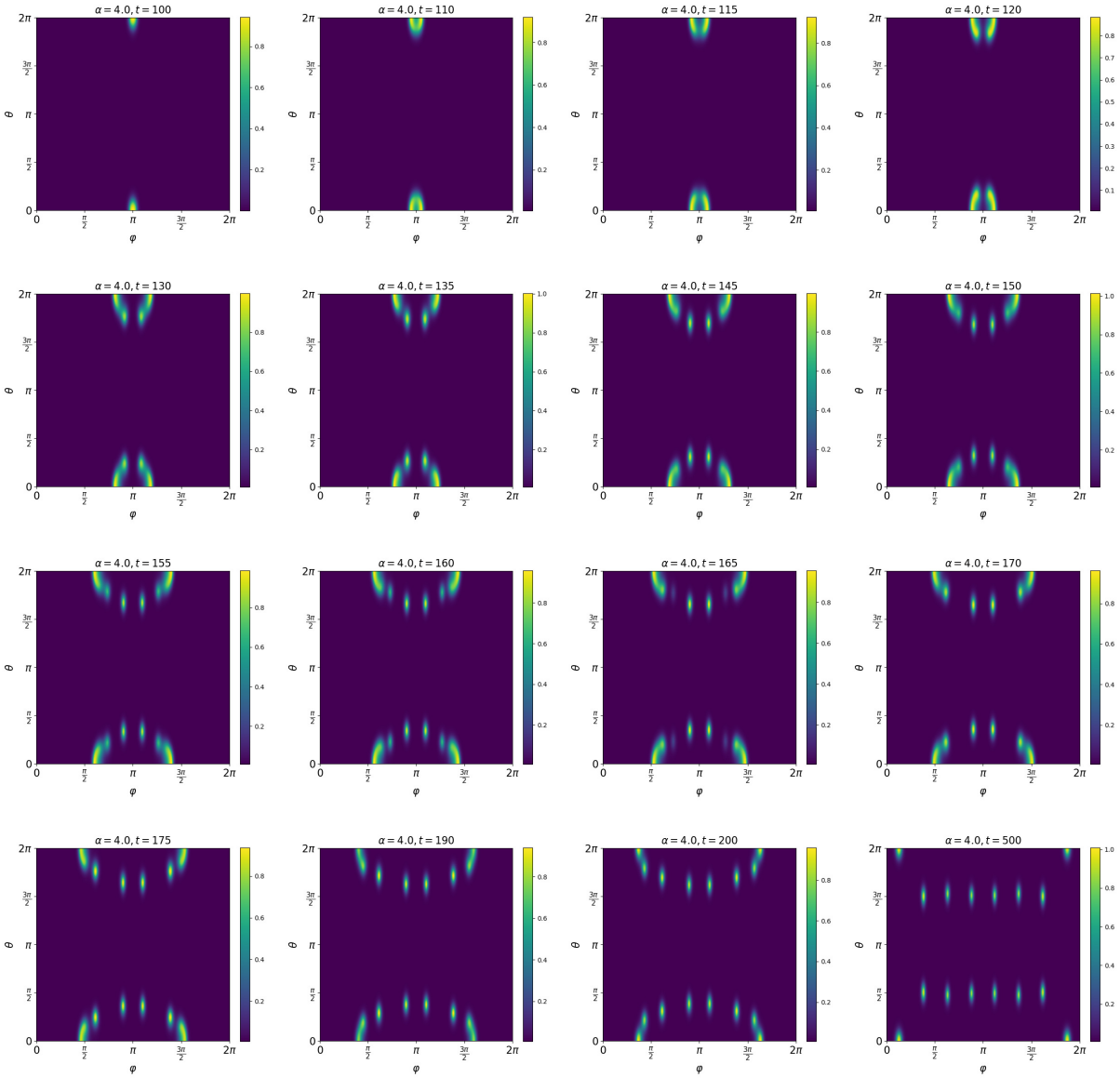

Figure 4.4: Evolution of the BRD model (1.3) from one spot centered at $(\theta_1, \varphi_1) = (0, \pi)$ on the torus of $R = 2.0$ and $r = 0.5$. The numerical parameters are $f = 0.7$, $\epsilon = 0.05$, $A = \frac{S_1}{2\pi Rr}$. When $t < 100$, $S_1 = 3$. When $t = 100$, we set $S_1 = 20$. Then, the division of spot is observed and a pattern of fourteen spots is formed.

Chapter 5

Comparison between the Spots on the Sphere and Torus

5.1 Quasi-stationary spot solution on the sphere

In [24, 29], quasi-stationary spot solutions and their dynamics of the BRD model (1.3) on the unit sphere are considered on the unit sphere endowed with the spherical coordinate system in $\mathbb{R}^3$,

$$\boldsymbol{x}_S(\theta_S, \varphi_S) = (\cos\varphi_S \sin\theta_S, \sin\varphi_S \sin\theta_S, \cos\theta_S)^T$$

for the longitudinal angular coordinate $\varphi_S \in [0, 2\pi)$ and the latitudinal coordinate $\theta_S \in (0, \pi)$. Two poles $\theta = 0$ and $\theta = \pi$ are not contained in this parameterization, but we can rotate the sphere so that there is no spot at the poles. In this section, following the asymptotic analysis in [24, 29], we extend quasi-stationary spot solutions and the evolution equation of the spots of RD model (1.1) on the unit sphere. Let $(\theta_{S,j}, \varphi_{S,j})$ denote the core of jth spot on the unit sphere and $\boldsymbol{x}_{S,j} = \boldsymbol{x}_S(\theta_{S,j}, \varphi_{S,j})$. Since $\frac{\partial \boldsymbol{x}_S}{\partial \theta_S} = (\cos\varphi_S \cos\theta_S, \sin\varphi_S \cos\theta_S, -\sin\theta_S)$, $\frac{\partial \boldsymbol{x}_S}{\partial \varphi_S} = (-\sin\varphi_S \sin\theta_S, \cos\varphi_S \sin\theta_S, 0)$, we have $\frac{\partial \boldsymbol{x}_S}{\partial \theta_S} \cdot \frac{\partial \boldsymbol{x}_S}{\partial \varphi_S} = 0$, $\left|\frac{\partial \boldsymbol{x}_S}{\partial \theta_S}\right| = 1$ and $\left|\frac{\partial \boldsymbol{x}_S}{\partial \varphi_S}\right| = \sin\theta_S$. Then, we introduce the following local coordinate $\boldsymbol{s} = (s_1, s_2)^T$ near the jth spot on the unit sphere:

$$s_1(\theta_S, \sigma) = \frac{1}{\epsilon}(\theta_S - \theta_{S,j}(\sigma)), \quad s_2(\varphi_S, \sigma) = \frac{\sin\theta_{S,j}}{\epsilon}(\varphi_S - \varphi_{S,j}(\sigma)), \quad \rho = \sqrt{s_1^2 + s_2^2}, \tag{5.1}$$

where $\sigma = \epsilon^2 t$. The Laplace–Beltrami operator on the unit sphere is defined by

$$\triangle_S = \frac{1}{\sin^2\theta_S}\frac{\partial^2}{\partial^2 \varphi_S} + \frac{1}{\sin\theta_S}\frac{\partial}{\partial \theta_S}\left(\sin\theta_S \frac{\partial}{\partial \theta_S}\right). \tag{5.2}$$

It follows from the local coordinate (5.1) that Laplace–Beltrami operator can be approximated by

$$\triangle_S = \frac{1}{\epsilon^2}\left(\triangle_{\boldsymbol{s}} + \epsilon \mathcal{N}_{S,j} + \mathcal{O}\left(\epsilon^2\right)\right), \tag{5.3}$$

where $\triangle_{\boldsymbol{s}} = \frac{\partial^2}{\partial s_1^2} + \frac{\partial^2}{\partial s_2^2}$ and

$$\mathcal{N}_{S,j} = \cot\theta_{S,j}\left(\frac{\partial}{\partial s_1} - 2s_1\frac{\partial^2}{\partial s_2^2}\right).$$

Owing to $|\varphi_S - \varphi_{S,j}| \le \mathcal{O}(\epsilon)$ in the jth inner spot, we obtain

$$\frac{\partial u}{\partial t} = \frac{\partial u}{\partial s_1}\frac{\partial s_1}{\partial \sigma}\frac{\partial \sigma}{\partial t} + \frac{\partial u}{\partial s_2}\frac{\partial s_2}{\partial \sigma}\frac{\partial \sigma}{\partial t} + \frac{\partial u}{\partial \sigma}\frac{\partial \sigma}{\partial t} = \epsilon \mathcal{L}_{S,j} u + \mathcal{O}(\epsilon^2) \tag{5.4}$$

and similarly

$$\frac{\partial v}{\partial t} = \epsilon \mathcal{L}_{S,j} v + \mathcal{O}(\epsilon^2),$$

where

$$\mathcal{L}_{S,j} = -\left(\frac{\mathrm{d}\theta_{S,j}}{\mathrm{d}\sigma}, \sin\theta_{S,j}\frac{\mathrm{d}\varphi_{S,j}}{\mathrm{d}\sigma}\right)\cdot \nabla_{\boldsymbol{s}}, \qquad \nabla_{\boldsymbol{s}} = \left(\frac{\partial}{\partial s_1}, \frac{\partial}{\partial s_2}\right). \tag{5.5}$$

Here $\mathcal{N}_{S,j}$ and $\mathcal{L}_{S,j}$ is different from $\mathcal{N}_j$ and $\mathcal{L}_j$ of the torus case, since they depend on the local coordinates. The solutions of (1.1) near the jth spot are expanded with respect to ϵ as follows.

$$u(s_1, s_2, \sigma) = \sum_{n=0}^{\infty} \epsilon^n u_{jn}, \qquad v(s_1, s_2, \sigma) = \sum_{n=0}^{\infty} \epsilon^n v_{jn}. \tag{5.6}$$

Since the core problem on the sphere is identical to that on the torus, we have the following results that are the same as those in the torus case:

$$u \sim -\epsilon^2 \frac{A}{a_1} + \sum_{j=1}^{N} u_{j0},$$

and

$$\triangle_S v + E = 2\pi \sum_{j=1}^{N} S_j \delta(\boldsymbol{x} - \boldsymbol{x}_j), \qquad |\boldsymbol{x} - \boldsymbol{x}_j| > \mathcal{O}(\epsilon), \quad j = 1, \dots, N, \tag{5.7}$$

$$v \sim v_{j0} + \epsilon v_{j1} \sim S_j \log\rho + \chi(S_j) + \epsilon v_{j1} + o(1), \quad |\boldsymbol{x} - \boldsymbol{x}_j| \to \mathcal{O}(\epsilon), \quad j = 1, \dots, N, \tag{5.8}$$

where $E = B - \frac{b_1}{a_1}A$. At next order, if we replace $\mathcal{N}_j$ and $\mathcal{L}_j$ of the torus case with $\mathcal{N}_{S,j}$ and $\mathcal{L}_{S,j}$, by introducing $\mathcal{P}_S = \triangle_{\boldsymbol{s}} + \mathcal{M}_j$, the next order equation is identical to that on the torus:

$$\mathcal{P}_S \boldsymbol{w}_{j1} = \triangle_{\boldsymbol{s}} \boldsymbol{w}_{j1} + \mathcal{M}_j \boldsymbol{w}_{j1} = -\mathcal{N}_{S,j} \boldsymbol{w}_{j0} + \begin{pmatrix} \mathcal{L}_{S,j} u_{j0} \\ 0 \end{pmatrix}, \tag{5.9}$$

where $\boldsymbol{w}_{jn} = (u_{jn}, v_{jn})^T$ and $\mathcal{M}_j$ is defined in (2.8). The source-neutral Green's function on the unit sphere, which is the solution of $\triangle_S L(\boldsymbol{x}_S; \boldsymbol{x}_{S,0}) = -\delta(\boldsymbol{x}_S - \boldsymbol{x}_{S,0}) + \frac{1}{4\pi}$ and $\int_S G \mathrm{d}\boldsymbol{x} = 0$, is given by

$$L(\boldsymbol{x}_S; \boldsymbol{x}_{S,0}) = -\frac{1}{2\pi}\log|\boldsymbol{x}_S - \boldsymbol{x}_{S,0}| + R_0, \tag{5.10}$$

where $R_0 = \frac{1}{4\pi}(\log 4 - 1)$. Then, by introducing $L_i(\boldsymbol{x}_S) = \log|\boldsymbol{x}_S - \boldsymbol{x}_{S,i}|$ the solution of (5.8) is

$$v = \sum_{j=1}^{N} S_j L_j(\boldsymbol{x}_S) - 4\pi R_0 E + \overline{v}, \qquad \text{where } \sum_{j=1}^{N} S_j = 2E. \tag{5.11}$$

By local coordinate (5.1), Trinh and Ward [29] shows the following results.

Theorem 5.1.1. (Lemma 1 in [29]) Suppose that $\theta_j \in (0,\pi)$. Then for $|\boldsymbol{x}_S - \boldsymbol{x}_{S,j}| = \mathcal{O}(\epsilon)$ and $|\boldsymbol{s}| = \mathcal{O}(1)$, we have

$$\boldsymbol{x}_S - \boldsymbol{x}_{S,j} = \epsilon \boldsymbol{J}_j \boldsymbol{s} + \mathcal{O}(\epsilon^2), \qquad |\boldsymbol{x}_S - \boldsymbol{x}_{S,j}| = \epsilon\rho + \frac{\epsilon^2}{2\rho} s_1 s_2^2 \cot\theta_{S,j}, \tag{5.12}$$

where $\boldsymbol{J}_j$ is the 3×2 matrix defined by

$$\boldsymbol{J}_j^T = \begin{pmatrix} \cos\varphi_{S,j}\cos\theta_{S,j} & \sin\varphi_{S,j}\cos\theta_{S,j} & -\sin\theta_{S,j} \\ -\sin\varphi_{S,j} & \cos\varphi_{S,j} & 0 \end{pmatrix}.$$

Then, using Theorem 5.1.1 and matching the leading order and next order of ϵ of (5.8) as $\boldsymbol{x}_S \to \boldsymbol{x}_{S,j}$ for $j = 1,\dots,N$, we obtain

$$S_j \log\epsilon - 4\pi R_0 E + \overline{v} + \sum_{\substack{i=1\\ i\neq j}}^{N} S_i L_{ij} = \chi(S_j), \tag{5.13}$$

$$v_{j1} = \frac{S_j}{2\rho^2} s_1 s_2^2 \cot\theta_{S,j} + \sum_{\substack{i=1\\ i\neq j}}^{N} S_i \left.\nabla_{(\theta_S,\varphi_S)} L_i\right|_{(\theta_S,\varphi_S)=(\theta_{S,j},\varphi_{S,j})} \cdot \left(s_1, \frac{1}{\sin\theta_{S,j}} s_2\right), \quad \text{as } |\rho|\to\infty, \tag{5.14}$$

where $L_{ij} = \log|\boldsymbol{x}_{S,i} - \boldsymbol{x}_{S,j}|$. Since S_j and $\overline{v}$ depends on the Green's function on the surface, the algebraic system of S_j and $\overline{v}$ of the torus case and the sphere case are different. By (5.13) and $\sum_{j=1}^N S_j = 2E$, we obtain following the nonlinear algebraic system for S_j, $j = 1,2,\dots,N$:

$$\boldsymbol{S} + \frac{1}{\log\epsilon}(\boldsymbol{I} - \boldsymbol{e}_0)\boldsymbol{L}\boldsymbol{S} - \frac{1}{\log\epsilon}(\boldsymbol{I} - \boldsymbol{e}_0)\boldsymbol{\chi} = \frac{2E}{N}\boldsymbol{e}, \tag{5.15}$$

where $\boldsymbol{e}_0 = \frac{1}{N}\boldsymbol{e}\boldsymbol{e}^T$ is the matrix whose components are all $\frac{1}{N}$ and

$$\boldsymbol{S} = \begin{pmatrix} S_1 \\ \vdots \\ S_N \end{pmatrix}, \quad \boldsymbol{e} = \begin{pmatrix} 1 \\ \vdots \\ 1 \end{pmatrix}, \quad \boldsymbol{\chi}(\boldsymbol{S}) = \begin{pmatrix} \chi(S_1) \\ \vdots \\ \chi(S_N) \end{pmatrix}, \quad \boldsymbol{L} = \begin{pmatrix} 0 & L_{12} & \cdots & L_{1N} \\ L_{21} & \ddots & & \vdots \\ \vdots & & & \\ L_{N1} & \cdots & & 0 \end{pmatrix}. \tag{5.16}$$

Then, $\overline{v}$ is given by

$$\overline{v} = -\frac{2E\log\epsilon}{N} + 4\pi R_0 E + \frac{1}{N}(\boldsymbol{e}^T\boldsymbol{\chi} - \boldsymbol{e}^T\boldsymbol{L}\boldsymbol{S}).$$

Suppose (5.15) has a solution. Then, there is a quasi-equilibrium solution $u_{\rm qe}$ and $v_{\rm qe}$ for RD model (1.1):

$$u_{\rm qe} \sim -\epsilon^2 E + \sum_{j=1}^{N} u_j(\epsilon^{-1}|\boldsymbol{x}_S - \boldsymbol{x}_{S,j}|), \tag{5.17}$$

$$v_{\rm qe} \sim \begin{cases} v_j(\epsilon^{-1}|\boldsymbol{x}_S - \boldsymbol{x}_{S,j}|), & |\boldsymbol{x}_S - \boldsymbol{x}_{S,j}| = \mathcal{O}(\epsilon), \\ \sum\limits_{i=1}^{N} S_i L_i(\boldsymbol{x}_S) - 4\pi R_0 E + \overline{v}, & |\boldsymbol{x}_S - \boldsymbol{x}_{S,j}| > \mathcal{O}(\epsilon). \end{cases} \tag{5.18}$$

For the BRD model (1.3), we have $E = A$. Hence, quasi-equilibrium solution of the BRD model (1.3) can be expressed as follow:

(Principal Result 2.1 in [24]) Let $\epsilon \to 0$. Suppose that the nonlinear algebraic system

$$\boldsymbol{S} + \frac{1}{\log \epsilon}(\boldsymbol{I} - \boldsymbol{e}_0)\boldsymbol{L}\boldsymbol{S} - \frac{1}{\log \epsilon}(\boldsymbol{I} - \boldsymbol{e}_0)\boldsymbol{\chi} = \frac{2A}{N}\boldsymbol{e}, \tag{5.19}$$

for the source strengths S_j, $j = 1, \cdots, N$, has a solution. Then, there is a quasi-equilibrium solution $u_{\rm qe}$ and $v_{\rm qe}$ for the Brusselator model (1.3) with leading-order uniformly valid asymptotics given by

$$u_{\rm qe} \sim -\epsilon^2 A + \sum_{j=1}^{N} u_j(\epsilon^{-1}|\boldsymbol{x} - \boldsymbol{x}_j|), \tag{5.20}$$

$$v_{\rm qe} \sim \begin{cases} v_j(\epsilon^{-1}|\boldsymbol{x}_S - \boldsymbol{x}_{S,j}|), & |\boldsymbol{x}_S - \boldsymbol{x}_{S,j}| = \mathcal{O}(\epsilon), \\ \sum\limits_{i=1}^{N} S_j L(\boldsymbol{x}_S; \boldsymbol{x}_{S,i}) - 4\pi R_0 A + \overline{v}, & |\boldsymbol{x}_S - \boldsymbol{x}_{S,j}| > \mathcal{O}(\epsilon), \end{cases} \tag{5.21}$$

where $\overline{v}$ is given by

$$\overline{v} = -\frac{2A \log \epsilon}{N} + 4\pi R_0 A + \frac{1}{N}(\boldsymbol{e}^T\boldsymbol{\chi} - \boldsymbol{e}^T\boldsymbol{L}\boldsymbol{S}). \tag{5.22}$$

To obtain the evolution equation for the slow spot dynamics, let us consider the following problem followed from (5.9) and (5.14):

$$\mathcal{P}_S \boldsymbol{w}_{j1} = \triangle_{\boldsymbol{s}} \boldsymbol{w}_{j1} + \mathcal{M}_j \boldsymbol{w}_{j1} = -\mathcal{N}_{S,j}\boldsymbol{w}_{j0} + \begin{pmatrix} \mathcal{L}_{S,j} u_{j0} \\ 0 \end{pmatrix}, \tag{5.23}$$

$$v_{j1} = \frac{S_j}{2\rho^2} s_1 s_2^2 \cot\theta_j + \sum_{\substack{i=1 \\ i \neq j}}^{N} S_i \, \nabla_{(\theta_S, \varphi_S)} L_i\big|_{(\theta_S, \varphi_S) = (\theta_{S,j}, \varphi_{S,j})} \cdot \left(s_1, \frac{1}{\sin\theta_{S,j}} s_2 \right), \quad \text{as } |\rho| \to \infty. \tag{5.24}$$

Since the boundary condition depends on the Green's function of surface, the boundary condition (5.24) of the sphere is different from the boundary condition of the torus (2.38). As similar to that on the torus, this equation is solved by considering the decomposition of $\boldsymbol{w}_{j1}$.

$$\boldsymbol{w}_{j1} = \begin{pmatrix} u_{j1} \\ v_{j1} \end{pmatrix} = \boldsymbol{w}^e_{j1} + \boldsymbol{w}^d_{j1}, \quad \boldsymbol{w}^e_{j1} = \begin{pmatrix} u^e_{j1} \\ v^e_{j1} \end{pmatrix}, \quad \boldsymbol{w}^d_{j1} = \begin{pmatrix} u^d_{j1} \\ v^d_{j1} \end{pmatrix}, \tag{5.25}$$

where $\boldsymbol{w}^e_{j1}$ and $\boldsymbol{w}^d_{j1}$ satisfy

$$\mathcal{P}_S \boldsymbol{w}^e_{j1} = -\mathcal{N}_{S,j}\boldsymbol{w}_{j0}, \quad \mathcal{P}_S \boldsymbol{w}^d_{j1} = \begin{pmatrix} \mathcal{L}_{S,j} u_{j0} \\ 0 \end{pmatrix}, \quad \boldsymbol{s} \in \mathbb{R}^2, \tag{5.26}$$

$$\boldsymbol{w}^e_{j1} \sim \begin{pmatrix} 0 \\ \frac{S_j}{2\rho^2} s_1 s_2^2 \cot\theta_{S,j} \end{pmatrix}, \quad \boldsymbol{w}^d_{j1} \sim \begin{pmatrix} 0 \\ \boldsymbol{\alpha}_{S,j} \cdot \boldsymbol{s} \end{pmatrix}, \quad \rho = |\boldsymbol{s}| \to \infty. \tag{5.27}$$

Here, the function $\boldsymbol{\alpha}_j = (\alpha_{S,j,1}, \alpha_{S,j,2})^T$ is given by

$$\boldsymbol{\alpha}_{S,j} = \begin{pmatrix} \alpha_{S,j,1} \\ \alpha_{S,j,2} \end{pmatrix} = \sum_{\substack{i=1 \\ i \neq j}}^{N} S_i \left. \begin{pmatrix} \frac{\partial L_i}{\partial \theta_S} \\ \frac{1}{\sin\theta_{S,j}} \frac{\partial L_i}{\partial \varphi_S} \end{pmatrix} \right|_{(\theta_S, \varphi_S) = (\theta_{S,j}, \varphi_{S,j})}. \tag{5.28}$$

The difference between $\alpha_{S,j}$ of the sphere case and α_j of the torus case is generated by the Green's functions and the local coordinates of the sphere and the torus. As shown in [29], $\boldsymbol{w}^e_{j1} = -\frac{s_2^2}{2}\cot\theta_{S,j}\frac{\partial \boldsymbol{w}_{j0}}{\partial s_1} + s_1 s_2 \cot\theta_{S,j}\frac{\partial \boldsymbol{w}_{j0}}{\partial s_2}$ is a solution of the first equation. The rest of the computation is similarly to that on the torus. Replacing $\mathcal{N}_j$ and $\mathcal{L}_j$ with $\mathcal{N}_{S,j}$ and $\mathcal{L}_{S,j}$ in the derivation of (2.49) and (2.50), we obtain the following evolution equation of RD model (1.1). The following results derived in [29] shows the evolution equation of spots of the BRD model (1.3) on the sphere, but it still holds for RD model (1.1).

(Principal Result 2 in [29]) Let $\epsilon \to 0$. Provided that there are no $\mathcal{O}(1)$ timescale instabilities of the quasi-equilibrium spot pattern, the time-dependent spot locations, $\boldsymbol{x}_j = (\cos\varphi_j \sin\theta_j, \sin\varphi_j \sin\theta_j, \cos\theta_j)^T$, vary on the slow time-scale $\sigma = \epsilon^2 t$, and satisfy the differential algebraic system:

$$\frac{\mathrm{d}\theta_{S,j}}{\mathrm{d}\sigma} = -\frac{2}{\mathcal{C}_j}\alpha_{S,j,1}, \qquad \sin\theta_{S,j}\frac{\mathrm{d}\varphi_j}{\mathrm{d}\sigma} = -\frac{2}{\mathcal{C}_j}\alpha_{S,j,2}, \quad j = 1, 2, \ldots, N, \tag{5.29}$$

where $\mathcal{C}_j$ is defined in (2.51) and

$$\begin{pmatrix}\alpha_{S,j,1}\\ \alpha_{S,j,2}\end{pmatrix} = \sum_{\substack{i=1\\ i\neq j}}^{N} S_i \left.\begin{pmatrix}\frac{\partial L_i}{\partial \theta_S}\\ \frac{1}{\sin\theta_{S,j}}\frac{\partial L_i}{\partial \varphi_S}\end{pmatrix}\right|_{(\theta_S,\varphi_S)=(\theta_{S,j},\varphi_{S,j})}. \tag{5.30}$$

By using cosine law $|\boldsymbol{x}_{S,i} - \boldsymbol{x}_{S,j}|^2 = 2(1-\cos\gamma_{ij})$, where γ_{ij} is the angle between $\boldsymbol{x}_{S,i}$ and $\boldsymbol{x}_{S,j}$ satisfying

$$\cos\gamma_{ij} = \cos\theta_{S,i}\cos\theta_{S,j} + \sin\theta_{S,i}\sin\theta_{S,j}\cos(\varphi_{S,i} - \varphi_{S,j}),$$

(5.30) can be expressed by

$$\begin{aligned}\frac{\mathrm{d}\theta_{S,j}}{\mathrm{d}\sigma} &= -\frac{1}{\mathcal{C}_j}\sum_{\substack{i=1\\ i\neq j}}^{N}\frac{S_i}{1-\cos\gamma_{ij}}(\sin\theta_{S,j}\cos\theta_{S,j} - \cos\theta_{S,j}\sin\theta_{S,j}\cos(\varphi_{S,j}-\varphi_{S,j})),\\ \sin\theta_{S,j}\frac{\mathrm{d}\varphi_{S,j}}{\mathrm{d}\sigma} &= -\frac{1}{\mathcal{C}_j}\sum_{\substack{i=1\\ i\neq j}}^{N}\frac{S_i}{1-\cos\gamma_{ij}}\sin\theta_{S,j}\sin(\varphi_{S,j}-\varphi_{S,j}),\end{aligned} \tag{5.31}$$

for $j = 1, 2, \ldots, N$. Writing $\boldsymbol{x}_{S,j}$ as a column vector, (5.31) is equivalent to

$$\frac{\mathrm{d}\boldsymbol{x}_{S,j}}{\mathrm{d}\sigma} = \frac{2}{\mathcal{C}_j}(\boldsymbol{I} - \mathcal{Q}_j)\sum_{\substack{i=1\\ i\neq j}}^{N}\frac{S_i\boldsymbol{x}_{S,i}}{|\boldsymbol{x}_{S,i}-\boldsymbol{x}_{S,j}|^2}, \qquad \mathcal{Q}_j = \boldsymbol{x}_{S,j}\boldsymbol{x}_{S,j}^T, \quad j = 1, 2, \ldots, N. \tag{5.32}$$

Since $\mathcal{C}(S)$ only depends on reaction terms of RD model (1.1), $\mathcal{C}(S)$ of the sphere case and the torus case are the same. Hence, the difference of the evolution equations of spots on the torus (2.52) and sphere (5.30) is only caused by the difference in the Green's functions and local coordinates of torus and sphere. Since the Green's function on the torus is difficult to express to the function of $\boldsymbol{x}$ and $\boldsymbol{x}_j$ as $\log|\boldsymbol{x}_S - \boldsymbol{x}_{S,j}|$ on the sphere, the evolution equation (2.52) on the torus is difficult to obtain the form as (5.32).

5.2 Dynamics of quasi-stationary localized spots on the sphere and torus

We compare the existence and stability of a single spot, two spots, N-ring and twisted and untwisted two N-rings on the unit sphere and torus. The comparison is based on our analysis and numerical simulations in Chapter 3 of the BRD model (1.3) on the torus and the numerical simulations of (5.32) of the BRD model (1.3) on the unit sphere carried in [14, 29]. For $2 < N \leq 10$, the numerical simulations of (5.19) and (5.32) of the BRD model (1.3) was carried in [14, 29] with parameter $f = 0.5$ and $\epsilon = 0.02$. In [14, 29], to generate N initial points, uniformly distributed random variables h_{θ_S} and h_{φ_S} in $(0, 1)$ were generated. Then, the spherical coordinates of initial spot center is given by $\theta_S = \cos^{-1}(2h_{\theta_S} - 1)$ and $\varphi_S = 2\pi h_{\varphi_S}$.

- Since the sphere has rotation invariance, the single spot is a stable equilibrium no matter where this spot is. In the meantime, torus is not constant curvature and the Green's function on the surface depends on the geometric property of the surface. For the case of torus, as shown in the proof of Theorem 3.2.1, there exists bifurcation $\alpha_s \approx 1.2010$ such that for $1 < \alpha < \alpha_s$, the single spot (θ_1, φ_1) on the torus is an equilibrium if and only if $\theta_1 = 0, \vartheta_s(\alpha), \pi, 2\pi - \vartheta_s(\alpha)$ where $\vartheta_s(\alpha) \in (0, \pi)$. The spots at $\theta_1 = 0$ and $\theta_1 = \pi$ on the torus are unstable, while those at $\theta_1 = \vartheta_s(\alpha)$ and $2\pi - \vartheta_s(\alpha)$ are stable. For $\alpha \geq \alpha_s$, the single spot (θ_1, φ_1) on the torus is an equilibrium if and only if $\theta_1 = 0$ or $\theta_1 = \pi$, the spot at $\theta_1 = 0$ is stable and the spot at $\theta_1 = \pi$ is unstable.

- For any two spot cores $(\theta_{S,1}, \varphi_{S,1})$ and $(\theta_{S,2}, \varphi_{S,2})$ on the sphere, we can rotate the sphere such that these cores are symmetric. Hence, for any two spots pattern, $S_1 = S_2 = E$ is a solution of (5.19). Then, Trinh and Ward [29] obtained the following result.

  Theorem 5.2.1. (Lemma 4 in [29]) Let $\gamma_{1,2} = \gamma_{1,2}(\sigma)$ denote the angle between the spot centers $\boldsymbol{x}_{S,1}$ and $\boldsymbol{x}_{S,2}$, i.e. $\boldsymbol{x}_{S,2}^T \boldsymbol{x}_{S,1} = \cos\gamma_{1,2}$. Then, provided that $S_1 = S_2 = E < \Sigma_2(f)$, we have for all time $\sigma = \epsilon^2 t \geq 0$ that

  $$\cos(\gamma_{1,2}/2) = \cos(\gamma_{1,2}(0)/2) e^{-E\sigma/|\mathcal{C}(E)|}. \tag{5.33}$$

  Since $\gamma_{1,2} \to \pi$ as $\sigma \to \infty$ for any $\gamma_{1,2}(0)$, the steady-state two-spot pattern will have spots centered at antipodal points on the sphere for any initial configuration of spots.

  Hence, any initial two-spot pattern on the sphere will move to be $\gamma_{12} = \pi$, the antipodal points on the sphere. Let us remember that the necessary condition of two spot equilibrium on the torus is $\varphi_1 - \varphi_2 = 0$ or $\varphi_1 - \varphi_2 = \pi$. The reason of the existence of necessary condition $\varphi_1 - \varphi_2 = 0$ is that the torus is a genus one surface. Since when $\varphi_1 - \varphi_2 \neq 0$ or π, two spots on the torus will move toward $\varphi_1 - \varphi_2 = \pi$, we obtain $\varphi_1 - \varphi_2 = 0$ is unstable.

- Let us consider a ring configuration of N spots at $\theta_{S,j} = \vartheta_{S,N}$ and $\varphi_{S,j} = (2j-1)\pi/N$ with the same strength $S_j = S_c$ on the unit sphere for $j = 1, \ldots, N$, which is called the N-ring at $\vartheta_{S,N}$. By the symmetry or (5.30), it is easy to confirm that N-ring at the equator $\vartheta_N = \frac{\pi}{2}$ of the sphere is an equilibrium. Theorem 5.2.1 and the numerical simulations of (5.19) and (5.32) in Section 5.1 of [29] shows that 2-rings and 3-rings at equator is stable, but N-rings at equator is unstable for $N \geq 4$. For the case of torus, the N-ring $\vartheta = 0$ and $\vartheta = \pi$ are equilibria for $\alpha > 1$ and there exist $\alpha_m(N)$ and $\alpha_M(N)$ such that N-ring equilibria $\vartheta = \vartheta_s \in (0, \pi)$ and $\vartheta = 2\pi - \vartheta_s$ exist for $\alpha \in (\alpha_m(N), \alpha_M(N))$

for $N \geq 2$. By our numerical computation, we found N-ring $\vartheta = \pi$ and $\vartheta = \vartheta_s \in (0, \pi)$ are unstable and the stability of N-ring $\vartheta = 0$ depends on α: there exists $\alpha_s(N)$ such that N-ring $\vartheta = 0$ is unstable for $1 < \alpha < \alpha_s(N)$ and stable for $\alpha \geq \alpha_s(N)$.

- For the case of sphere, when $N = 8$, numerical result in Section 5.1 of [29] showed that there exist $\theta_S \approx 55.6^\circ$ such that the two twisted 4-rings $(\vartheta_{S,1}, \vartheta_{S,2}) = (\theta_S, 2\pi - \theta_S)$ are a stable equilibrium pattern (Figure 10 in [29]). Numerical result in [29] also indicated that the two untwisted 4-rings on the sphere are unstable and the configuration tends to the twisted two 4-rings $(\vartheta_{S,1}, \vartheta_{S,2}) = (\theta_S, 2\pi - \theta_S)$ as time increases. In the meantime, for the case of torus, the untwisted two N-rings equilibrium $(\vartheta_1, \vartheta_2) = (\vartheta_N(\alpha), 2\pi - \vartheta_N(\alpha))$ exists for $\alpha > 1$ and is unstable as shown in Figure 3.12. The stability of the twisted two N-rings equilibrium $(\vartheta_1, \vartheta_2) = (\vartheta_N(\alpha), 2\pi - \vartheta_N(\alpha))$ on the torus depends on α as shown in Figure 3.12. And we found that there exist stable two N-rings equilibrium $(\vartheta_1, \vartheta_2) = (0, \pi)$ and stable special two N-rings equilibrium $(\vartheta_1, \vartheta_2) = (\vartheta_a(\alpha), \vartheta_b(\alpha))$ on the torus depending on α as shown in Figure 3.13, where $\vartheta_a \in (0, \pi)$, $\vartheta_b \in (\pi, 2\pi)$ satisfying $2\pi < \vartheta_a + \vartheta_b < 3\pi$.

- In [14, 29], it is suggested that there exists a relationship between elliptic Fekete points and stable equilibrium on the sphere when $-\frac{1}{\log \epsilon} \ll 1$, which is reviewed as follows. Let us consider the following regular perturbation expansion. For $-\frac{1}{\log \epsilon} \ll 1$ and given spots cores (θ_j, φ_j) on the torus, $j = 1, \ldots, N$, suppose that $E \sim \mathcal{O}(1)$ and $S_j \sim \mathcal{O}(1)$ for $j = 1, \ldots, N$, we then obtain the following regular perturbation expansion:

$$\mathbf{S} = \mathbf{S}_0 + \frac{1}{\log \epsilon}\mathbf{S}_1 + \frac{1}{(\log \epsilon)^2}\mathbf{S}_2 + \cdots, \tag{5.34}$$

where $\mathbf{S} = (S_1, \ldots, S_N)$ and $\mathbf{S}_i = (S_{1,i}, \ldots, S_{N,i})^T$ for $i = 0, 1, 2, \ldots$. Similarly, we have

$$\boldsymbol{\chi} = \boldsymbol{\chi}_0 + \mathcal{O}\left(\frac{1}{\log \epsilon}\right), \tag{5.35}$$

where $\boldsymbol{\chi} = (\chi(S_{1,0}; f), \ldots, \chi(S_{N,0}; f))^T$. By substituting (5.34) and (5.35) into (2.29), matching the leading order and next order of $\frac{1}{\log \epsilon}$, we obtain $\mathbf{S}_0 = \frac{2\pi r R E}{N}\boldsymbol{e}$ and $\mathbf{S}_1 = (I - \boldsymbol{e}_0)\chi_0 - (I - \boldsymbol{e}_0)(\mathcal{G} - \mathbf{P} + \mathcal{K} + \mathcal{Q})\mathbf{S}_0$. When $\mathbf{S}_0 = \frac{2\pi r R E}{N}\boldsymbol{e}$, we have $(I - \boldsymbol{e}_0)\chi_0 = 0$ and $(I - \boldsymbol{e}_0)\mathcal{K} = 0$. Then, we obtain

$$\mathbf{S} \sim \frac{2\pi r R E}{N}\left(\boldsymbol{e} - \frac{1}{\log \epsilon}(I - \boldsymbol{e}_0)(\mathcal{G} - \mathbf{P} + \mathcal{Q})\boldsymbol{e}\right). \tag{5.36}$$

Hence, under the assumption, we obtain $S_j \to S_c = \frac{2\pi r R E}{N}$ as $-\frac{1}{\log \epsilon} \to 0$. Similarly, for the case of the unit sphere, as shown in [29], when $E \sim \mathcal{O}(1)$ and $S_j \sim \mathcal{O}(1)$ for $j = 1, \ldots, N$, the regular perturbation expansion of (5.19) yields

$$\boldsymbol{S} \sim \frac{2E}{N}(\boldsymbol{e} - \frac{1}{\log \epsilon}(\boldsymbol{I} - \boldsymbol{e}_0)\boldsymbol{L}\boldsymbol{e}), \tag{5.37}$$

where $\boldsymbol{L}$ is defined in (5.16). Let $\{\boldsymbol{x}_{S,1}, \ldots, \boldsymbol{x}_{S,N}\}$ be a set of points on the unit sphere. Then, elliptic Fekete points is the point set on the unit sphere such that this sets globally minimizes the discrete logarithmic energy

$$V = -\sum_{i=1}^{N}\sum_{j=i+1}^{N} \log|\boldsymbol{x}_{S,i} - \boldsymbol{x}_{S,j}|. \tag{5.38}$$

If we ignore the constraint (5.19) and set $S_j = 1$ in (5.30), we obtain

$$\frac{\mathrm{d}V}{\mathrm{d}\sigma} = \sum_{j=1}^{N} \left(\frac{\partial V}{\partial \theta_{S,j}} \frac{\mathrm{d}\theta_{S,j}}{\mathrm{d}\sigma} + \frac{\partial V}{\partial \varphi_{S,j}} \frac{\mathrm{d}\varphi_{S,j}}{\mathrm{d}\sigma} \right) = \frac{2}{\mathcal{C}(1)} \sum_{j=1}^{N} \left(\alpha_{S,j,1}^2 + \alpha_{S,j,2}^2 \right) \leq 0, \tag{5.39}$$

where $\mathcal{C}(1) < 0$. Hence, it seems that there exists a relationship between elliptic Fekete point set and equilibrium of (5.32) and (5.19) when $\frac{1}{\log \epsilon} \to 0$. [29] found that the cores of the stable twisted two 4-rings $(\vartheta_{S,1}, \vartheta_{S,2}) = (\theta_S, 2\pi - \theta_S)$ on the sphere is an elliptic Fekete point set, where $\theta_S \approx 55.6^\circ$. Jamieson-Lane et al. [14] concluded that equilibrium spot configurations for $N = 3, \ldots, 10$ in their numerical simulations having a large basin of attraction are indeed elliptic Fekete point sets.

In the case of torus, let us define the energy function $V_{\mathbb{T}_{R,r}}(\theta_1, \ldots, \theta_N, \varphi_1, \ldots, \varphi_N)$ of N-spot pattern as follow:

$$\begin{aligned} &V_{\mathbb{T}_{R,r}}(\theta_1, \ldots, \theta_N, \varphi_1, \ldots, \varphi_N) \\ &= -\sum_{j=1}^{N} \sum_{i=j+1}^{N} \widetilde{G}_i(\theta_j, \varphi_j)) - \sum_{j=1}^{N} \left(2\pi F(\theta_j) + \frac{1}{4\pi \mathcal{A}} K^2(\theta_j) - \frac{1}{2} \int_0^{\theta_j} \frac{\sin\theta}{\alpha - \cos\theta} \mathrm{d}\theta \right). \end{aligned} \tag{5.40}$$

The function $V_{\mathbb{T}_{R,r}}$ is periodic satisfying $V_{\mathbb{T}_{R,r}}(\theta_1, \ldots\ldots, \theta_N, \varphi_1, \ldots, \varphi_N) = V_{\mathbb{T}_{R,r}}(\theta_1, \ldots, \theta_j + 2\pi, \ldots, \theta_N, \varphi_1, \ldots, \varphi_N) = V_{\mathbb{T}_{R,r}}(\theta_1, \ldots, \theta_N, \varphi_1, \ldots, \varphi_j + 2\pi, \ldots, \varphi_N)$ for any $j = 1, \ldots, N$. If we fix $S_j = 1$ in (2.52) and ignore the constraint (2.29), $V_{\mathbb{T}_{R,r}}$ satisfies

$$\frac{\partial V_{\mathbb{T}_{R,r}}}{\partial \theta_j} = -r\alpha_{j,1}, \qquad \frac{\partial V_{\mathbb{T}_{R,r}}}{\partial \varphi_j} = -(R - r\cos\theta_j)\alpha_{j,2}.$$

Hence, if we fix $S_j = 1$ in (2.52) and ignore the constraint (2.29), $V_{\mathbb{T}_{R,r}}$ is regarded as a Lyapunov function, since

$$\frac{\mathrm{d}V_{\mathbb{T}_{R,r}}}{\mathrm{d}\sigma} = \sum_{j=1}^{N} \left(\frac{\partial V_{\mathbb{T}_{R,r}}}{\partial \theta_j} \frac{\mathrm{d}\theta_j}{\mathrm{d}\sigma} + \frac{\partial V_{\mathbb{T}_{R,r}}}{\partial \varphi_j} \frac{\mathrm{d}\varphi_j}{\mathrm{d}\sigma} \right) = \frac{2}{\mathcal{C}(1)} \sum_{j=1}^{N} (\alpha_{j,1}^2 + \alpha_{j,2}^2) \leq 0. \tag{5.41}$$

The local and global minima of the energy $V_{\mathbb{T}_{R,r}}(\theta_1, \ldots, \theta_N, \varphi_1, \ldots, \varphi_N)$ depend not only on N, but also on α. Investigating the relationship of minima of the energy $V_{\mathbb{T}_{R,r}}$ and stable equilibria of (2.52) for $-\frac{1}{\log \epsilon} \ll 1$ is left open for future research.

Chapter 6

Summary

By using the method of matched asymptotic expansions, we have constructed quasi-stationary states consisting of localized spots appearing in the reaction-diffusion system (1.1) on the surface of a torus. Under the assumption that these localized spots persist stably for a long time, the ODEs describing the slow dynamics of the spot cores are derived in the slow-time scale $\sigma = \epsilon^2$. Utilizing the analytic expression of the Green's function of the Laplace–Beltrami operator on the toroidal surface, we derive the ODEs analytically, thereby investigating the existence of equilibria with a mathematical rigor. We have considered the five kinds of spot configurations: spots at the outermost or the innermost, a single spot, two spots, the N-ring configuration where N localized spots are equally spaced along a latitudinal line, and the two N-rings configuration where N localized spots are equally spaced along a latitudinal line and the other N localized spots are equally spaced along another latitudinal line. The theoretical results agree with nonlinear evolutions of the BRD model (1.3) that are obtained by numerical means, which are summarized and compared with the dynamics of results on the sphere [14, 29].

- Spots at the outermost ($\theta_j = \pi$) or the innermost ($\theta_j = 0$) locations on the torus, $j = 1, 2, \ldots, N$ are always equilibria in θ direction, i.e., $\frac{\mathrm{d}\theta_j}{\mathrm{d}\sigma} = 0$ if $\theta_i = 0$ or π for $i = 1, 2, \ldots, N$.

- The single spots at the outermost ($\theta_1 = \pi$) and the innermost ($\theta_1 = 0$) locations on the torus are always equilibria for $\alpha > 1$. On the other hand, there exist special locations $\theta_1 = \vartheta_s(\alpha) \in (0, \pi)$ and $2\pi - \vartheta_s(\alpha) \in (\pi, 2\pi)$ at which the single spot becomes an equilibrium for $1 < \alpha < \alpha_s \approx 1.201$. The single spot at $\theta_1 = \pi$ is always linearly unstable, and those at $\theta_1 = \vartheta_s(\alpha)$ and $2\pi - \vartheta_s(\alpha)$ are stable as long as they exist. The single spot at $\theta = 0$ is unstable for $1 < \alpha < \alpha_s$, whereas its stability changes when $\vartheta_s(\alpha) \to 0$ as $\alpha \to \alpha_s$. It is interesting to consider a geometric or physical interpretation of this special angle $\vartheta_s(\alpha)$, which is a future problem. Let us remember that a single point on the sphere at any location is always a stable equilibrium [29].

- Quasi-stationary states consisting of two localized spots are necessarily on the axial section of the torus, i.e., $\varphi_1 = \varphi_2$ or $|\varphi_2 - \varphi_1| = \pi$. We obtain $\varphi_1 = \varphi_2$ is unstable, the spots will move to $|\varphi_2 - \varphi_1| = 0$ after perturbation. In the meantime, two spots patterns on the sphere are equilibria if and only if spots centered at antipodal points [29].

- The N-ring ($N \geq 2$) at the outermost ($\theta = \pi$) and the innermost ($\theta = 0$) latitudinal lines on the torus are equilibria for $\alpha > 1$. We also obtain a range of the aspect ratio

$\alpha \in (\alpha_m(N), \alpha_M(N))$ such that there exists $\vartheta_N(\alpha) \in (0, \pi)$ for $N \geq 2$. We observe the linear stability of these N-ring configurations of the BRD model on the torus. The outermost N-ring is always unstable, while there exists an aspect ratio $\alpha_s(N)$ such that the innermost one is unstable (resp., neutrally stable) for $1 < \alpha < \alpha_s(N)$ (resp., $\alpha \geq \alpha_s(N)$). N-ring at $\vartheta_N(\alpha)$ and $2\pi - \vartheta_N(\alpha)$ are unstable equilibria as long as they exist. Quasi-stationary solutions of the BRD model consisting of the unstable N-ring are numerically investigated. The unstable N-ring spots are moving toward stable quasi-stationary states having nonsymmetric configuration of N spots, indicating the existence of more nontrivial spot equilibria that are stable. On the other hand, for the sphere case, the N-ring at equator is a stable (resp., unstable) equilibrium for $N \leq 3$ (resp., $N \geq 4$).

- The twisted and untwisted two N-rings at $(\vartheta_1, \vartheta_2) = (0, \pi)$ are equilibria on the torus for $\alpha > 1$. In addition, the strengths of two N-rings at $(\vartheta_1, \vartheta_2) = (0, \pi)$ are not identical, nor they are uniquely obtained. We also obtain the existence of equilibria for the twisted and untwisted two N rings at $(\vartheta_1, \vartheta_2) = (\vartheta_N, 2\pi - \vartheta_N)$ with identical strength $S_j = S_c$, $j = 1, 2, \ldots, 2N$. For $\alpha > 1$, there exists $\vartheta_N(\alpha)$ such that the untwisted two N rings at $(\vartheta_1, \vartheta_2) = (\vartheta_N(\alpha), 2\pi - \vartheta_N(\alpha))$ is an equilibrium and unstable. We also obtain a range of the aspect ratio $\alpha \in (1, \alpha_d(N))$ where there exists the twisted two N-rings at $(\vartheta_1, \vartheta_2) = (\vartheta_N(\alpha), 2\pi - \vartheta_N(\alpha))$. Our numerical results obtain the stability of the twisted two N rings at $(\vartheta_1, \vartheta_2) = (\vartheta_N(\alpha), 2\pi - \vartheta_N(\alpha))$ is complicated and we obtain a bifurcation diagram showing the relationship between the twisted two N-rings at $(\vartheta_1, \vartheta_2) = (\vartheta_N(\alpha), 2\pi - \vartheta_N(\alpha))$ and the twisted two N-rings at $(\vartheta_1, \vartheta_2) = (0, \pi)$. In the meantime, the two twisted 4-rings at $(\vartheta_1, \vartheta_2) = (\vartheta_N, 2\pi - \vartheta_N)$ on the sphere is stable [29].

- By carrying the numerical simulation of (5.32) and (5.19), the stable equilibria of evolution equation (5.32) coincide with elliptic Fekete point for $N = 2, \ldots, 10$ is found in [14, 29]. For the case of torus, we derive the energy $V_{\mathbb{T}_{R,r}}$ related to evolution equation (2.52), but the relationship between the minima of $V_{\mathbb{T}_{R,r}}$ and equilibria of (2.52) is left open for future research.

Appendix A

Asymptotic Expansions of the Green's Function

We introduce the asymptotic expansion and the partial derivative of the Green's function the which are used in the derivation in Chapter 2. The asymptotic expansion of the Green's function (2.15) with respect to ϵ up to $\mathcal{O}(\epsilon)$ is provided in what follows. Since

$$\begin{aligned}
\frac{\zeta(\theta,\varphi)}{\zeta(\theta_i,\varphi_i)} &= e^{i(\varphi-\varphi_i)}\exp\left(-\int_{\theta_i}^{\theta}\frac{\mathrm{d}\eta}{\alpha-\cos\eta}\right) \\
&= 1 + i(\varphi-\varphi_i) - \frac{r}{R-r\cos\theta_i}(\theta-\theta_i) - \frac{1}{2}(\varphi-\varphi_i)^2 - i\frac{r}{R-r\cos\theta_i}(\varphi-\varphi_i)(\theta-\theta_i) \\
&\quad + \frac{1}{2}\left(\frac{r^2}{(R-r\cos\theta_i)^2} + \frac{r^2\sin\theta_i}{(R-r\cos\theta_i)^2}\right)(\theta-\theta_i)^2 + \cdots \\
&= 1 - \frac{\epsilon}{R-r\cos\theta_i}y_1 - \frac{\epsilon^2}{2(R-r\cos\theta_i)^2}y_2^2 + \frac{\epsilon^2(1+\sin\theta_i)}{2(R-r\cos\theta_i)^2}y_1^2 \\
&\quad + \frac{i\epsilon}{R-r\cos\theta_i}y_2 - i\frac{\epsilon^2}{(R-r\cos\theta_i)^2}y_1y_2 + \mathcal{O}(\epsilon^3),
\end{aligned} \tag{A.1}$$

we obtain, as $\boldsymbol{x}\to\boldsymbol{x}_i$,

$$\begin{aligned}
&\log\left|1-\frac{\zeta(\theta,\varphi)}{\zeta(\theta_i,\varphi_i)}\right| - \log\rho \\
&= \log\left|-y_1 - \frac{\epsilon y_2^2}{2(R-r\cos\theta_i)} + \frac{\epsilon(1+\sin\theta_i)y_1^2}{2(R-r\cos\theta_i)} + i\left(y_2 - \frac{\epsilon y_1y_2}{(R-r\cos\theta_i)}\right) + \mathcal{O}(\epsilon^2)\right| \\
&\quad + \log\left|\frac{\epsilon}{R-r\cos\theta_i}\right| - \log\rho \\
&= \frac{1}{2}\log\left((y_1^2+y_2^2)\left(1 + \frac{\epsilon}{(R-r\cos\theta_i)(y_1^2+y_2^2)}(-y_1y_2^2 - (1+\sin\theta_i)y_1^3 + \mathcal{O}(\epsilon))\right)\right) \\
&\quad + \log\epsilon - \log(R-r\cos\theta_i) - \log\rho \\
&= \log\epsilon - \log(R-r\cos\theta_i) - \frac{\epsilon(1+\sin\theta_i)y_1}{2(R-r\cos\theta_i)} + \frac{\epsilon\sin\theta_i y_1y_2^2}{2\rho^2(R-r\cos\theta_i)} + \mathcal{O}(\epsilon^2).
\end{aligned} \tag{A.2}$$

Regarding $W_j(\theta,\varphi)$, setting $E_{i,j}=\exp\left(-\int_{\theta_i}^{\theta_j}\frac{\mathrm{d}\eta}{\alpha-\cos\eta}\right)$ and $s=\exp(-2\pi\mathcal{A})$, we obtain

$$\begin{aligned}
h_{i,j,n}=&\left.\frac{\partial\log\left|\left(1-e^{-2n\pi\mathcal{A}}\frac{\zeta(\theta,\varphi_j)}{\zeta(\theta_i,\varphi_i)}\right)\left(1-e^{-2n\pi\mathcal{A}}\left(\frac{\zeta(\theta,\varphi_j)}{\zeta(\theta_i,\varphi_i)}\right)^{-1}\right)\right|}{\partial\theta}\right|_{\theta=\theta_j}\\
=&\frac{1}{\alpha-\cos\theta_j}\left(\frac{s^n\cos(\varphi_j-\varphi_i)E_{i,j}-s^{2n}E_{i,j}^2}{1-2s^n\cos(\varphi_j-\varphi_i)E_{i,j}+s^{2n}E_{i,j}^2}-\frac{s^n\cos(\varphi_j-\varphi_i)E_{i,j}^{-1}-s^{2n}E_{i,j}^{-2}}{1-2s^n\cos(\varphi_j-\varphi_i)E_{i,j}^{-1}+s^{2n}E_{i,j}^{-2}}\right)\\
=&\frac{1}{\alpha-\cos\theta_j}\frac{(E_{i,j}^{-1}-E_{i,j})\left(-(1+s^{2n})s^n\cos(\varphi_j-\varphi_i)+s^{2n}(E_{i,j}^{-1}+E_{i,j})\right)}{(1+s^{2n}-s^n\cos(\varphi_j-\varphi_i)(E_{i,j}+E_{i,j}^{-1}))^2+(s^n\sin(\varphi_j-\varphi_i)(E_{i,j}-E_{i,j}^{-1}))^2},
\end{aligned}\tag{A.3}$$

$$\begin{aligned}
w_{i,j,n}=&\left.\frac{\partial\log\left|\left(1-e^{-2n\pi\mathcal{A}}\frac{\zeta(\theta_j,\varphi)}{\zeta(\theta_i,\varphi_i)}\right)\left(1-e^{-2n\pi\mathcal{A}}\left(\frac{\zeta(\theta_j,\varphi)}{\zeta(\theta_i,\varphi_i)}\right)^{-1}\right)\right|}{\partial\varphi}\right|_{\varphi=\varphi_j}\\
=&\frac{s^n\sin(\varphi_j-\varphi_i)E_{i,j}}{1-2s^n\cos(\varphi_j-\varphi_i)E_{i,j}+s^{2n}E_{i,j}^2}+\frac{s^n\sin(\varphi_j-\varphi_i)E_{i,j}^{-1}}{1-2s^n\cos(\varphi_j-\varphi_i)E_{i,j}^{-1}+s^{2n}E_{i,j}^{-2}},\\
=&\frac{\sin(\varphi_j-\varphi_i)s^n\left(\left(E_{i,j}+E_{i,j}^{-1}\right)(1+s^{2n})-4s^n\cos(\varphi_j-\varphi_i)\right)}{(1+s^{2n}-s^n\cos(\varphi_j-\varphi_i)(E_{i,j}+E_{i,j}^{-1}))^2+(s^n(E_{i,j}-E_{i,j}^{-1})\sin(\varphi_j-\varphi_i))^2},
\end{aligned}\tag{A.4}$$

$$\begin{aligned}
t_{i,j}=&\left.\frac{\partial\log\left|1-\frac{\zeta(\theta,\varphi_j)}{\zeta(\theta_i,\varphi_i)}\right|}{\partial\theta}\right|_{\theta=\theta_j}\\
=&\frac{1}{\alpha-\cos\theta_j}\frac{(1-\cos(\varphi_j-\varphi_i)E_{i,j})\cos(\varphi_j-\varphi_i)E_{i,j}-\sin^2(\varphi_j-\varphi_i)E_{i,j}^2}{(1-\cos(\varphi_j-\varphi_i)E_{i,j})^2+(\sin(\varphi_j-\varphi_i)E_{i,j})^2}\\
=&\frac{1}{\alpha-\cos\theta_j}\frac{\cos(\varphi_j-\varphi_i)E_{i,j}-E_{i,j}^2}{(1-\cos(\varphi_j-\varphi_i)E_{i,j})^2+(\sin(\varphi_j-\varphi_i)E_{i,j})^2},
\end{aligned}\tag{A.5}$$

and

$$\begin{aligned}
o_{i,j}=&\left.\frac{\partial\log\left|1-\frac{\zeta(\theta_j,\varphi)}{\zeta(\theta_i,\varphi_i)}\right|}{\partial\varphi}\right|_{\varphi=\varphi_j}\\
=&\frac{(1-\cos(\varphi_j-\varphi_i)E_{i,j})\sin(\varphi_j-\varphi_i)E_{i,j}+\sin(\varphi_j-\varphi_i)\cos(\varphi_j-\varphi_i)E_{i,j}^2}{(1-\cos(\varphi_j-\varphi_i)E_{i,j})^2+(\sin(\varphi_j-\varphi_i)E_{i,j})^2}\\
=&\frac{\sin(\varphi_j-\varphi_i)E_{i,j}}{(1-\cos(\varphi_j-\varphi_i)E_{i,j})^2+(\sin(\varphi_j-\varphi_i)E_{i,j})^2}.
\end{aligned}\tag{A.6}$$

When $\theta_i=\theta_j$, we have $E_{i,j}=E_{i,j}^{-1}=1$ and $\sin(\varphi_j-\varphi_i)=0$ for $\varphi_i=\varphi_j$, (A.3) and (A.4) yield

$$\left.\frac{\partial\log W_j(\theta,\varphi_j)}{\partial\theta}\right|_{\theta=\theta_j}=0,\qquad\left.\frac{\partial\log W_j(\theta_j,\varphi)}{\partial\varphi}\right|_{\varphi=\varphi_j}=0.\tag{A.7}$$

Appendix B

An Algorithm to Solve $\boldsymbol{g}(\boldsymbol{S}) = \mathbf{0}$

In order to construct the localized spot solution of BRD model (1.3), we need to solve the nonlinear equation $\boldsymbol{g}(\boldsymbol{S}) = \mathbf{0}$ (2.29) for S_j, $j = 1, \ldots, N$. We introduce the numerical method to solve (2.29) as follows, which are used in the numerical computation of Chapter 3. The parameters are set as $\Delta S = 10^{-8}$ and $tol = 10^{-8}$.

(Step 0) Computing $\overline{\chi}(S)$ for discrete values $S = 0.001, 0.002, \ldots, 8.000$ by solving the boundary value problem (2.53), we approximate the map $\overline{\chi}(S)$ by using the cubic spline interpolation. The initial guess is given by $\boldsymbol{S}^{(0)} = (S_c, \ldots, S_c)^T$ with $S_c = 2\pi RrE/N$ and set $k = 0$. This step is done only once.

(Step 1) Compute $\boldsymbol{\chi}(\boldsymbol{S}^{(k)})$ and $\boldsymbol{\chi}(\boldsymbol{S}^{(k)} \pm \Delta S \boldsymbol{e}_j)$ for $j = 1, \ldots, N$, where $\boldsymbol{e}_j$ is the unit vector whose jth component is 1. Each component of $\boldsymbol{\chi}$ is obtained from the piecewise cubic approximation of $\overline{\chi}(S)$ constructed in Step 0.

(Step 2) Compute the Jacobi matrix $\mathcal{J}(\boldsymbol{S}) = \{J_{ij}(\boldsymbol{S})\}$, $i, j = 1, \ldots, N$ of $\boldsymbol{g}(\boldsymbol{S})$ at $\boldsymbol{S} = \boldsymbol{S}^{(k)}$. Each entity is approximated by the central finite difference.

$$J_{ij}\left(\boldsymbol{S}^{(k)}\right) = \frac{g_i\left(\boldsymbol{S}^{(k)} + \Delta S \boldsymbol{e}_j\right) - g_i\left(\boldsymbol{S}^{(k)} - \Delta S \boldsymbol{e}_j\right)}{2\Delta S},$$

in which g_i is the ith component of $\boldsymbol{g}$.

(Step 3) Solve the linear equation $\mathcal{J}(\boldsymbol{S}^{(k)})\Delta \boldsymbol{g} = \boldsymbol{g}(\boldsymbol{S}^{(k)})$ with respect to $\Delta \boldsymbol{g}$.

(Step 4) If $|\Delta \boldsymbol{g}| < tol$, then $\boldsymbol{S}^{(k)}$ is the approximate solution of $\boldsymbol{S}$, and we go to Step 5. Otherwise, we set $\boldsymbol{S}^{(k+1)} = \boldsymbol{S}^{(k)} - \Delta \boldsymbol{g}$ and $k = k + 1$. Then we go back to Step 1.

(Step 5) The constant $\overline{v}$ is computed from the approximate solution through (2.28).

Appendix C

A Brief Introduction of Surface Finite Element Method

In this chapter, we briefly introduce surface finite element method and give an example of the discrete BRD model (1.3) by this method.

C.1 Piecewise linear hat function

Definition C.1.1. A k-simplex σ in $\mathbb{R}^n$ with $0 \leq k \leq n$ is a convex hull of $(k+1)$ ordered vertices $\{v_0, v_1, \ldots, v_k\}$, where $v_0, v_1, \ldots, v_k \in \mathbb{R}^n$ satisfy that $(v_1 - v_0, v_2 - v_0, \ldots, v_k - v_0)$ are linearly independent. Then, the k-simplex σ can be written as

$$\sigma = \left\{ \sum_{i=0}^{k} \lambda_i v_i \middle| \sum_{i=0}^{k} \lambda_i = 1, 0 \leq \lambda_i \right\}.$$

We use $[v_0, v_1, \ldots, v_k]$ to represent the k-simplex σ with vertices $\{v_0, v_1, \ldots, v_k\}$. For example, in $\mathbb{R}^3$, a 0-simplex is a vertex, 1-simplex is an edge, a 2-simplex is a triangle, and a 3-simplex is a tetrahedron.

Definition C.1.2. Let $\sigma_a = [v_{a_0}, \ldots, v_{a_i}], \sigma_b = [v_{b_0}, \ldots, v_{b_j}]$ be simplices in $\mathbb{R}^n$. Then σ_b is said to be a face of σ_a, if $\{v_{b_0}, \ldots, v_{b_j}\} \subset \{v_{a_0}, \ldots, v_{a_i}\}$.

For example, $[v_0]$ and $[v_1]$ are the faces of $[v_0, v_1]$.

Definition C.1.3. A simplicial complex K in $\mathbb{R}^{n+1}$ is a collection of simplices σ_i in $\mathbb{R}^{n+1}$ such that

(i) If simplex $\sigma \in K$, then every face of σ belongs to K,

(ii) If simplices $\alpha, \beta \in K$, then $\alpha \cap \beta = \emptyset$ or $\alpha \cap \beta$ is the common face of α and β.

The dimension of the largest dimensional simplex in K is called the dimension of K.

Definition C.1.4. n-dimensional simplicial complex M in $\mathbb{R}^{n+1}$ is called simplicial surface if M satisfies that for every k-simplex $s_1 \in M$, $0 \leq k < n$, there exists a n-simplex $s_2 \in M$ such that s_1 is a face of s_2.

Hence, a simplicial surface M in $\mathbb{R}^3$ is a set of closed triangles satisfying that the intersection of two different closed triangles in M is empty or a vertex of each of the triangles or an edge of each of the triangles.

Definition C.1.5. Let M be a simplicial surface in $\mathbb{R}^{n+1}$ and set $\{v_i\}_{i=0}^m$ denote the vertices set of M. The piecewise linear hat function $\phi_i : M \to \mathbb{R}$ corresponding to v_i is defined as follow:

(i) For any vertex v_j,

$$\phi_i(v_j) = \delta_{ij}, \tag{C.1}$$

where δ is Kronecker delta function.

(ii) For any k-simplex $\Gamma_s = [v_{s0}, v_{s1}, \ldots, v_{sk}] \in M$, $\phi_i : \Gamma_s \to \mathbb{R}$ is a linear function defined as follows. For any $p = (x_{p,1}, x_{p,2}, \ldots, x_{p,n+1}) \in \Gamma_s \in \mathbb{R}^{n+1}$, there exists a unique set $a_0, \ldots, a_k \in \mathbb{R}$, such that $p = a_0 v_{s0} + \cdots a_k v_{sk}$. Then, $\phi_i(p)$ is defined by

$$\phi_i(p) = \phi_i(a_0 v_{s0} + \cdots a_k v_{sk}) = a_0\phi_i(v_{s0}) + \cdots a_k\phi_i(v_{sk}). \tag{C.2}$$

Since ϕ_i equals 1 at v_i and equals 0 at other vertices, it looks like a hat. Let M be a simplicial surface in $\mathbb{R}^3$. The set $\{v_i\}_{i=0}^m$ is vertices set of M. By Definition C.1.5, we obtain for triangle $\triangle_{v_iv_jv_k}$, $\phi_i : \triangle_{v_iv_jv_k} \to \mathbb{R}$ can be expressed by

$$\phi_i(q) = 1 - \frac{\left|\overrightarrow{qv_i} \cdot \overrightarrow{h}\right|}{h^2}, \tag{C.3}$$

where h is the height of edge $[v_k, v_j]$ in $\triangle v_iv_jv_k$ as shown in Figure C.1 and $\overrightarrow{h} = \overrightarrow{pv_i}$. Here p is the perpendicular foot on the line of $[v_j, v_k]$.

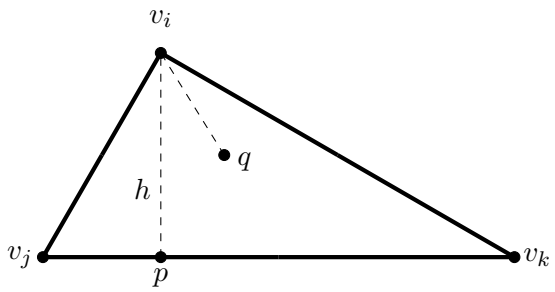

Figure C.1: The figure corresponds to (C.3) and Theorem C.2.3. h is the height of $[v_j, v_k]$ and p is the perpendicular foot.

Let $u : M \to \mathbb{R}$ be a continuous scalar function, and $\{\sigma_k\}$ be the triangle set of M. Let $\mathrm{I\!I}_h$ denote the Lagrange interpolation operator of M which is defined by

$$\mathrm{I\!I}_h u = \sum_{i=0}^{n} u(v_i)\phi_i, \tag{C.4}$$

where ϕ_i is the piecewise linear hat function of v_i.

C.2 Surface finite element method and approximation

In this section, based on [8, 9, 10], we introduce some basic notations of surface finite element method. Let Γ be a compact smooth oriented connected surface in $\mathbb{R}^{n+1}$. We suppose that there exists a smooth level set function $d(x)$, $x \in \mathbb{R}^{n+1}$ satisfying

$$\Gamma = \{x \in \mathcal{S} | d(x) = 0\}, \tag{C.5}$$

where $\mathcal{S}$ is an open set of $\mathbb{R}^{n+1}$ which depends on $d(x)$ satisfying $\nabla d \neq 0$ in $\mathcal{S}$ and $d \in C^2(\mathcal{S})$. We can choose signed distance function to be $d(x)$, and $v(x) = \nabla d(x)$ to be the unit normal of Γ. Then, we choose $\mathcal{S}$ to satisfy that for any $x \in \mathcal{S}$, the exists an unique $y(x) \in \Gamma$ such that

$$x = y(x) + d(x)v(y(x)). \tag{C.6}$$

Definition C.2.1. The projection matrix P of Γ is defined by $\forall x \in \Gamma$, for any vector $X \in \mathbb{R}^{n+1}$ such that

$$P(x)X = X - (X \cdot v)v. \tag{C.7}$$

And (i, j)-element of $P(x)$ can be express by

$$P(x)_{ij} = \delta_{ij} - v(x)_i v(x)_j. \tag{C.8}$$

where δ is the Kronecker delta.

Let functions $f \in C^2(\mathcal{S})$ and $g \in C^1(\mathcal{S})$. Then, the gradient and Laplace–Beltrami operator of f on Γ is defined by:

Definition C.2.2. The tangential gradient of f on Γ is defined by

$$\nabla_\Gamma f = \nabla f - (\nabla f \cdot v)\, v = P \nabla f. \tag{C.9}$$

The components of the tangent gradient is denoted by $\nabla_\Gamma f = (\underline{D}_1 f, \ldots, \underline{D}_{n+1} f)$. Then, the Laplace–Beltrami operator on Γ is defined by

$$\triangle_\Gamma f = \nabla_\Gamma \cdot \nabla_\Gamma f = \sum_{i=1}^{n+1} \underline{D}_i \underline{D}_i f. \tag{C.10}$$

As proofed in [10], the Green's identity of Laplace–Betrami $\triangle_\Gamma$ is given by

Theorem C.2.1.

$$\int_\Gamma g \triangle_\Gamma f = \int_{\partial\Gamma} g \nabla f \cdot u - \int_\Gamma \nabla_\Gamma g \cdot \nabla_\Gamma f, \tag{C.11}$$

where u is the unit normal on $\partial\Gamma$, tangential to Γ.

Let Γ be a compact smooth oriented connected surface in $\mathbb{R}^3$ and be approximated by a simplicial surface Γ_h, a triangulated surface consisting of triangles, h denote the maximum diameter of triangles in Γ_h and inner radius of triangles be bounded below by ch with some constant $c > 0$. The vertices set of Γ_h is denoted by $\{v_i\}_{i=1}^n$, where $v_i \in \Gamma$ and the piecewise linear hat function corresponding to v_i is denoted by ϕ_i for $i = 1, 2, \ldots, n$. Suppose that for every $y \in \Gamma$, there only exists a unique $x \in \Gamma_h$ satisfying

$$x(y) = y + d(x(y))v(y). \tag{C.12}$$

Then, from (C.6) and (C.12), there exists a bijective function between Γ and Γ_h. For any function $f \in C^0(\Gamma_h)$, f^l denotes the lift of f onto Γ by

$$f^l(y) = f(x(y)), \quad y \in \Gamma. \tag{C.13}$$

Similarly, for any function $g \in C^0(\Gamma)$, g^{-l} denotes the inverse function onto Γ_h by

$$g^{-l}(x) = g(y(x)), \quad x \in \Gamma_h. \tag{C.14}$$

Let us define operator $\amalg_h^l : C^0(\Gamma) \to C^0(\Gamma)$ by $\amalg_h^l g = (\amalg_h g^{-l})^l$ for $g \in C^0(\Gamma)$. The following estimate bewteen g and $\amalg_h^l g$ is derived in [10]

Theorem C.2.2. For any $g \in W^{2,2}(\Gamma)$, we have

$$||g - \amalg_h^l g||_{L^2(\Gamma)} + h||\nabla_\Gamma(g - \amalg_h^l g)||_{L^2(\Gamma)} \leq ah^2(||\nabla_\Gamma^2 g||_{L^2(\Gamma)} + h||\nabla_\Gamma g||_{L^2(\Gamma)}), \tag{C.15}$$

where $a \in \mathbb{R}$ is a constant independent of h, $W^{k,p}$ is Sobolev space, $\nabla_\Gamma^2 f^l$ and $\nabla_{\Gamma_h}^2 f$ denote the second tagential derivatives matrix of f^l and f. The component of $\nabla_\Gamma^2 f^l$ and $\nabla_{\Gamma_h}^2 f$ can be express by $(\nabla_\Gamma^2 f^l)_{ij} = \underline{D_i D_j f^l}$, $(\nabla_{\Gamma_h}^2 f)_{ij} = \underline{D_{h,i} D_{h,j}} f$. The L^2-norm of the vector and matrix denotes the L^2-norm of its components.

Using Green's identity (C.11) and the piecewise linear hat function of finite element method, some partial differential equation can be approximated by linear system of equations. For example, if Γ is a surface without boundary in $\mathbb{R}^3$ approximated by Γ_h with vertices set $\{v_1, \ldots, v_n\}$, we can approximate the heat equation $a_t = \triangle_\Gamma a$ on Γ as follows. Let ϕ_i denote the piecewise linear hat function of vertex i of Γ_h , $i = 1, \ldots, n$. Let $\widetilde{a}(\cdot, t) \in C^2(\Gamma_h)$ be the weak solution of the following equation: for $i = 1, 2, \ldots, n$,

$$\int_{\Gamma_h} \phi_i \widetilde{a}_t \mathrm{d}S = \int_{\Gamma_h} \phi_i \triangle_{\Gamma_h} \widetilde{a} \mathrm{d}S. \tag{C.16}$$

By using Green's identity (C.11) and $\partial\Gamma_h = \emptyset$, we obtain

$$\int_{\Gamma_h} \phi_i \widetilde{a}_t \mathrm{d}S = -\int_{\Gamma_h} \nabla_{\Gamma_h} \phi_i \nabla_{\Gamma_h} \widetilde{a} \mathrm{d}S, \tag{C.17}$$

Setting

$$\widetilde{a}(\cdot, t) = \sum_{i=0}^{n} \widetilde{a}_i(t)\phi_i(\cdot), \quad \widetilde{a}_i(0) = a(v_i, 0), \quad i = 1, \ldots, n, \tag{C.18}$$

we obtain

$$M\partial_t \hat{a}(t) = -N\hat{a}(t), \tag{C.19}$$

where

$$\hat{a}(t) = \begin{pmatrix} \widetilde{a}_1(t) \\ \vdots \\ \widetilde{a}_n(t) \end{pmatrix}, \tag{C.20}$$

and the element of matrices M and N are

$$M_{ij} = \int_{\Gamma_h} \phi_i \phi_j \mathrm{d}S, \qquad N_{ij} = \int_{\Gamma_h} \nabla\phi_i \cdot \nabla\phi_j \mathrm{d}S, \quad i, j = 1, \ldots, n. \tag{C.21}$$

Another example about BRD model on the toroidal surface with the backward Euler method is shown inappendix C.3. As shown in the above example, we need to compute $\int_{\Gamma_h} \phi_i \phi_j \mathrm{d}S$ and $\int_{\Gamma_h} \nabla\phi_i \cdot \nabla\phi_j \mathrm{d}S$. The following facts are useful:

Theorem C.2.3. For any triangle $\triangle v_i v_j v_k$, the following facts hold.

$$(i) \quad \nabla\phi_i = \frac{\overrightarrow{h}|v_j v_k|}{2h|\triangle v_i v_j v_k|}, \tag{C.22}$$

$$(ii) \quad \int_{\triangle v_i v_j v_k} \nabla\phi_i \cdot \nabla\phi_i \mathrm{d}S = \frac{1}{2}(\cot\angle v_i v_j v_k + \cot\angle v_j v_k v_i), \tag{C.23}$$

$$(iii) \quad \int_{\triangle v_i v_j v_k} \nabla\phi_j \cdot \nabla\phi_k \mathrm{d}S = -\frac{1}{2}\cot\angle v_k v_i v_j, \tag{C.24}$$

$$(iv) \quad \int_{\triangle v_i v_j v_k} \phi_i^2 \mathrm{d}S = \frac{1}{6}\left|\triangle v_i v_j v_k\right|, \tag{C.25}$$

$$(v) \quad \int_{\triangle v_i v_j v_k} \phi_j \phi_k \mathrm{d}S = \frac{1}{12}\left|\triangle v_i v_j v_k\right|, \tag{C.26}$$

where $|\triangle v_i v_j v_k|$ denotes the area of $\triangle v_i v_j v_k$, $|v_j v_k|$ denotes the length of edge $[v_j, v_k]$. The height of $\triangle v_i v_j v_k$ corresponding to v_i is denoted by h and we use $\overrightarrow{h}$ to denote the vector of height, from p to v_i. Here p is the perpendicular foot on the line of $[v_j, v_k]$ as shown in Figure C.1.

Proof. (i): By the definition of piecewise linear hat function, we obtain

$$\nabla\phi_j = \frac{\overrightarrow{h}}{h^2} = \frac{\overrightarrow{h}|v_j v_k|}{h^2|v_j v_k|} = \frac{\overrightarrow{h}|v_j v_k|}{2h|\triangle v_i v_j v_k|}.$$

(ii): From (C.22), we obtain

$$\begin{aligned}\int_{\triangle v_i v_j v_k} \nabla\phi_i \cdot \nabla\phi_i \mathrm{d}S &= \int_{\triangle v_i v_j v_k} \left(\frac{|v_j v_k|}{2|\triangle v_i v_j v_k|}\right)^2 \mathrm{d}S = \frac{|v_j v_k|^2}{4|\triangle v_i v_j v_k|} = \frac{|v_j v_k|}{2h} \\ &= \frac{1}{2}(\cot\angle v_i v_j v_k + \cot\angle v_j v_k v_i).\end{aligned}$$

(iii): Since the included angle between $\nabla\phi_j$ and $\nabla\phi_k$ is $(\pi - \angle v_k v_i v_j)$ and the area of $\triangle v_i v_j v_k$ can be expressed by $|\triangle v_i v_j v_k| = \frac{1}{2}|v_k v_i||v_i v_j|\sin\angle v_k v_i v_j$, we obtain

$$\begin{aligned}\int_{\triangle v_i v_j v_k} \nabla\phi_j \cdot \nabla\phi_k \mathrm{d}S &= \int_{\triangle v_i v_j v_k} \cos(\pi - \angle v_k v_i v_j)\frac{|v_k v_i|}{2|\triangle v_i v_j v_k|}\frac{|v_i v_j|}{2|\triangle v_i v_j v_k|}\mathrm{d}S \\ &= -\frac{1}{2}\frac{|v_k v_i||v_i v_j|\cos\angle v_k v_i v_j}{|v_k v_i||v_i v_j|\sin\angle v_k v_i v_j} = -\frac{1}{2}\cot\angle v_k v_i v_j.\end{aligned}$$

(iv):

$$\begin{aligned}\int_{\triangle v_i v_j v_k} \phi_i \phi_i \mathrm{d}S &= \int_0^h \left(\frac{\eta}{h}\right)^2 \frac{h-\eta}{h}|v_j v_k|\mathrm{d}\eta = \frac{|v_j v_k|}{h^3}\int_0^h h\eta^2 - \eta^3 \mathrm{d}\eta \\ &= \frac{|v_j v_k|}{h^3}\left(\frac{1}{3}h^4 - \frac{1}{4}h^4\right) = \frac{1}{12}h|v_j v_k| = \frac{1}{6}\left|\triangle v_i v_j v_k\right|.\end{aligned}$$

(v) Let $f_j, f_k : [p_j, p_k] \to \mathbb{R}$ be the linear functions on the edge $[p_j, p_k]$ satisfying

$$f_j(p_j) = a, f_j(p_k) = 0, f_k(p_j) = 0, f_k(p_k) = b$$

and the length of $[p_j, p_k]$ is denoted by l. Then, we obtain

$$\begin{aligned}\int_{p_j p_k} f_j f_k \mathrm{d}x &= \int_0^l a\left(1-\frac{x}{l}\right) b\frac{x}{l}\mathrm{d}x = ab\int_0^l \left(\frac{x}{l}-\frac{x^2}{l^2}\right)\mathrm{d}x \\ &= ab\left(\frac{1}{2}l-\frac{1}{3}l\right) = \frac{1}{6}abl.\end{aligned}$$

Using the equation above, we obtain

$$\begin{aligned}\int_{\triangle v_i v_j v_k} \phi_j\phi_k \mathrm{d}S &= \int_0^h \frac{1}{6}\left(1-\frac{\eta}{h}\right)^2 |v_j v_k|\left(1-\frac{\eta}{h}\right)\mathrm{d}\eta \\ &= \frac{1}{6h^3}|v_j v_k|\int_0^h (h-\eta)^3 \mathrm{d}\eta = \frac{1}{12}\left|\triangle v_i v_j v_k\right|. \qquad \square\end{aligned}$$

C.3 Discrete approximation of the Brusselator reaction-diffusion system on the toroidal surface

In this section, we introduce how to obtain the discrete equations of the BRD model (1.3) by finite element method on the toroidal surface $\mathbb{T}_{R,r}$ with the backward Euler method as follows. Let $\widetilde{\mathbb{T}}_{R,r}$ denote the triangulation mesh with n vertices of the toroidal surface $\mathbb{T}_{R,r}$. Let ϕ_i denote the piecewise linear hat function of vertex i of mesh, $i = 1, \ldots, n$. Let $\widetilde{u}(\cdot,t), \widetilde{v}(\cdot,t)$ be the approximate solution of $u(\cdot,t)$ and $v(\cdot,t)$, $\widetilde{u}(t) = \sum_{i=1}^n \widetilde{u}_i(t)\phi_i(\cdot)$ and $\widetilde{v}(t) = \sum_{i=1}^n v_i(t)\phi_i(\cdot)$, where $\widetilde{u}_i(t)$ and $\widetilde{u}_i(v)$ denote the value of $\widetilde{u}$ and $\widetilde{v}$ at vertex i of the mesh at time t satisfying $\widetilde{u}_i(0) = u(v_i, 0)$ and $\widetilde{v}_i(0) = v(v_i, 0)$. We use the backward Euler method to compute $\widetilde{u}(\cdot,t), \widetilde{v}(\cdot,t)$ numerically with time step Δt. Then, $\widetilde{u}_t(\cdot,t)$ is approximated by

$$\widetilde{u}_t(\cdot,t) \approx \frac{\widetilde{u}(\cdot,t+\Delta t)-\widetilde{u}(\cdot,t)}{\Delta t}.$$

Since $(\widetilde{u}(\cdot,t+\Delta t)-\widetilde{u}(\cdot,t))^2 = \mathcal{O}(\Delta t^2)$ and $(\widetilde{u}(\cdot,t+\Delta t)-\widetilde{u}(\cdot,t))(\widetilde{v}(\cdot,t+\Delta t)-\widetilde{v}(\cdot,t)) = \mathcal{O}(\Delta t^2)$, $\widetilde{u}^2(\cdot,t+\Delta t)\widetilde{v}(\cdot,t+\Delta t)$ can be approximated by

$$\begin{aligned}\widetilde{u}^2(\cdot,t+\Delta t)\widetilde{v}(\cdot,t+\Delta t) =& \left[\widetilde{u}(\cdot,t)+(\widetilde{u}(\cdot,t+\Delta t)-\widetilde{u}(\cdot,t))\right]^2\left[\widetilde{v}(\cdot,t)+(\widetilde{v}(\cdot,t+\Delta t)-\widetilde{v}(\cdot,t))\right] \\ =& \widetilde{u}^2(\cdot,t)\widetilde{v}(\cdot,t)+2\widetilde{u}(\cdot,t)\widetilde{v}(\cdot,t)\widetilde{u}(\cdot,t+\Delta t) \\ & -2\widetilde{u}^2(\cdot,t)\widetilde{v}(\cdot,t)+\widetilde{u}^2(\cdot,t)\widetilde{v}(\cdot,t+\Delta t)-\widetilde{u}^2(\cdot,t)\widetilde{v}(\cdot,t)+\mathcal{O}(\Delta t^2) \\ \approx& 2\widetilde{u}(\cdot,t)\widetilde{v}(\cdot,t)\widetilde{u}(\cdot,t+\Delta t)+\widetilde{u}^2(\cdot,t)\widetilde{v}(\cdot,t+\Delta t)-2\widetilde{u}^2(\cdot,t)\widetilde{v}(\cdot,t).\end{aligned}$$

Then, $\widetilde{u}(\cdot,t)\widetilde{v}(\cdot,t)\widetilde{u}(\cdot,t+\Delta t)$, $\widetilde{u}(\cdot,t)^2\widetilde{v}(\cdot,t+\Delta t)$ and $\widetilde{u}(\cdot,t)^2\widetilde{v}(\cdot,t)$ can be approximated by $k_1(\cdot,t,\Delta t)$, $k_2(\cdot,t,\Delta t)$ and $k_3(\cdot,t)$, respectively:

$$\begin{aligned}k_1(\cdot,t,\Delta t) &= \sum_{i=1}^n \widetilde{u}_i(t)\widetilde{v}_i(t)\widetilde{u}_i(t+\Delta t)\phi_i(\cdot), \\ k_2(\cdot,t,\Delta t) &= \sum_{i=1}^n \widetilde{u}_i^2(t)\widetilde{v}_i(t+\Delta t)\phi_i(\cdot), \\ k_3(\cdot,t) &= \sum_{i=1}^n \widetilde{u}_i^2(t)\widetilde{v}_i(t)\phi_i(\cdot).\end{aligned}$$

Next, we consider the weak solution $\widetilde{u}_i(t+\Delta t), \widetilde{v}_i(t+\Delta t)$ of the following equations that for $i = 1, \dots n$,

$$\int_{\widetilde{\mathbb{T}}_{R,r}} \phi_i \frac{\widetilde{u}(\cdot, t+\Delta t) - \widetilde{u}(\cdot, t)}{\Delta t} \mathrm{d}S = \int_{\widetilde{\mathbb{T}}_{R,r}} \phi_i \epsilon^2 \triangle_{\widetilde{\mathbb{T}}_{R,r}} \widetilde{u}(\cdot, t+\Delta t) \mathrm{d}S + \int_{\widetilde{\mathbb{T}}_{R,r}} \phi_i (\epsilon^2 A - \widetilde{u}(\cdot, t+\Delta t)) \mathrm{d}S + \int_{\widetilde{\mathbb{T}}_{R,r}} \phi_i f(2k_1(\cdot, t, \Delta t) + k_2(\cdot, t, \Delta t) - 2k_3(\cdot, t)) \mathrm{d}S,$$

$$\int_{\widetilde{\mathbb{T}}_{R,r}} \phi_i \tau \frac{\widetilde{v}(\cdot, t+\Delta t) - \widetilde{v}(\cdot, t)}{\Delta t} \mathrm{d}S = \int_{\widetilde{\mathbb{T}}_{R,r}} \phi_i \triangle_{\widetilde{\mathbb{T}}_{R,r}} \widetilde{v}(\cdot, t+\Delta t) \mathrm{d}S + \int_{\widetilde{\mathbb{T}}_{R,r}} \phi_i \frac{1}{\epsilon^2} \widetilde{u}(\cdot, t+\Delta t) \mathrm{d}S - \int_{\widetilde{\mathbb{T}}_{R,r}} \phi_i \frac{1}{\epsilon^2} (2k_1(\cdot, t, \Delta t) + k_2(\cdot, t, \Delta t) - 2k_3(\cdot, t)).$$

Here $\triangle_{\widetilde{\mathbb{T}}_{R,r}} = \nabla_{\widetilde{\mathbb{T}}_{R,r}} \cdot \nabla_{\widetilde{\mathbb{T}}_{R,r}}$ where $\nabla_{\widetilde{\mathbb{T}}_{R,r}}$ is defined by (C.9) on each triangle. Let us define

$$p(\cdot, t, \Delta t) = \frac{1}{\Delta t} \widetilde{u}(\cdot, t) + \epsilon^2 A - 2f k_3(\cdot, t) = \sum_{i=1}^{n} p_i(t, \Delta t) \phi_i(\cdot),$$
$$q(\cdot, t, \Delta t) = \frac{\tau}{\Delta t} \widetilde{v}(\cdot, t) + \frac{2}{\epsilon^2} k_3(\cdot, t) = \sum_{i=1}^{n} q_i(t, \Delta t) \phi_i(\cdot),$$

where $p_i = \frac{1}{\Delta t} \widetilde{u}_i(t) + \epsilon^2 A - 2f \widetilde{u}_i^2(t) \widetilde{v}_i(t)$ and $q_i = \frac{\tau}{\Delta t} \widetilde{u}_i(t) + \frac{2}{\epsilon^2} \widetilde{u}_i^2(t) \widetilde{v}_i(t)$. By Green's identity (C.11), we obtain

$$\int_{\widetilde{\mathbb{T}}_{R,r}} \phi_i p(\cdot, t, \Delta t) \mathrm{d}S = \int_{\widetilde{\mathbb{T}}_{R,r}} \phi_i \frac{\widetilde{u}(\cdot, t+\Delta t)}{\Delta t} \mathrm{d}S + \int_{\widetilde{\mathbb{T}}_{R,r}} \nabla_{\widetilde{\mathbb{T}}_{R,r}} \phi_i \cdot \nabla_{\widetilde{\mathbb{T}}_{R,r}} \widetilde{u}(\cdot, t+\Delta t) \mathrm{d}S + \int_{\widetilde{\mathbb{T}}_{R,r}} \phi_i \widetilde{u}(\cdot, t+\Delta t) \mathrm{d}S - \int_{\widetilde{\mathbb{T}}_{R,r}} \phi_i f(2k_1(\cdot, t, \Delta t) + k_2(\cdot, t, \Delta t)) \mathrm{d}S,$$

$$\int_{\widetilde{\mathbb{T}}_{R,r}} \phi_i q(\cdot, t, \Delta t) \mathrm{d}S = \int_{\widetilde{\mathbb{T}}_{R,r}} \phi_i \tau \frac{\widetilde{v}(\cdot, t+\Delta t)}{\Delta t} \mathrm{d}S + \int_{\widetilde{\mathbb{T}}_{R,r}} \nabla_{\widetilde{\mathbb{T}}_{R,r}} \phi_i \cdot \nabla_{\widetilde{\mathbb{T}}_{R,r}} \widetilde{v}(\cdot, t+\Delta t) \mathrm{d}S - \int_{\widetilde{\mathbb{T}}_{R,r}} \phi_i \frac{1}{\epsilon^2} \widetilde{u}(\cdot, t+\Delta t) \mathrm{d}S + \int_{\widetilde{\mathbb{T}}_{R,r}} \phi_i \frac{1}{\epsilon^2} (2k_1(\cdot, t, \Delta t) + k_2(\cdot, t, \Delta t)) \mathrm{d}S.$$

Then, we obtain the matrix form of discrete Brusselator RD system

$$\begin{pmatrix} MA(t, \Delta t) + N & MB(t) \\ MC(t) & MD(t, \Delta t) + N \end{pmatrix} \begin{pmatrix} U(t+\Delta t) \\ V(t+\Delta t) \end{pmatrix} = \begin{pmatrix} MP(t, \Delta t) \\ MQ(t, \Delta t) \end{pmatrix}, \tag{C.27}$$

where

$$U(t+\Delta t) = \begin{pmatrix} \widetilde{u}_1(t+\Delta t) \\ \vdots \\ \widetilde{u}_n(t+\Delta t) \end{pmatrix}, \quad V(t+\Delta t) = \begin{pmatrix} \widetilde{v}_1(t+\Delta t) \\ \vdots \\ \widetilde{v}_n(t+\Delta t) \end{pmatrix}, \quad P(t) = \begin{pmatrix} p_1(t) \\ \vdots \\ p_n(t) \end{pmatrix}, \quad Q(t) = \begin{pmatrix} q_1(t) \\ \vdots \\ q_n(t) \end{pmatrix},$$
$$M = \begin{pmatrix} X_{1,1} & \cdots & X_{1,n} \\ \vdots & \ddots & \vdots \\ X_{n,1} & \cdots & X_{n,n^2} \end{pmatrix}, \quad N = \begin{pmatrix} Y_{1,1} & \cdots & Y_{1,n} \\ \vdots & \ddots & \vdots \\ Y_{n,1} & \cdots & Y_{n,n} \end{pmatrix},$$

$$A(t,\Delta t)=\begin{pmatrix} a_1(t,\Delta t) & 0 & 0 & \cdots & 0\\ 0 & a_2(t,\Delta t) & 0 & \cdots & 0\\ 0 & 0 & a_3(t,\Delta t) & \cdots & 0\\ \vdots & \vdots & \vdots & \ddots & \vdots\\ 0 & 0 & 0 & \cdots & a_n(t,\Delta t)\end{pmatrix},\quad B(t)=\begin{pmatrix} b_1(t) & 0 & 0 & \cdots & 0\\ 0 & b_2(t) & 0 & \cdots & 0\\ 0 & 0 & b_3(t) & \cdots & 0\\ \vdots & \vdots & \vdots & \ddots & \vdots\\ 0 & 0 & 0 & \cdots & b_n(t)\end{pmatrix},$$

$$C(t,\Delta t)=\begin{pmatrix} c_1(t,\Delta t) & 0 & 0 & \cdots & 0\\ 0 & c_2(t,\Delta t) & 0 & \cdots & 0\\ 0 & 0 & c_3(t,\Delta t) & \cdots & 0\\ \vdots & \vdots & \vdots & \ddots & \vdots\\ 0 & 0 & 0 & \cdots & c_n(t,\Delta t)\end{pmatrix},\quad D(t)=\begin{pmatrix} d_1(t) & 0 & 0 & \cdots & 0\\ 0 & d_2(t) & 0 & \cdots & 0\\ 0 & 0 & d_3(t) & \cdots & 0\\ \vdots & \vdots & \vdots & \ddots & \vdots\\ 0 & 0 & 0 & \cdots & d_n(t)\end{pmatrix}.$$

Here $a_i(t,\Delta t)=\frac{1}{\Delta t}+1-2f\widetilde{u}_i(t)\widetilde{v}_i(t)$, $b_i(t)=-f\widetilde{u}_i^2(t)$, $c_i(t)=\frac{1}{\epsilon^2}(-1+2\widetilde{u}_i(t)\widetilde{v}_i(t))$, $d_i(t,\Delta t)=\frac{\tau}{\Delta t}+\frac{1}{\epsilon^2}\widetilde{u}_i^2(t)$, $X_{i,j}=\int_{\widetilde{\mathbb{T}}_{R,r}}\phi_i\phi_j\mathrm{d}S$ and $Y_{i,j}=\int_{\widetilde{\mathbb{T}}_{R,r}}\nabla_{\widetilde{\mathbb{T}}_{R,r}}\phi_i\cdot\nabla_{\widetilde{\mathbb{T}}_{R,r}}\phi_j\mathrm{d}S$ for $i,j=1,\ldots,n$. For given Δt and initial data $u(\cdot,0)$ and $v(\cdot,0)$, we have $\widetilde{u}_i(0)=u(v_i,0)$ and $\widetilde{v}_i(0)=v(v_i,0)$, $i=1,2,\ldots,n$. Then, by (C.27) and Theorem C.2.3, we can obtain the numerical results of $\widetilde{u}_i(t)$ and $\widetilde{v}_i(t)$.

References

[1] Y. A. Astrov and H.-G. Purwins, *Plasma spots in a gas discharge system: birth, scattering and formation of molecules*, Physics Letters A, 283 (2001), pp. 349–354.

[2] Y. A. Astrov and H.-G. Purwins, *Spontaneous division of dissipative solitons in a planar gas-discharge system with high ohmic electrode*, Physics Letters A, 358 (2006), pp. 404–408.

[3] G. Bader and U. Ascher, *A new basis implementation for a mixed order boundary value ODE solver*, SIAM Journal on Scientific and Statistical Computing, 8 (1987), pp. 483–500.

[4] Y. CHANG, J. C. TZOU, M. J. WARD, and J. C. WEI, *Refined stability thresholds for localized spot patterns for the Brusselator model in* $\mathbb{R}^2$, European Journal of Applied Mathematics, 30 (2019), p. 791–828.

[5] W. Chen and M. J. Ward, *The stability and dynamics of localized spot patterns in the two-dimensional Gray–Scott model*, SIAM Journal on Applied Dynamical Systems, 10 (2011), pp. 582–666.

[6] P. W. Davies, P. Blanchedeau, E. Dulos, and P. D. Kepper, *Dividing blobs, chemical flowers, and patterned islands in a reaction-diffusion system*, The Journal of Physical Chemistry A, 102 (1998), pp. 8236–8244.

[7] A. Doelman, R. A. Gardner, and T. J. Kaper, *Stability analysis of singular patterns in the 1d gray-scott model: a matched asymptotics approach*, Physica D: Nonlinear Phenomena, 122 (1998), pp. 1–36.

[8] G. Dziuk and C. M. Elliott, *Finite elements on evolving surfaces*, IMA Journal of Numerical Analysis, 27 (2007), pp. 262–292.

[9] G. Dziuk and C. M. Elliott, *Surface finite elements for parabolic equations*, Journal of Computational Mathematics, (2007), pp. 385–407.

[10] G. Dziuk and C. M. Elliott, *Finite element methods for surface PDEs*, Acta Numerica, 22 (2013), pp. 289–396.

[11] M. R. Garvie and C. Trenchea, *Identification of space-time distributed parameters in the gierer–meinhardt reaction-diffusion system*, SIAM Journal on Applied Mathematics, 74 (2014), pp. 147–166.

[12] D. Iron and M. J. Ward, *The dynamics of multispike solutions to the one-dimensional gierer–meinhardt model*, SIAM Journal on Applied Mathematics, 62 (2002), pp. 1924–1951.

[13] D. Iron, M. J. Ward, and J. Wei, *The stability of spike solutions to the one-dimensional gierer–meinhardt model*, Physica D: Nonlinear Phenomena, 150 (2001), pp. 25–62.

[14] A. Jamieson-Lane, P. H. Trinh, and M. J. Ward, *Localized spot patterns on the sphere for reaction-diffusion systems: Theory and open problems*, in Mathematical and Computational Approaches in Advancing Modern Science and Engineering, Springer International Publishing, 2016, pp. 641–651.

[15] T. Kolokolnikov and M. J. Ward, *Reduced wave green's functions and their effect on the dynamics of a spike for the gierer–meinhardt model*, European Journal of Applied Mathematics, 14 (2003), pp. 513–545.

[16] T. Kolokolnikov, M. J. Ward, and J. Wei, *The existence and stability of spike equilibria in the one-dimensional gray–scott model: The pulse-splitting regime*, Physica D: Nonlinear Phenomena, 202 (2005), pp. 258–293.

[17] T. Kolokolnikov, M. J. Ward, and J. Wei, *Spot self-replication and dynamics for the Schnakenburg model in a two-dimensional domain*, Journal of Nonlinear Science, 19 (2009), pp. 1–56.

[18] S. Kondo and T. Miura, *Reaction-diffusion model as a framework for understanding biological pattern formation*, Science, 329 (2010), pp. 1616–1620.

[19] K.-J. Lee, W. D. McCormick, J. E. Pearson, and H. L. Swinney, *Experimental observation of self-replicating spots in a reaction–diffusion system*, Nature, 369 (1994), pp. 215–218.

[20] F. Mazzia, J. R. Cash, and K. Soetaert, *Solving boundary value problems in the open source software R: package bvpSolve*, Opuscula Mathematica, 34 (2014), pp. 387–403.

[21] A. Nakamasu, G. Takahashi, A. Kanbe, and S. Kondo, *Interactions between zebrafish pigment cells responsible for the generation of turing patterns*, Proceedings of the National Academy of Sciences, 106 (2009), pp. 8429–8434.

[22] Q. Ouyang and H. L. Swinney, *Transition from a uniform state to hexagonal and striped turing patterns*, Nature, 352 (1991), pp. 610–612.

[23] I. Prigogine and R. Lefever, *Symmetry breaking instabilities in dissipative systems. II*, The Journal of Chemical Physics, 48 (1968), pp. 1695–1700.

[24] I. Rozada, S. J. Ruuth, and M. J. Ward, *The stability of localized spot patterns for the Brusselator on the sphere*, SIAM Journal on Applied Dynamical Systems, 13 (2014), pp. 564–627.

[25] T. Sakajo and Y. Shimizu, *Point vortex interactions on a toroidal surface*, Proceedings of the Royal Society A: Mathematical, Physical and Engineering Sciences, 472 (2016), p. 20160271.

[26] T. Sakajo and P. Wang, *Spot dynamics of a reaction-diffusion system on the surface of a torus*, SIAM Journal on Applied Dynamical Systems, 20 (2021), pp. 1053–1089.

[27] L. J. Shaw and J. D. Murray, *Analysis of a model for complex skin patterns*, SIAM Journal on Applied Mathematics, 50 (1990), pp. 628–648.

[28] Z. Tan, S. Chen, X. Peng, L. Zhang, and C. Gao, *Polyamide membranes with nanoscale turing structures for water purification*, Science, 360 (2018), pp. 518–521.

[29] P. H. Trinh and M. J. Ward, *The dynamics of localized spot patterns for reaction-diffusion systems on the sphere*, Nonlinearity, 29 (2016), pp. 766–806.

[30] A. M. Turing, *The chemical basis of morphogenesis*, Philosophical Transactions of the Royal Society of London. Series B, Biological Sciences, 237 (1952), pp. 37–72.

[31] J. J. Tyson, *Some further studies of nonlinear oscillations in chemical systems*, The Journal of Chemical Physics, 58 (1973), pp. 3919–3930.

[32] J. C. Tzou and L. Tzou, *Spot patterns of the Schnakenberg reaction–diffusion system on a curved torus*, Nonlinearity, 33 (2019), pp. 643–674.

[33] J. C. Tzou and M. J. Ward, *The stability and slow dynamics of spot patterns in the 2D Brusselator model: The effect of open systems and heterogeneities*, Physica D: Nonlinear Phenomena, 373 (2018), pp. 13–37.

[34] V. K. Vanag, *Waves and patterns in reaction–diffusion systems. belousov–zhabotinsky reaction in water-in-oil microemulsions*, Physics-Uspekhi, 47 (2004), pp. 923–941.

[35] V. K. Vanag and I. R. Epstein, *Localized patterns in reaction-diffusion systems*, Chaos: An Interdisciplinary Journal of Nonlinear Science, 17 (2007), p. 037110.

[36] S. Vey and A. Voigt, *Amdis: adaptive multidimensional simulations*, Computing and Visualization in Science, 10 (2007), pp. 57–67.

[37] T. Witkowski, S. Ling, S. Praetorius, and A. Voigt, *Software concepts and numerical algorithms for a scalable adaptive parallel finite element method*, Advances in computational mathematics, 41 (2015), pp. 1145–1177.